# Identification of Nonlinearities in Joints of a Wing Structure

Thesis submitted in accordance with the requirements of the University of Liverpool for the degree of Doctor in Philosophy

by

Mohd Shahrir Mohd Sani

April 2016

*To my family*

# Abstract

Nonlinear structural identification is essential in engineering. The powerful finite element method can only produce accurate results when accurate values of the structural parameters are used. As new materials are being used and structures become slender and lighter, nonlinear behaviour of structures becomes more important. There have been many studies into the development and application of system identification methods for structural nonlinearity based on changes in natural frequencies, mode shapes and damping ratios. A great challenge is to identify nonlinearity in large structural systems. Much work has been undertaken in the development of nonlinear system identification methods (e.g. Hilbert Transform, NARMAX, and Proper Orthogonal Decomposition), however, it is arguable that most of these methods are cumbersome when applied to realistic large structures that contain mostly linear modes with some local nonlinearity (e.g. aircraft engine pylon attachment to a wing). In this thesis, a multi-shaker force appropriation method is developed to determine the underlying linear and nonlinear structural properties through the use of the measurement and generation of restoring force surfaces. One undamped mode is excited in each multi-shaker test. Essentially, this technique is a derivative of the restoring surface method and involves a non-linear curve fitting performed in modal space. A reduced finite element model is established and its effectiveness in revealing the nonlinear characteristics of the system is discussed. The method is demonstrated through both numerical simulations and experiments on a simple jointed laboratory structure with seeded faults, which represents an engine pylon structure that consists of a rectangular wing with two stores suspended underneath.

# Acknowledgements

I would like to express my sincerest gratitude to my primary supervisor, **Prof. Huajiang Ouyang**, for his invaluable supports, encouragements and supervision throughout the duration of this research. His continuous guidance has enabled me to complete my work successfully. I also would like to thank **Prof. Jonathan Cooper** for his valuable input and time serving my second supervisor.

Special thanks are due to Principal Experimental Officer of Dynamics Lab, **Dr. Simon James**, for his valuable advice in conducting my experimental work. I would like express my appreciation to **Mr. Steve Bode** in helping me in performing MIMO Normal Mode Testing.

Special appreciation to **Dr. Nurul, Dr. Hamed Haddad, Dr. Marco Prandina, Dr. Sham, Dr. Yazdi, Dr. John, Dr. Fiza, Mr. Amin** and **Dr. Dan Stancioiu** for their discussion and advice.

My greatest appreciation to my wife, **Mrs. Haslizahanim Mohd Razali**, who endured this long process with me, sacrificed almost everything to enable me reaching my dreams while always offering support and love without fail. For my daughter, **Sufi Tihani** and my son, **Muhammad Syabil Hazim**, who are always my inspirations. It would not have been possible for me to complete my research without the outstanding moral support from my mum, **Hajjah Asmah Omar**.

Finally, I would like to greatly acknowledge the support by the **Malaysian Ministry of Higher Education (MOHE)** and the **Universiti Malaysia Pahang (UMP)** throughout the duration of this research.

# Contents

# List of Figures

## Chapter 2



## Chapter 3

## Chapter 4

## Chapter 5



## Chapter 6

# List of Tables

## Chapter 3



## Chapter 4

## Chapter 5

## Chapter 6

# List of Symbols and Abbreviations

| | |
|---|---|
| $x$ | displacement |
| $\dot{x}$ | velocity |
| $\ddot{x}$ | acceleration |
| $t$ | time |
| $E$ | Young's modulus |
| $G$ | shear modulus |
| $v$ | Poisson's ratio |
| $\rho$ | mass density |
| $\omega$ | frequency |
| $\omega_n$ | natural frequency |
| $f(t)$ | applied force |
| $\lambda$ | eigenvalues |
| $\Phi$ | mode shapes |
| $\zeta_n$ | modal damping |
| $r$ | number of response |
| $e$ | number of excitations |
| $\mathbf{M}$ | mass matrix |
| $\mathbf{C}$ | damping matrix |
| $\mathbf{K}$ | stiffness matrix |
| $\mathbf{p}$ | modal displacement matrix |
| $\mathbf{\Phi}$ | modal vector matrix |
| $\mathbf{H}(\omega)$ | frequency response function matrix |
| $\mathbf{g}_{nl}$ | stiffness nonlinearity matrix |
| Re | real number |
| Im | imaginary number |

| | |
|---|---|
| 3D | three dimensional |
| ARMA | auto regressive moving average with exogenous input |
| CF | crest factor |
| CRP | conditioned reverse path |
| DFT | discrete Fourier transform |
| DOF | degree of freedom |
| EMA | experimental modal analysis |
| FDFI | frequency domain direct parameter identification |
| FE | finite element |
| FFT | fast Fourier Transform |
| FRF | frequency response function |
| HMT | hybrid modal techniques |
| HT | Hilbert transform |
| HVD | Hilbert vibration decomposition |
| LSCE | least squares complex exponential |
| MDOF | multi degree of freedom |
| MMIF | multivariate mode indicator function |
| MPI | modal purity index |
| MSE | mean square error |
| NARMAX | nonlinear auto regressive moving average with exogenous input |
| NKV | nonlinear Kelvin Voigt |
| NLRDM | nonlinear resonant decay method |
| NNMs | nonlinear normal modes |
| RF | restoring forces |
| RFS | restoring force surface |
| RMS | root mean square |
| RP | reverse path |
| SDOF | single degree of freedom |
| SNR | signal to noise ratio |
| SVD | singular value decomposition |

# Chapter 1

# Introduction

## 1.1 Background

Most engineering structures experience vibration due to some sources of excitation. Examples of these sources are: impact or rotational out of balance forces, aerodynamic forces acting on a wing structure, the irregularities of a road surface. It is therefore important that vibration levels can be anticipated and reduced if necessary. In aerospace structures, where safety is important, investigation of the structure's dynamic behaviour is required in the event of aerodynamic instability or flutter due to excessive response levels.

A mathematical model for structure can be derived using Finite Element (FE) analysis in order to predict its dynamic behaviour. Essentially, the structure is approximated by a series of masses and springs with damping assumed in some appropriate ways. The FE model is constructed to estimate the modal parameters such as undamped natural frequencies, normal mode shapes and modal damping values to be obtained. The modelling accuracy of the structures depends on the experience of the analyst and on the adequacy of the structural idealisation. The main advantage of FE analysis is that it does not require a physical structure test to be performed, and the effect of modifying a structure can be quickly assessed. However, FE has its limitations, particularly in modeling joints accurately. For an example, when an elastic connection is assumed to be rigid (fixed) or when an eccentricity of a beam or a plate connection is omitted from the model (Mottershead et al., 2011). The user of FE should be alert of several sources of modeling error and carry out essential adjustment to those aspects of the model that cannot corrected by

changing the values of selected model updating parameters. Idealisation errors from the simplification of structure, for example, when a plate is treated like a beam which might be erroneous depending on the length to width ratio of the plate and frequency range to be covered. Others typical idealisation error arises from inaccurate assignment of mass properties, errors in connectivity of the mesh, erroneous modeling of boundary conditions and erroneous geometrical shape assumptions.

Modal testing is a common method to measure the dynamics response of a structure under some operating conditions. Ewins (1995) described that modal testing is the name given to the process by which a mathematical model is derived from measured vibration data. Model derivation relies on the test that is carried out, but it may describe the system in terms of either undamped or damped normal modes or complex modes. If a perfect undamped normal mode is excited, then all points in the system would vibrate in monophase and in quadrature to the excitation at the corresponding undamped natural frequency. However, if the system vibrates in one of its complex modes, the behaviour is different in that it vibrates at the damped natural frequency and all the points in the system do not move in monophase. The mode's shapes are thus complex to accommodate the resulting phase relationships.

The response of linear structures will be the superposition of all modes of vibration. If the structure could be made to vibrate in one mode only, then the vibrating shape will be the normal mode shape. Pure or undamped normal modes are the characteristic shapes in the absence of damping, whereas damped normal modes include damping effects. Damping is the energy dissipation process in the structure and has the effect of reducing, restricting or preventing its oscillations. Commonly, there are two types of damping in structures: viscous damping with damping forces proportional to velocity, and hysteretic damping with damping forces proportional to displacement.

In this project, force appropriation and restoring forces methods were applied to a model of an aircraft wing and pylon experimental structure. A pylon is a part of an aircraft's structure, which connects or is attached to an engine, a wing or the fuselage. Basically, the main function of a pylon is to support an engine through the wings of an aircraft. The experimental structure under this investigation consisted of a rectangular wing with two stores suspended underneath.

## 1.2 Force Appropriation Method

The force appropriation method is a technique of exciting a single mode of a structure by applying multiple forces. This method involves analysing the frequency response function (FRF) matrix in order to obtain a set of multiple exciter force patterns and undamped natural frequencies. Normal modes of the system can be excited in isolation.

The force appropriation method or the phase resonance approach is used to determine the multi-point force vector that will induce single-mode behaviour, thus allowing each normal mode to be identified in isolation. The method can be classified into two categories, direct or iterative approaches. Breitbach (1973) developed iterative force appropriation methods, but these were complicated to apply because of the long computing time. Morosow and Ayre (1978) also observed that the iterative approach was difficult to implement due to limited the requirement of a suitable initial force vector and convergence problems. Therefore, most researchers only considere the direct force appropriation method to extract eigenvalues and eigenvectors of structures.

Otte et al. (1992) presented a normal mode force appropriation method to extract undamped natural frequencies and normal-mode shapes of a structure. It is different from the phase separation technique in that the individual modes of the system are excited in sequence and mode shapes are measured directly at each resonance

condition. The force appropriation method is an approach of exciting a single mode of a structure by applying multiple forces in a certain pattern at the corresponding frequency (Cooper et al., 1993). The modal frequency and ideal pattern of excitation for a given mode are estimated by a procedure based on multivariate mode indicator function (MMIF). MMIF was developed by Williams et al. (1986) and used to automate the tuning of real normal modes in sine dwell ground vibration testing. MMIF utilizes an eigenvalue solution method on a set of FRF's to isolate modes.

They also applied advanced curve fitting algorithms, which can provide phase and kinetic energy information for mode identification. The minimal eigenvalues were declared as undamped natural frequencies for this method.

In the aerospace industry, normal mode force appropriation has been used for flight flutter or ground vibration testing (Hamilton et al., 1985; Williams et al., 1986; Brillhart and Hunt, 1992; Alexiou and Wright, 1993; Degener, 1995; Deforges et al., 2004). These approaches are most advantageous in the condition of significant modal overlap, where modes are close in frequency by damping forces. The advantages of this approach are accurate, easily compared with FE results and smoothness of mode shapes. However, the disadvantages for this method are that it needs extra analysis and longer testing time for adequate excitation.

Wright et al. (1999) suggested that the direct appropriation method of the normal modes should undergo three stages. Initially, FRF matrices are measured for multiple excitations and response positions by random or stepped sine signal. Then, the undamped natural frequencies of the normal modes were estimated using one of a number of matrix based approaches. The final step of this procedure is to apply force vectors according to each interested mode and the relevant undamped natural frequency of structure. Furthermore, the authors made a wide-ranging review of several normal mode force appropriation algorithms such as square FRF matrix by the Asher method, Trail-Nash method and Gauss-Siedel method, rectangular FRF matrix methods using MMIF and extended Asher method, rectangular FRF matrix

methods with rank reduction by modified MMIF and Juang-Wright method. The algorithm comparison is very important in order to avoid longer computational or measurement time due to multi point excitations. Details about force appropriation theory will be explained clearly in subchapter 3.2

## 1.3 Restoring Forces Method

Initially, Masri and Caughey (1979) introduced the restoring forces surface (RFS) to identify nonlinearity in single-degree of freedom (SDOF) systems by exploiting Newton's 2nd law to directly measure restoring and dissipative forces in the system. This technique expresses the nonlinear component of SDOF systems with measured parameters, displacement $(x)$ and velocity $(\dot{x})$, and time $(t)$. Three dimensional surface is displayed by plotting a 3D graph with three axes: restoring forces (RF) versus displacement $(x)$ versus velocity $(\dot{x})$. This method is based on curve fitting the restoring forces in terms of velocity and displacement to obtain a non-parametric model of the system. Chebyshev polynomials can be used to characterize the resulting surface. The shape of the graph can reveal the type of nonlinearity such as cubic stiffness, bilinear stiffness, saturation, clearance or blacklash, Coulomb friction or nonlinear damping.

The restoring forces method was extended by Masri et al. (1982) to identify multi-degree of freedom (MDOF) systems by transforming the equations of motion from physical to modal space using the modal matrix of the underlying linear system. For a linear proportionally damped system, this transformation will yield uncoupled equations, one for each of the normal modes of the system. However, for non-proportionally damped system, this transformation will result in the presence of damping coupling terms in the modal equation of motion. The parametric identification method by force state mapping technique was developed by Crawley and Aubert (1986), which is similar to restoring force method. Experiments were carried out to demonstrate the technique and results showed strong structural nonlinearities that were a cubic hardening spring, friction, and impact phenomena. In

addition, Dimitriadis and Cooper (1998) attempted to identify MDOF nonlinear aeroelastic systems based on the restoring force method. The authors considered time response at similar amplitudes and achieved a constant nonlinear restoring force. There was a good agreement with the actual system, and this method is capable of identifying a wide range of nonlinearities including discontinuous and hysteresis types. Furthermore, numerical and experimental identifications of a clamped-free nonlinear beam were conducted by Kerschen et al. (2001) using the restoring force method to identify piecewise and bilinear stiffness characteristics. A filtering procedure was applied to remove other modes' contributions.

Advantages of using a restoring forces method over other approaches are listed below:

- any type of excitation signal can be applied in this method
- the resulting mathematical model is a continuous model underlying the theory of modal analysis.
- it allows any type of nonlinearity to be identified
- it is a simple and quick identification method and is relatively straightforward mathematically and computationally
- the method can be extended to identify multi degrees of freedom systems
- it can yield visual information about the type of the nonlinearity present, especially for non-polynomial nonlinearities identification (Worden, 1992)

Details about the theory of the restoring forces theory will be explained in more detail in section 3.5

## 1.4 Research Goal and Objectives

The main goal of this research was to present a method for nonlinear identification in the joints of a wing structures. The proposed method is an efficient tool to identify large and complex nonlinear structures. Four objectives were identified as follows:

- To model and simulate various types of nonlinearity such as cubic, free play and bilinear
- To perform finite element modelling and normal mode analysis of a wing structure
- To perform modal testing using hammer, single shaker and multi shakers. However, for nonlinear identification, multi shakers were applied to the wing structure
- To identify nonlinearities in the joints of wing structure using a combination of Force Appropriation and Restoring Forces methods.

## 1.5 Research Scope

The scope of this research includes the following steps:

a) Finite element modelling was performed on a single engine pylon and an overall wing structure using MSC Nastran and Patran. Normal mode analysis was executed to determine natural frequencies and mode shapes. Mass and stiffness matrices were extracted using Matlab code based on the numerical output file.
b) Modal testing was carried out using a hammer and a single shaker to extract modal properties. The results from this test were compared with the numerical results.
c) Multi-input multi-output (MIMO) Sine Testing and MIMO Normal Mode testing were carried out to perform a nonlinear test on the pylon and wing

structure. Time domain results were obtained at different levels of excitation forces.

d) Validation by nonlinear identification method was carried out for a single pylon and the overall wing structure.

## 1.6 List of Publication

- **M.S.M. Sani**, H. Ouyang, J.E. Cooper and C.K.E.N.C.K. Husin. "Smart Methodology of Stiffness Nonlinearity Identification Vibration System", 2nd International Conference on Mechanical Engineering Research 2013 (ICMER 2013), 1-3 July 2013, Bukit Gambang Resort, Gambang, Pahang Malaysia.

## 1.7 Thesis Overview

This thesis consists of seven chapters, namely introduction, literature review, theory of force appropriation and restoring forces methods, experimental modal analysis of structure, finite element model updating of structures, nonlinear identification on structures, and conclusions and future work.

Chapter 1 gives an overview of the background, an introduction to the force appropriation and restoring force methods, the goal and objectives, and the scopes of this PhD project.

Chapter 2 reviews the single degree of freedom systems, multi degree of freedom systems, modal testing methods, finite element model updating methods, sources of nonlinearity, previous work on nonlinear identification of structures and excitation signals.

Chapter 3 covers some fundamental theoretical concepts. The development of force appropriation method including the Asher method, modified Asher method, Trail-Nash method, extended Asher method, multivariate mode indicator function (MMIF) and Juang-Wright method are discussed. The theory of restoring forces method will be covered to identify nonlinearities of the system. Implementation at different type of excitation, integration of measured time data, and estimation of mass and modal matrices are explored.

Chapter 4 addresses the experimental modal testing of a wing structure. A description about hardware, software and experimental setup is made for modal tests using a hammer, a single shaker and multi shakers. Experimentally determined appropriated force patterns obtained from a single pylon and wing FRF data are presented for two-exciter or shaker test configuration. MIMO sine testing and MIMO normal mode testing results are discussed in this chapter.

Chapter 5 presents the finite element analysis and model updating of a single engine pylon and overall wing structure. Model updating is used to minimise the discrepancies of modal properties between experimental and numerical results.

Chapter 6 discusses nonlinear identification of the single engine pylon and overall wing structure results. The combination force appropriation method and restoring forces was applied to the structure to identify stiffness nonlinearity.

Chapter 7 gives the overall conclusions, suggestions and recommendations for future studies.

# Chapter 2

# Literature Review

## 2.1 Introduction

Structural identification is a systematic approach to identifying structural parameters from input-output test data performed on structures using vibration sensing devices. System identification plays a significant role for a structural dynamics researcher to carry out numerical studies and obtain experimental results. Since the early 1960's, system identification has developed rapidly, and it has become a major research direction and new discipline in vibration, control and system engineering since the beginning of 1970's (Zhang, 2004).

Linear dynamic system identification to identify frequencies, damping and mode shapes has been widely studied by researchers in many different fields and is now a mature scientific discipline over last decades (Dearson, 1994; Ewins, 1999; Worden and Tomlinson, 2001). Modal analysis is the most popular method for performing linear system identification in structural dynamics.

Some published works on fundamental vibration theory, structural dynamics, nonlinear dynamics identification methods are reviewed in this chapter, with attention given to how detection, localization and characterization have been done due to its relevance to this research.

## 2.2 Review on Single Degree of Freedom (SDOF) Theory

The dynamics of an SDOF system is shown in Figure 2.1, and the equation of motion can be written as

$$m\ddot{x} + g(\dot{x}, x) = f(t) \tag{2.1}$$

where $m$ is the mass, $\ddot{x}$ is the acceleration, $f(t)$ is any applied force and $g(\dot{x}, x)$ is the restoring force, which is a function of velocity, $\dot{x}$ and displacement, $x$ . Equation (2.1) can be rewritten for the restoring force as below

$$g(\dot{x}, x) = f(t) - m\ddot{x} \tag{2.2}$$

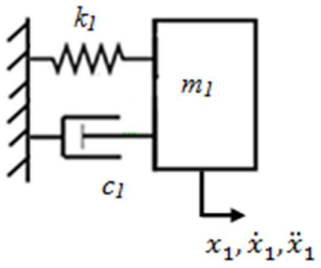


Figure 2.1: A single degree of freedom

Thus, if the input force, mass, and acceleration are known, the restoring force for the system can be estimated. If the system is time invariant, the restoring force uniquely represents the behaviour of the system and for the SDOF system, this restoring force may be written as

$$g(\dot{x}, x) = kx + c\dot{x} \tag{2.3}$$

where $c$ is the viscous damping and $k$ is the stiffness coefficient.

An undamped free vibration SDOF is obtained by considering a system with no external force as

$$m\ddot{x} + kx = 0 \tag{2.4}$$

Ignoring the trivial solution where $x(t) = 0$, which corresponds to no motion, it is known that the solution of equation (2.4) is

$$x = x_o e^{i\omega t} \tag{2.5}$$

where i is the imaginary unit $(\sqrt{-1})$, $x_o$ represents the amplitude of the displacement and $\omega$ is the angular frequency of vibration. Substituting equation (2.5) into (2.4) and solving for $\omega$, the natural frequency $\omega_n$ is obtained as

$$\omega_n = \sqrt{\frac{k}{m}} \tag{2.6}$$

which corresponds to the frequency at which the system naturally vibrates once it has been set into motion. In forced vibration case, consider a harmonic excitation of the form

$$f(t) = f_o e^{i\omega t} \tag{2.7}$$

where $f_o$ is the amplitude of the force, it is a normal procedure to study the behaviour of the system by using the output such as displacement, velocity and acceleration from frequency response function (FRF). For an undamped system excited by a harmonic force, the FRF can be expressed as

$$h(\omega) = \frac{x_o}{f_o} = \frac{1}{k-\omega^2 m} \tag{2.8}$$

where $h(\omega)$ is the receptance of the system.

## 2.3 Review on Multi Degree of Freedom Vibration Theory

Most engineering structures are continuous and have more than one degree of freedom. Normally, any real continuous system has an infinite number of degrees of freedom (DOF), but is usually described approximately over a frequency range of interest by a discrete, linear and time invariant mathematical model with a finite number of DOF ($n$),

$$\mathbf{M}\ddot{\mathbf{x}} + \mathbf{C}\dot{\mathbf{x}} + \mathbf{K}\mathbf{x} = \mathbf{f}(t) \tag{2.9}$$

where $\mathbf{x}$ is the ($n$∗1) column vector containing physical displacements, $\mathbf{f}$ is a vector of forces, and $\mathbf{M}$, $\mathbf{C}$ and $\mathbf{K}$ are the ($n$∗$n$) physical mass, damping and stiffness matrices of the system, respectively. Basically the continuous system is discretised into 'lumps' whose displacements become the unknowns, as in the finite element (FE) method. Provided that an adequate number of degrees of freedom are represented, equation (2.9) can be used to provide a good estimation of the physical system over the frequency range of interest. If the system is undamped, free vibration solution of the equation means that all points move in or out of phase at the same frequency $\omega$, namely

$$\mathbf{x} = \mathbf{x_o} e^{i\omega t} \tag{2.10}$$

So that

$$[\mathbf{K} - \omega^2 \mathbf{M}]\mathbf{x_o} = 0 \tag{2.11}$$

where $\mathbf{x_o}$ represents the peak displacement. Equation (2.11) is in fact an eigenvalue problem, the solution of which yields $n$ eigenvalues and eigenvectors, and hence, the undamped natural frequencies is $\omega_j$ and the undamped normal mode shapes is $\mathbf{\Phi}_j$ (where $j = 1, 2, 3 \ldots n$) of the system.

In practice, only a limited set of modes ($N<<n$) are used to represent the modal behaviour of a physical structure. Equation (2.9) can be reduced to contain $N$ DOF by considering a transformation to modal displacements,

$$\mathbf{x} = \mathbf{\Phi}\,\mathbf{p} \tag{2.12}$$

where $\mathbf{p}$ is the ($N*1$) modal displacement vector and $\mathbf{\Phi}$ is the ($n*N$) modal matrix containing mode shape data for $N$ modes. By substituting equation (2.12) into equation (2.9), and pre-multiply with the mode shape transpose, $\mathbf{\Phi}^{\mathrm{T}}$

$$\mathbf{\Phi}^{\mathrm{T}}\mathbf{M}\mathbf{\Phi}\ddot{\mathbf{p}} + \mathbf{\Phi}^{\mathrm{T}}\mathbf{C}\mathbf{\Phi}\dot{\mathbf{p}} + \mathbf{\Phi}^{\mathrm{T}}\mathbf{K}\mathbf{\Phi}\mathbf{p} = \mathbf{\Phi}^{\mathrm{T}}\mathbf{f}(t) \tag{2.13}$$

By using the orthogonality of the modes, equation (2.13) becomes

$$\bar{\mathbf{M}}\ddot{\mathbf{p}} + \bar{\mathbf{C}}\dot{\mathbf{p}} + \bar{\mathbf{K}}\mathbf{p} = \bar{\mathbf{f}} \tag{2.14}$$

where $\bar{\mathbf{M}} = \mathbf{\Phi}^{\mathrm{T}}\mathbf{M}\mathbf{\Phi} = [\bar{\mathrm{M}}_{rr}]$ and $\bar{\mathbf{K}} = \mathbf{\Phi}^{\mathrm{T}}\mathbf{K}\mathbf{\Phi} = [\bar{\mathrm{K}}_{rr}]$ are the ($N*N$) diagonal matrices containing modal mass and stiffness, respectively and $\bar{\mathbf{f}}$ are the modal force vector. If the structure has proportional damping, $\bar{\mathbf{C}} = \mathbf{\Phi}^{\mathrm{T}}\mathbf{C}\mathbf{\Phi} = [\bar{\mathrm{C}}_{rr}]$, which is also a ($N*N$) diagonal matrix, and equation (2.14) reduces to

$$\bar{\mathrm{M}}_{rr}\ddot{p}_r + \bar{\mathrm{C}}_{rr}\dot{p}_r + \bar{\mathrm{K}}_{rr}p_r = \bar{\mathrm{f}}_r \tag{2.15}$$

A typical modal displacement $p_r$ represents the amount of the $r^{th}$ undamped normal mode present in the response. If this is the case, then equation (2.15) is uncoupled, so that each mode can be excited independently at its natural frequency using the corresponding modal force. Most real structures are non-proportionally damped, resulting in a fully populated $\bar{\mathbf{C}}$ matrix such that the modal equations are coupled, and a single modal force will excite other modes. Therefore, modal forces will need to be applied to all modes to counteract forces due to damping coupling and excite only the mode of interest.

Consider a mono-phase (the term mono-phase being used to describe a phase relationship between the force components of 0 or π radians), sinusoidal force input of the form $\mathbf{f}e^{i\omega t}$ where $\mathbf{f}$ is a vector of real forces applied at frequency, $\omega$ . Then for phase resonance, the resultant mono-phase response of the system will lag the excitation vector by an angle,

$$\hat{\mathbf{x}} = \mathbf{x_o} e^{i(\omega t - \theta)} \tag{2.16}$$

where $\hat{\mathbf{x}}$ is a complex vector containing amplitude and phase information and $\mathbf{x_o}$ is the vector of the peak response amplitude. Substituting equation (2.16) into equation (2.9) gives,

$$([\mathbf{K} - \omega^2 \mathbf{M}] + \mathrm{i}\omega\mathbf{C})\mathbf{x_o} e^{-i\theta} = \mathbf{f} \tag{2.17}$$

which can be expressed in terms of its real and imaginary components,

$$([\mathbf{K} - \omega^2 \mathbf{M}]cos\theta + \omega\,\mathbf{C}\,sin\theta)\mathbf{x_o} = \mathbf{f} \tag{2.18}$$

and,

$$([\mathbf{K} - \omega^2 \mathbf{M}]sin\theta + \omega\,\mathbf{C}\,cos\theta)\mathbf{x_o} = \mathbf{0} \tag{2.19}$$

respectively. All the response locations on the structure move coherently in quadrature with the excitation when the phase lag angle, $\theta = \frac{\pi}{2}$. At a quadrature phase, equations (2.18) and (2.19) become,

$$\omega \mathbf{C}\, \mathbf{x_o} = \mathbf{f} \tag{2.20}$$

and

$$[\mathbf{K} - \omega^2 \mathbf{M}]\mathbf{x_o} = 0 \tag{2.21}$$

From equation (2.15), it is possible to see that at quadrature phase, $\omega$ is equal to the undamped natural frequency, $\omega_j$ of the $j^{th}$ mode and $\mathbf{x_o}$ is the corresponding undamped normal mode shape, $\mathbf{\Phi}_j$. Thus, the physical force distribution required to excite the $j^{th}$ undamped normal mode will be:

$$\mathbf{f} = \omega_j \mathbf{C} \mathbf{\Phi}_j \tag{2.22}$$

which is known as the appropriated force vector. Expressing equation (2.22) in a combination form for a system with $n$ DOF of interest,

$$[\mathbf{f}_1 \quad \mathbf{f}_2 \quad \dots \quad \mathbf{f}_n] = [\mathbf{C}][\mathbf{\Phi}_1 \quad \mathbf{\Phi}_2 \quad \dots \quad \mathbf{\Phi}_n] \begin{bmatrix} \omega_1 & 0 & \dots & 0 \\ 0 & \omega_2 & \dots & 0 \\ 0 & 0 & \dots & 0 \\ 0 & 0 & \dots & \omega_n \end{bmatrix} \tag{2.23}$$

Then, in simple notation, the matrix of appropriated physical force vectors is

$$\mathbf{F} = \mathbf{C}\, \mathbf{\Phi}[\ddots] \tag{2.24}$$

where $[\ddots]$ is the diagonal matrix containing the natural frequencies. Multiplying equation (2.24) by the transpose of the modal matrix $\mathbf{\Phi}^{\mathrm{T}}$ leads to the matrix of appropriated modal force vectors

$$\bar{\mathbf{f}} = \bar{\mathbf{C}}\,[\ddot{\cdot}] \tag{2.25}$$

If the damping is proportional, then $\bar{\mathbf{C}}$ and hence $\bar{\mathbf{f}}$ will be diagonal. Thus, the modal forces in matrix $\bar{\mathbf{f}}$ are,

$$\mathbf{f}_{ij} = 0 \text{ if } i \neq j \tag{2.26}$$

$$\mathbf{f}_{ij} \neq 0 \text{ if } i = j \tag{2.27}$$

The expressions show the appropriate force distribution to excite the $j^{th}$ mode, which provides a modal force in mode $j$ only.

If the structure is non-proportionally damped, then the modal damping, $\bar{\mathbf{C}}$ and the modal forces $\bar{\mathbf{f}}$ will be fully populated. In order to excite a normal mode, modal forces have to be introduced, which will counteract forces due to damping coupling and cause response only in the mode of interest. Unfortunately, in normal practice, the damping distribution is not known, so the appropriated force vectors cannot be determined theoretically. Instead, the forces must be determined experimentally in some other ways.

In modal testing, response data are usually measured from a limited number of response $r$ for $e$ (number of excitation) applied forces (where $e \leq r << n$). Thus, the mathematics needs to be revised for the subset of positions. By using equation (2.16), it is possible to relate the physical and the principal coordinates,

$$\mathbf{x}_r = \mathbf{\Phi}_r\,\mathbf{p} \tag{2.28}$$

and therefore,

$$\bar{\mathbf{f}} = \mathbf{\Phi}^{\mathrm{T}}\mathbf{f}_e \tag{2.29}$$

where $[\boldsymbol{\Phi}_r]_{r*N}$ and $[\boldsymbol{\Phi}_e]_{e*N}$ are the sub matrices of the modal matrix; $\mathbf{x}_r$ and $\mathbf{f}_e$ are the physical response and applied force vectors, respectively. Thus if the applied forces are in mono-phase and harmonic, then

$$\mathbf{f}_e = \hat{\mathbf{f}}_e e^{i\omega t} \tag{2.30}$$

and thus,

$$\mathbf{x}_r = \hat{\mathbf{x}}_r e^{i\omega t} = \boldsymbol{\Phi}_r \hat{\mathbf{p}} e^{i\omega t} \tag{2.31}$$

where ^ denotes complex values containing both amplitude and phase information. By using equations (2.14), (2.28) and (2.29), it is possible to show that,

$$\hat{\mathbf{p}} = [\overline{\mathbf{K}} - \omega^2 \overline{\mathbf{M}} + \mathrm{i}\omega \overline{\mathbf{C}}]^{-1} \overline{\mathbf{f}} \tag{2.32}$$

$$\hat{\mathbf{x}}_r = \boldsymbol{\Phi}_r [\overline{\mathbf{K}} - \omega^2 \overline{\mathbf{M}} + \mathrm{i}\omega \overline{\mathbf{C}}]^{-1} \boldsymbol{\Phi}_r{}^{\mathrm{T}} \mathbf{f}_e \tag{2.33}$$

or,

$$\mathbf{H}(\omega) = [\boldsymbol{\Phi}_r]_{r*N} [\overline{\mathbf{K}} - \omega^2 \overline{\mathbf{M}} + \mathrm{i}\omega \overline{\mathbf{C}}]^{-1}{}_{N*N} [\boldsymbol{\Phi}_e]^{\mathrm{T}}{}_{N*e} \tag{2.34}$$

where $\mathbf{H}(\omega)$ is the complex FRF matrix. Equation (2.34) shows the rank problem clearly. The rank of $\mathbf{H}(\omega)$ is $N$, even though its dimensions are $(r* e)$. In any frequency range, the effective value of $N$ is equal to the effective number of degrees of freedom, $n*$ (i.e. the number of modes that determine $\mathbf{H}(\omega)$ ). The matrices $\overline{\mathbf{K}}$, $\overline{\mathbf{M}}$ and $\overline{\mathbf{C}}$ are not known and therefore, equations (2.33) and (2.34) can be expressed in alternative forms,

$$\hat{\mathbf{x}}_r = [\mathbf{A}(\omega) + \mathrm{i}\mathbf{B}(\omega)] \mathbf{f}_e \tag{2.35}$$

and,

$$\mathbf{H}(\omega) = \mathbf{A}(\omega) + \mathrm{i}\mathbf{B}(\omega) \tag{2.36}$$

where $[\mathbf{A}(\omega) + i\mathbf{B}(\omega)]$ is the $(r * e)$ complex FRF matrix at frequency $\omega$ relating the $r$ responses to $e$ excitation forces. Equation (2.36) will be discussed further in the theory of force appropriation method in Chapter 3.

## 2.4 Modal Testing

Modal testing has always provided a major contribution to understand many vibration phenomena in real practice. This experimental test is a process applied to the tested parts or structures with the aim to get the mathematical description of their dynamic behaviour (Bilosova, 2011). The vibration of structures is difficult to predict and would be tough to avoid due to their flexible nature, which occurs when they are subjected to some forms of excitation. Excitation may, for example, take the form of aerodynamic loading, impact or rotational out of balance forces. The extent of vibration will depend not only on the type of excitation, but also on the properties of the structure. Although sometimes beneficial, vibration is usually unwanted and can be problematic, causing anything from terrible failure to general human discomfort. Mathematical models expressing the dynamic behaviour of structures are therefore obtained, so that the structural dynamic behaviour due to specific excitation patterns and structural modifications can be predicted.

Vibration testing in its simplest form consists of measuring the dynamic response of a structure under specific operating conditions. However, information concluded from such a test is of limited use. It is usual to determine the modal properties of the structure by means of a controlled excitation. Modal testing (Ewins, 1995) is the term used to describe the determination of a mathematical model of the dynamic behaviour of a structure from measured vibration test data. The extraction of modal properties from measured vibration test data is commonly referred to as modal analysis. The results usually take the form of frequencies, mode shapes and damping

ratios for each mode. However, results can equally be expressed in terms of modal mass, damping and stiffness matrices and mode shapes; such modal results are associated with a transformation from physical to modal space. Depending on the type of modal test performed, two distinct forms of modal parameters can be identified, namely, complex (damped) or real (undamped) modes. In general, these results are obtained from the so-called phase separation and phase resonance techniques (Niedbal, 1985). By performing a modal test, modal parameters of the system can be determined, thus having a base for solving many problems caused by structural vibrations (Bilosova, 2011).

A pure or normal mode is a characteristic free vibration shape of the undamped structure. In contrast, a complex mode involves vibration at the damped natural frequency, but all points do not move in mono-phase; nodal points do not remain stationary, but appear to move during the vibration cycle. Different points on the structure reach their maximum amplitude at differing instants in time. The mode shape is often referred to as complex where the magnitude and phase angles of the mode are presented in the form of complex plane or the Argand diagram. The complex mode corresponds to free vibration of the damped structure. Complex modes occur in experimental data because of actual damping may not be represented by proportional viscous damping. The mode shapes of the undamped model are also mode shapes of damped system when proportional viscous damping is considered.

A widely accepted approach for deriving a mathematical model to determine the dynamic properties of structures is the use of finite element (FE) analysis (Zienkiewicz and Taylor, 1994). Here the structure is essentially approximated by a series of masses and springs, with damping assumed in some approximate manners. The use of FE has many advantages since it does not require physical structural testing to be performed and allows the effects of structural modifications to be determined cost-effectively. However, FE has its limitations and many aspects of structures, such as damping and joints, cannot be adequately represented. Thus, experimental vibration testing is required if the mathematical model is to be

validated and, if necessary, updated. Based on modal updating of analytical and FE models using experimental data, it can be concluded that integration of modal analysis is in a total engineering approach (Maia and Silva, 1997).

### 2.4.1 Phase Separation Testing

Phase separation techniques are very flexible in their applications since the input could be FRF, response spectra or transmissibility function, which may have been obtained in vibration test (Ley et al., 2009). The phase separation test aims to excite all of the modes at the same time in the frequency range of interest using one or more exciters [(Stahle, 1962), (Allemang and Brown, 1986)]. The force input in this test can be random, transient, sinusoidal or chirp excitation provided by shakers. Then, a complex mode model is a derivation by curve fitting a mathematical model to the measured test data in the frequency or time domain. A popular method in the frequency domain technique is the Frequency Domain Direct Parameter Identification (FDPI) method (Lembregts et al., 1989). In addition, the multiple input Least Squares Complex Exponential (LSCE) or Poly reference method (Deblauwe et al., 1987) is also a popular time domain technique. The complex mode model is expressed in terms of damped natural frequencies, complex mode shapes and damping ratios. If the system is under the special condition of proportional damping, where the physical damping matrix can be expressed as a linear combination of the physical mass and/or stiffness matrices, the results of a phase separation test will give the complex mode shapes, which are related to the undamped (normal) mode shapes by a factor of proportionality, i.e. the normal modes may be extracted. However, under the more general case of non-proportional damping, the complex mode can be very different from the normal mode; there is no simple transformation between the complex and normal modes, thus making the phase separation results difficult to compare with those from FE analysis. In addition, the complex nature of the complex mode renders it, in general, difficult to interpret physically.

Frequently, as a general and simple approximation, the modal damping matrix is assumed to be proportional. Consistent with such an approximation, a diagonal modal damping matrix is defined in terms of a damping ratio per mode. Such a representation of the damping is referred to as modal damping. The concept of modal damping is invalid for non-proportionally damped systems because of the non-diagonal form of the modal damping matrix.

### 2.4.2 Phase Resonance Testing

Phase resonance testing is distinct from phase separation testing in that it aims to excite each undamped normal mode of the structure in turn using several exciters (Alexiou and Wright, 1993). This is achieved by the application of a pattern of multiple mono-phase sinusoidal forces at each undamped natural frequency; the pattern is chosen such that the so-called phase resonance condition is achieved when all response points move in mono-phase and in quadrature with the applied excitation. Thus, each normal mode shape may be measured directly. The mono-phase force pattern required to isolate the normal mode (also known as appropriated force vector) and the undamped natural frequency are obtained from one of the number of force appropriation methods (Hamilton, 1993), which may be iterative, but are usually based on an analysis of the measured FRF matrix (direct methods). Therefore, the advantage of such approach is that the resulting normal mode identified using phase resonance tests can be compared directly with the undamped normal modes resulting from an FE analysis. Then, correcting an FE model can be done to minimise the error between experimental and numerical results. Most of the force appropriation methods such as Asher, Traill-Nash, Multivariate Mode Indicator Function (MMIF), Juang and Wright method have been developed based on phase resonance testing.

### 2.4.3 Phase Separation versus Phase Resonance

Several key points were highlighted in general, comparing the phase separation and the phase resonance approaches (Cooper and Wright, 1997). One advantage of the phase resonance approaches is that the quality of the normal mode may be quantified since it can be evaluated against the phase resonance condition. Phase Separation approaches depend on stability plots to distinguish between structural and/or computational modes; however, the results cannot readily be quality assessed. In addition, the phase separation approach obtains a global estimate of the modal parameters by analysing all measurement data simultaneously. Therefore, the results are compromised for all measurement positions leading to the possibility of errors in the estimated complex mode shapes. The estimated modal parameters can also be affected by the presence of out of band modes, which are only roughly represented in the phase separation approaches by the so-called residual terms, which can introduce errors into the complex mode shapes. In contrast, in the phase resonance test, the structure will vibrate in the normal mode, which is measured directly so the structure acts as a filter and smooth mode shapes are obtained. When the damping is proportional, the complex mode derived from the phase separation approach is related to the real normal mode. However, when the damping is non-proportional, complex mode can be significantly different from normal mode; there is no simple transformation between the two. Also, the frequency resulting from the phase separation approaches is different from the frequency of the undamped system (Holmes et al., 1996), and the concept of modal damping becomes invalid.

Thus, phase resonance approaches have many advantages over phase separation approaches due to the quality of results which they produce. Nevertheless, the extra test time and the positioning of exciters associated with such an approach have to be considered. However, for non-proportionally damped structures, phase resonance approach is a more suitable choice because results are in the form where they can be quality assessed and compared with those from FE analysis.

The main difficulties with normal mode testing based phase resonance are the selection of excitation locations, the tuning of force pattern and the choice of excitation frequency (Maia and Silva, 1997). The complete process has to be repeated for each different mode and consequently, the testing time can be lengthy.

## 2.5 Finite Element Model Updating

Finite element (FE) models are widely used to predict dynamic characteristics of engineering structures. These models often give results that have discrepancy from test results and therefore, need to be updated to minimise error. Model updating is a part of verification and validation of numerical models. There are many techniques that have been proposed for this process by which finite element models of structures are adjusted by varying the parameters of numerical models to suit modal testing measured data. The simplest way to perform modal updating is simply by changing the values of some model parameters of FE model, running the normal mode analysis and comparing the updated results with the measured data. However, this type of manual FE model adjustment of parameters using trial- and-error process is tedious and there is no guarantee to get the right match. Trial and error approach is inefficient because a large amount of unnecessary repetitive processes is required for the correlation. Furthermore, this way highly depends on the individual's skills in order to minimise the error between FE model and modal test data.

Continuous improvement has been made on model updating in the last few decades in order to improve the correlation between numerical model of structures and test data through modal testing. Rodden (1967) is one of the pioneers who identified the structural influence coefficients through free-free ground vibration test to measure natural frequencies and mode shapes. Systematic approach of model updating via improvement of stiffness and mass parameter of FE model was performed by

Berman and Flannelly (1971). In their findings, the achievement was only via mass matrix, but not through stiffness matrix because it did not fit the true stiffness matrix.

By assuming that the mass matrix is correct, Baruch (1978) applied Lagrange multipliers to update the stiffness matrix by minimising the error between updated and analytical stiffness matrices. A similar approach was employed by Berman and Nagy (1983) to update the mass matrix of a large numerical model and also include updated stiffness matrix with two constraint equations. Further investigation by Wei (1980) and Ceasar (1986) used the same approach to see the possibility of this method to be used to affect structural changes.

Model updating based on optimisation has been developed in recent years. In order to minimise the defined objective function, this method permits a number of model parameters to be adjusted systematically. Kim and Park (2001) defined an objective function in model updating as a set of function involving the weighted sum of the differences between experimental and analytical results: often the natural frequencies, mode shapes and FRF. An optimization process or the set-up of objective functions and design variables is an important step in model updating. There are some papers that comprehensively discussed and demonstrated the results obtained from model updating using optimisation approach. Marwala (2010) developed the response surface method for FE model updating. The updated parameters of the FE model were calculated using genetic algorithm by optimising the surface response equation. Saada et al. (2013) improved a particle swarm optimisation algorithm to facilitate updating FE models in accordance with experimentally determined natural frequencies to predict the damage location. Multi objective optimisation technique was introduced by Kim and Park (2001) in model updating to optimise several objective terms simultaneously.

Model updating through iterative methods use sensitivity based methods in order to reduce the discrepancy between FE eigenvalues and eigenvectors with test data. Such iterative method leads to physically meaningful parameters if convergence is

achieved (Ceasar, 1987). Natke (1998), Imegrun and Visser (1991), Mottershead and Friswell (1993), Mottershead et al. (2010) presented mathematical approach and extensive surveys on model updating. In addition, Friswell and Mottershead (1995) wrote a comprehensive textbook on finite element model updating.

Damage identification using iterative model updating was presented by Fritzen et al. (1998); Abu Hussain et al. (2009a); Abu Hussain et al. (2009b) and Yunus et al. (2011). In structural engineering, model updating is often used for non-destructive damage assessment. By calibrating stiffness parameters of FE models based on experimentally obtained (modal) data, structural damage can be identified, quantified and located (Simoen et al., 2015).

Many researchers have studied FE model updating on structural joints in mechanical structures. Kim et al. (1989) and Arruda and Santos (1993) developed FE model updating using mechanical joints to identify stiffness and damping joint properties. Palmonella et al. (2003) modelled three different FE models of spot weld joints to improve the numerical data by optimising values of parameters of spot welds model. Mottershead et al. (2006) employed the model updating method to converge a set of identical physical structure welded with spot weld joints. Other works on model updating of joints such as bolts, fastener, welding were explored by Abu Hussain et al. (2010); Abdul Rani (2012); Yunus (2012) and Gant et al. (2013).

Stochastic model updating is a new trend in structural dynamic modification. Abu Hussain et al. (2012) observed how stochastic updating can be adequately performed using the perturbation method of structures with bolted joints. The authors also studied a set of welded structures using two parameters weighting matrix approaches. Appropriate weighting must be used in order to obtain excellent convergence between the predicted mean natural frequencies and their measured data. A three degree-of-freedom numerical model and a double-hat structure formed by a number of bolted joints were employed to illustrate the implementation of stochastic model updating and Monte Carlo method (Rui et al., 2013).

## 2.6 Sources of Nonlinearity

Generally, most structures exhibit some degrees of nonlinearity characteristics (Platten et al., 2002). A nonlinear system is able to demonstrate extremely complex behaviour which linear systems cannot. Furthermore, nonlinear dynamic analysis becomes very important for the diagnosis of faults in structures. In a recent review, Kerschen et al. (2006) stated that the five typical sources of nonlinearities in structural dynamics were as follows: geometric nonlinearity, inertia nonlinearity, material nonlinearity, damping dissipation and boundary conditions.

Any structure that has large deflections or angular motions would contribute to geometric nonlinearities. Amabili and Paidoussis (2003); Nayfeh and Pai (2004) mentioned that large elastic displacements and rotations in structures also introduce geometric nonlinearities, which arise from the potential energy of the system. Large deformations may cause nonlinear strain-displacement or curvature-displacement relations. A common example for this source of nonlinearity is a short and thin cantilever beam that tends to exhibit geometric nonlinearity when large deformations occur.

In an equation of motion, inertia nonlinearity can be derived based on nonlinear terms containing velocities and accelerations from the kinetic energy of the system. Inertia nonlinearity is derived from nonlinear terms containing velocities and/or accelerations in the equations of motion. Malatkar (2003) stated that nonlinear damping, which has a similar term, was different from nonlinear inertia and also mentioned that the kinetic energy of the system is the source of inertia nonlinearity. For example, the equations describing the motion of an elastic pendulum (a mass attached to a spring) and those describing the transverse motion of an extensional cantilever beam. Furthermore, nonlinear inertia in a beam can arise from longitudinal and rotary inertia forces (Atluri, 1973).

Material nonlinearity occurs when the constitutive law relating stresses and strains is nonlinear. Rubber is a common example for this source of nonlinearity. Richards and Singh (2001) used rubber as an isolator to mount a system. On the other hand, material nonlinearity also can be observed in foam structures (White et al., 2000). Kümmel et al. (1998) observed nonlinear material behaviour experimentally and considered the effect in an oscillator.

Damping dissipation is an essentially nonlinear and understood phenomenon (Kerschen et al., 2006). Hysteretic damping, aerodynamics drag and Coulomb friction are common examples of nonlinear damping. Nonlinear aerodynamic damping were found experimentally by Anderson et al. (1996), which was significant for large amplitude first-mode vibrations of slender excited beams. Shi and Atluri (1991) reported that slipping in nonlinear flexible connections occur in frame-type structures with hysteretic damping at the structural joints. Hysteretic damping modelling using Nonlinear Kelvin Voigt (NKV) model with stiffness and damping characteristics were developed by Bratosin and Sireteanu (2002). Ouyang et al. (2006) showed that damping in bolted joints is nonlinear, as shown in the hysteresis loop plot and the frequency spectra of the relative angular displacement of bolted joints.

Due to boundary conditions, nonlinearity can exist too. Loose joints, clearance, contact with rigid constraints and free surface in fluids are common examples for this source of nonlinearity. Agarwal and Gupta (1987) investigated the effect of boundary conditions on nonlinear phenomena in optical resonators. Turner (2004) studied nonlinear vibrations of a linear beam with cantilever-Hertizian contact boundary conditions. Findings from that study showed that an amplitude–frequency curve indicates nonlinear softening behaviour.

## 2.7 Nonlinear Identification Methods

In this section, nonlinear identification methods are discussed. Detection, localization and identification of nonlinearity are very significant in nonlinear structural dynamics area (Arslan, 2008). Kerschen (2002) observed that an identification process involved three stages: detection, characterisation and parameter estimation as shown in Figure 2.2.

Identification of nonlinear systems is an essential part of the verification and validation process. Roache (1998) showed that verification is a process where computations in mathematics are performed correctly. On the other hand, validation refers to formulating mathematical model and selecting coefficient to describe the systems.

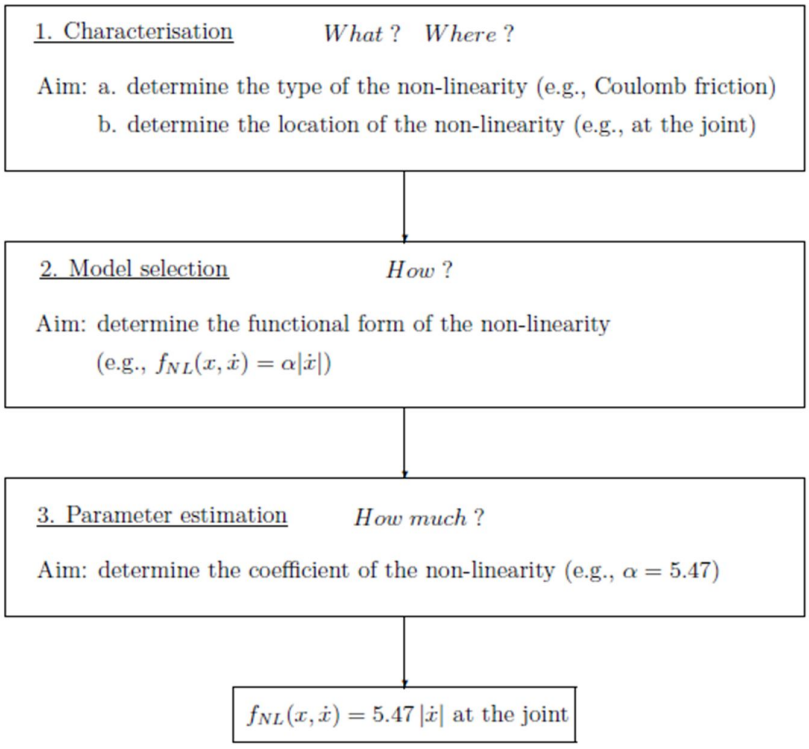


Figure 2.2: Identification Process (Kerschen, 2002)

There have been many studies on the use of system identification methods to identify structural nonlinearity, which include changes in natural frequencies, mode shapes and damping ratios. Kerschen et al., (2006) classified nonlinear identification methods into seven categories: bypassing nonlinearity, linearisation, time domain method, frequency domain method, modal methods, time-frequency analysis, black box modelling and structural model updating. The following is a brief description of the most popular techniques that have been carried out in the last thirty years.

Ibanez (1973) seemed to be a pioneer in nonlinear identification research area. Authors obtained dynamic properties such as damping, eigen-frequencies, mode shapes, and nonlinear effects from experimental data. Masri and Caughey (1979) introduced the restoring forces surface (RFS) to identify nonlinearity in single-degree of freedom (SDOF) systems by exploiting Newton's 2nd law to directly measure restoring and dissipative forces in the system. This technique expresses the nonlinear component of SDOF systems by measuring three different parameters; displacement ($y$), velocity ($\dot{y}$), and time ($t$). These parameters are plotted with 3D diagram with three axes; restoring forces (RF) versus displacement ($y$) versus velocity ($\dot{y}$). Chebyshev polynomials can be used to characterize the resulting surface. The shape of the diagram can reveal the type of nonlinearity such as cubic stiffness, bilinear stiffness, saturation, clearance or blacklash, Coulomb friction or nonlinear damping.

RFS was extended by Masri et al. (1982) to identify multi-degree of freedom (MDOF) systems by transforming the equations of motion from physical to modal coordinate space. The method can be used with deterministic or random excitation to identify dynamic systems with arbitrary nonlinearities, including those with hysteretic characteristics. Authors claimed that RFS is more efficient than the Weiner-kernel approach in identifying nonlinear dynamic systems of the types considered. The parametric identification method by force state mapping technique was developed by Crawley and Aubert (1986), which is similar to RFS. They carried out experiments to demonstrate the technique and the results showed strong

structural nonlinearities, which were cubic hardening spring, friction, and impact phenomena. In addition, Dimitriadis and Cooper (1998) attempted to identify MDOF systems using a variant of RFS method, which considers time response at similar amplitudes, and subsequently, constant nonlinear restoring forces could be achieved. This approach allows the identification of small systems with the least-squares method. Nevertheless, there is a limitation to large systems that requires the try-and-error method to detect the location of nonlinearity. Kerschen et al. (2001) applied RFS method for two different cases: a symmetrical nonlinear beam with piecewise linear stiffness and an asymmetrical nonlinear beam with bilinear stiffness. The polynomial model identifies a significant cubic stiffness with mean square error (MSE) of 1.70% and the non-polynomial model achieved an MSE of 1.80%. It shows that both models gave similar results. For bilinear stiffness, the authors concluded that reliable identification has been achieved with similar MSE and good fitting of restoring forces.

Simon and Tomlinson (1984) used the Hilbert transform (HT) method to identify linear and nonlinearity of structures in frequency domain. The HT approach has been shown to be a suitable tool to identify nonlinearity and it has the capacity to quantify nonlinearity, subject to the input excitation being sinusoidal. Tomlinson (1987) described the development in the use and application of HT for identifying and quantifying nonlinearity using simulated and experimental FRF. Calculation of HTs was carried out in the time domain employing the fast Fourier transform (FFT) procedures and new correction terms were proposed. Linearisation with HT and random excitation methods were applied to experimental data to reveal similar trends in the extracted modal parameters. Feldman (2012) developed an HT method for identification of mechanical time-varying vibration systems under free and forced vibration regimes. Three groups of dynamic time-varying SDOF systems are investigated in this research: This method is useful for modelling complex structure responses and is important when internal resonances are present between the modes. This approach is based on the HT of input/output signals in a time domain to extract

instantaneous dynamic structure characteristics such as natural frequencies, stiffness and damping.

Feldman (2007) proposed a new method for analysing and identifying nonlinear vibration of structures by considering the primary and higher harmonics of the solution. The method is based on two other HT methods: the method for extracting instantaneous frequency and Hilbert Vibration Decomposition (HVD) method that splits non-stationary wideband oscillating signal into separate components. Instantaneous modal parameters from nonlinear systems are oscillating functions due to divergences from a linear relationship between specific input and output of the system. These nonlinear distortions are characterised by the appearance in the output of a system of frequencies, which are linear combinations of the fundamental frequencies and all the high harmonics present in the signals. Furthermore, HVD considers the high super harmonics, which are more precise identification of nonlinear systems, including nonlinear elastic and damping force characteristics.

Reverse path (RP) method allows proper estimate of frequency response functions (FRF) and distributed nonlinearity coefficients. Bendat (1990) introduced the RP method and was followed by Rice and Fitzpatrick (1991) who used this method for MDOF systems. Nevertheless, this method requires external force to be applied at the location of nonlinearity.

In addition, reverse path spectral approach was studied by Richard and Singh (1998) for identifying nonlinear systems using Gaussian random excitation. They developed the technique for the underlying linear systems without contaminating effects from the nonlinearities. The authors estimated the conditioned FRF and identified nonlinearities by estimating the coefficients of analytical functions. This method was successfully simulated in several systems: a three-degree-of-freedom system with an asymmetric nonlinearity, a three-degree of freedom system with distributed nonlinearities and a five-degree-of-freedom system with multiple nonlinearities and multiple excitations. Marchesiello (2003) extended this method to conditioned

reverse path (CRP) to separate nonlinear part of the equation of motion from the linear part and construct the ranking of uncorrelated response part in the frequency domain. The author claimed that CRP was very straightforward to identify nonlinearity for MDOF system using random excitation. However, some refinement is needed to improve the discrimination performance and to reduce analyst interaction.

Lin et al. (1993) proposed an extension of the method to detect nonlinearity from analysis of complex modes. For SDOF systems, two complex nonlinear equations are built by considering two points of equal magnitude before and after resonance. They also considered MDOF systems and successfully solved a numerical case for a two-degree of freedom system. However, Siller (2004) tried a similar approach, but concluded that the method only applied to systems with friction damping or weak stiffness nonlinearity. He explained further that for strong cubic stiffness systems, it is impossible to locate a point of similar magnitude after resonance.

Slaats et al. (1995) put forward three mode types: tangent modes, modal derivatives and static modes for reducing nonlinear dynamical from finite element discretisation. Tangent modes are acquired from an eigenvalue analysis with a tangent stiffness matrix where modal derivatives (second order terms) with respect to modal coordinates containing the reduction information. However, integration of nonlinear dynamic system was reduced by a set of tangent modes, which would contribute to poor results of large displacement. Static modes can be obtained by an incremental Newton-Raphson iteration rule, which ignores the inertia terms. In this paper, positive influence on computational time was highlighted for nonlinear dynamic reduction technique by numerical examples.

Shaw and Pierre (1993) developed a systematic approach to identify only weak nonlinear and continuous systems using nonlinear normal modes (NNMs). This method conserves the physical nature of nonlinear mode shapes and modal dynamics parameter. By using asymptotic series expansions and transformation, the authors

demonstrated how an approximate nonlinear superposition could be employed to rebuild the overall motion from individual nonlinear modal dynamics. Subsequently, Boivin et al. (1995) introduced some modifications to this method, which allows performing a legitimate modal analysis from free response of nonlinear systems. They discovered some desirable properties for the modal analysis of linear system based on geometric approach. This methodology ignores the modelled modes invariant from non-modelled ones to reduce the set of equations. Pesheck et al. (2001) investigated the multimode invariant manifold method to generate reduced order models for MDOF nonlinear vibration systems. This method is useful for modelling complex structure responses and is important when internal resonances are present between the modes. Noël et al. (2016) developed a two-step methodology integrating system identification and numerical continuation for the experimental extraction of nonlinear modes under broadband forcing. Firstly, input and output were acquired to derive an experimental state space model of the structure. Then, the second step was to convert this state space model into a model in modal space whereby nonlinear normal modes were computed using shooting and pseudo-arc length continuation. The accuracy of the method was demonstrated numerically by considering noise perturbations. Gavassoni et al. (2015) investigated the nonlinear vibration of a two-degree-of-freedom conceptual model of an offshore compliant articulated tower using NNMs method. Buoyancy, added mass, ocean currents and wave effects are considered in the analysis. The elastic restoring forces were modeled, based on Augusti's model, using two orthogonal rotational springs. The invariant-manifold approach was applied to the equations of motion, and the resulting equations were solved through an asymptotic expansion. The derived nonlinear normal modes are then used to reduce the problem to a single degree-of-freedom nonlinear oscillator in each mode. The comparisons between numerical solutions and reduced order model confirm that nonlinear normal modes are a good alternative for the nonlinear analysis of an articulated tower and similar offshore structures.

An identification of weak nonlinearity of structure has been developed by Rice (1995) using the first order function of cubic stiffness nonlinearity. The author described an approach where underlying nonlinear differential equation governing the system is identified. This approach receives the input data in time domain with different levels of excitation and builds the variations of stiffness and damping ratios. A mounted commercial aircraft trim panel was tested to demonstrate this technique.

Soize and Le Fur (1997) presented an identification formula based on a stochastic linearization method with random coefficients. The model was defined as a multidimensional linear second-order dynamic system with random coefficients. Furthermore, an optimisation technique was developed to identify the parameters of the probability law of random coefficients. However, the authors concluded that this method could be improved by introducing some statistical dependence between the components of the random coefficients expressed in the modal coordinates in order to model the coupling of the eigenvectors induced by the weak nonlinearities.

Rosa et al. (1999) developed an optimization approach to estimate the modal parameters of nonlinear systems using goal programming. This method is performed in the frequency domain in order to minimise the total squared error between experimental and estimated values of nonlinear FRFs. Its main purpose was to obtain better accuracy than classical methods in complex cases: highly damped systems, systems of high modal density and noisy experimental data. The results from this goal programming were compared with those obtained from a classical estimation method, the orthogonal polynomials method. They found that this algorithm could produce high-accuracy results even when using poor initial estimates.

The force-state mapping technique for nonlinear systems was developed by Al-Hadid and Wright (1989). They simplified the identification procedure by Masri and Caughey (1979) in order to identify nonlinearity for SDOF and MDOF systems. In addition, the authors used a simple methodology, faster and more accurate for

identifying the type and location of discrete nonlinear elements in a lumped-parameter system.

McEwan et al. (2001) proposed a method for modelling large-deflection beams using a combined modal or finite element analysis of dynamic response. They developed a special code to construct static nonlinear test cases subjected to prescribed modal forces and resultant modal displacements. Then, regression analysis is applied in order to extract the nonlinear stiffness coefficients. The beam problem can then be solved for any force-time history in the reduced degree of freedom modal system. Singular value decomposition (SVD) is required for finding the pseudo-inverse of a rectangular matrix and solving systems that are suspected to be ill-conditioned.

Siller (2004) presented two methods: direct path and hybrid modal techniques (HMT) in order to identify nonlinearity from FRF as the input data. The direct path method is a technique to manipulate physical coefficients stored in system matrices. The author stated that optimisation of this method was validated against real measurement and it was found that the nonlinear characteristic was predicted with good accuracy. HMT is similar to a nonlinear superposition technique, in which the underlying linear system is expressed in generalized modal coordinates, while the nonlinearities are kept in the physical domain. The function of the hybrid coordinates is a significant feature to localize the nonlinearities of the system. The author also introduced fast approximation technique (FAT) to allow analytical derivation via newly developed expressions, which establish a link with other nonlinear methods and standard modal analysis techniques.

The auto regressive moving average with exogenous inputs (ARMA) model is one of the popular identification methods in time domain. Based on ARMA, Leontaritis and Billings (1985) proposed the nonlinear auto-regressive moving average with exogenous inputs (NARMAX) model. This model works on discrete time and is a nonlinear version of the discrete time ARMA model used in a number of linear methods. It allows the estimation of higher order FRFs by harmonic probing

(Billings et al., 1989). Basically, most of the works carried out using this model were based on single input/output data, and it looks most suited to relatively low order complex nonlinear systems. This model does not lend itself simply to acquire a significant physical parametric model and large order multi input-multi output (MIMO) systems that would lead to a massive number of terms. Nevertheless, Thouverez and Jezequel (1996) attempted to identify a modal space model using NARMAX by reducing the model order and catering for larger systems. Billings et al. (1989) applied orthogonal estimator in order to improve model selection and parameter estimation methods in NARMAX model. Genetic algorithms approach in NARMAX model was successfully developed by Chen et al. (2007).

Claeys et al. (2016) applied a nonlinear vibration simulation method to a test structure with friction joints. There were four main steps involved in this method: finite element modeling, model reduction, nonlinear simulation and comparison with experimental results. The simulated multi-harmonic response due to friction was in good agreement with measurement. The scanning laser vibrometer was used to measure nonlinear behaviour near the contacts in experiment. This study concluded that nonlinear simulation method was relevant in simulating the evolution of the frequency response due to friction in frequency shifts and energy dissipation.

Mareishi et al. (2014) investigated the nonlinear free vibration of piezoelectric laminated composite beams and the effects of the temperature rise and the volume fraction of the piezoelectric fibers on the nonlinear fundamental natural frequencies of the piezoelectric fiber reinforced composites. The authors found that the intermediate volume fraction did not have the intermediate critical temperature while in mechanical bifurcation analysis, the intermediate volume fraction was corresponding to the intermediate critical mechanical load. Another finding was that an increase in volume fraction of piezoelectric fibers, enhanced the bending stiffness of the laminated beam and led to a decrease in dimensionless static central deflection and an increase in fundamental natural frequencies of the hybrid laminated beams. Guo and Zhang (2016) analysed the nonlinear vibration behaviour of a reinforced

composite plate with the carbon nanotubes (CNT) under combined parametric and forcing excitations. The Galerkin procedure was used to determine a second order nonlinear ordinary differential equations, which included the square and cubic nonlinear terms, the parametric excitation and the forcing excitation terms. The results of numerical simulation showed the complex nonlinear vibration response in the CNT composite rectangular thin plate under combined parametric and forcing excitations.

## 2.8 Nonlinear Resonant Decay Method (NLRDM)

The nonlinear resonant decay method (NLRDM) deals with nonlinear dynamics system using a model based in linear space. This model comprises of the underlying linear system and extra terms that correspond to nonlinear behaviour. Wright et al. (2001) stated that nonlinear identification is very significant in structural dynamics and receives considerable attention in the literature with many different approaches. Nevertheless, the practical application of these methods to the modelling of vibration system is far less well developed. Experimental modal analysis for MDOF linear structures are moderately mature, but not for nonlinear structures.

There have been many studies to identify structural nonlinearities based on vibration data, but most methods are only suitable for a small number of degrees of freedom and less nonlinear terms. NLRDM attempts to address this issue as it is a technique to identify nonlinear systems with higher degree of freedom. Wright et al. (2001) was the first to propose NLRDM for weak nonlinear systems using a model based in modal space. This method is fundamentally based upon an expansion of the original restoring force surface approach in modal space by Masri et al. (1982) and takes advantage of the methodologies for normal mode force appropriation (Williams et al., 1986).

Basically, the resulting continuous time model is based in modal space. Platten et al. (2009a) proposed that the identification of nonlinearity could be performed in modal space using modal responses or in physical space using measured inputs and responses for parameter estimation. The main advantage of modal space models is less computing time where running in fewer degrees of freedoms than for the equivalent physical space model. In addition, the authors believed that most modes of the real structures behave linearly at the response levels of interest. However, for remaining modes which behave nonlinearly, some modes will be coupled to each other, and some will be independent. Most aircraft researchers (Wright et al., 2001; Gloth and Sinapius, 2004; Göge et al., 2005) focused on modal models due to a high level of complexity of aircraft structures and made the assumption that aircraft structures are mostly linear systems that contain some weak nonlinear modes. These modes behave linearly under small amplitudes of excitation. Therefore, a linear modal model is a good basis for a nonlinear model because it gives a good estimation of the true aircraft structure at low excitation levels.

NLRDM was the first approach to develop the application of appropriated excitation to nonlinear systems to limit the number of responding modes. According to Platten et al. (2009b), modes in NLRDM can be classified into three categories: (i) modes that behave linearly, (ii) modes that behave nonlinearly but are not nonlinearly coupled to other modes, and (iii) modes that are nonlinear and are nonlinearly coupled to other modes. They found that each mode from (ii) and (iii) could be identified using a relatively-low-order model in which a limited number of nonlinear modal terms can be used to identify any mode behaving as nonlinear.

Figure 2.3 shows the flow of the identification process using NLRDM for a large system (Platten et al., 2009a). Furthermore, the approach may be regarded as an addition to the standard ground vibration test where multiple exciters and normal mode tuning are involved.

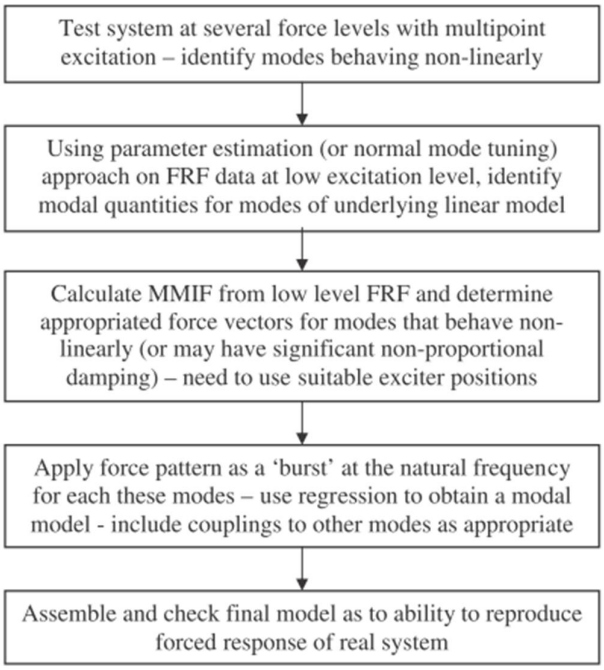


Figure 2.3: Flow diagram of identification process for high order systems (Platten et al., 2009a)

In the first step, the authors classified linear and nonlinear modes by carrying out a modal test with multi-exciters and random (or multi-sine) excitation was performed at several excitation levels to check on homogeneity. It is expected that some modal peaks would demonstrate nonlinear effects, whereas other modes would be largely unaffected by an increase in excitation level. The modes may then be classified largely as linear or nonlinear. Kragh (2010) stated that homogeneity is the simplest way to detect nonlinearities. Furthermore, homogeneity is best visualized in the frequency domain through the distortion of FRF's.

Secondly, the authors identified modal parameters underlying the linear system. An FRF matrix at a low excitation level was used to estimate the modal parameters for the so-called linear modes using a parameter estimation algorithm (e.g. least-squares complex exponential). On the other hand, the FRF matrix may be used to estimate the appropriated force vector for each mode of interest. By normal mode

tuning, the mode shape can be estimated either using 'soft tuning' (using FRF matrix) or 'hard tuning' (low level excitation on structure). This approach is slower, but it has to be used to gain an improved mode shape estimate for any close mode or any fitted mode shape that is not real, and may therefore, be non-proportionally damped. The aim of this stage is to establish a suitable modal matrix for transformation between physical and modal spaces. In addition, for any mode that behaves linearly in the homogeneity test and is proportionally damped, the estimated modal parameters may be used in the final model. Nevertheless, those parameters for modes that behave nonlinearly will need to be identified separately using NLRDM.

Thirdly, the authors applied a mode-by-mode excitation to test structures, and MMIF was then calculated from the low level FRF matrix and force vectors determined for each mode of interest (i.e. those affected by nonlinearity or non-proportional damping). Wright et al. (2001) believed that it is very important to choose suitable number and location of exciter positions. The appropriated force vector is applied as a burst sine excitation to each mode in turn, at a level big enough to excite any nonlinear behaviour present. If the modes are nonlinearly uncoupled, then the appropriated modes should dominate the response in the steady-state phase. If they are nonlinearly coupled, other modes may also exhibit a significant response. During the decay, the presence of linear damping couplings as well as nonlinear couplings between the modes will be noticeable.

Fourthly, the authors employed a mode-by-mode identification by suitable curve fitting to identify the linear and nonlinear modal parameters for each mode. Either the purely modal model or a combination of physical and modal models is selected for curve-fitting to appropriate a basis function that can represent the true nonlinearity in the system. Essentially, the burst appropriation excitation should allow a large model to be identified approximately mode by mode by curve-fitting a series of relatively small modal models.

Finally, the authors assembled modal equations and the final model was validated against suitable right input–output data obtained from the actual system. The procedure described above will not succeed when applied to a system undergoing limit cycle or chaotic oscillations. In the presence of limit cycle or any other self-excited oscillations, it will not be possible to obtain a decaying response from the system. Furthermore, if the system undergoes chaotic oscillations at particular amplitudes and frequencies of the excitation force, there will be several internal resonances that will most likely excite all modes, even the ones that are not nonlinearly coupled.

Sarmast and Wright (2010) investigated the residual effects when applying NLRDM identification. The authors are concerned with the inclusion of residual modes when applying NLRDM on multi degree of freedom. The lower residual region was observed to contain rigid body modes and would affect the result in the region of interest. The effect of the upper residual area in the modelling of the system within the range of interest was observed through several case studies. The authors concluded that measuring any rigid body mode is difficult because it needs to be setup at very low frequency and excitation is inaccurate.

## 2.9 Review of Shaker Excitation Signals

A brief review of shaker excitation signals is provided. A discussion on improved FRF estimation in case of MIMO sine sweep data can be found in (Gloth and Sinapius, 2004; Orlando et al., 2008). The level of excitation is very important to make sure that energy is distributed uniformly (Atkins and Worden, 1997). If the level is too low, nonlinearity will not be sufficiently excited. However, if the level is too high, the response will be dominated by the higher order terms and the lower order properties will not fit accurately. A review is now given on shaker excitation signals aiming to get improved FRF estimates.

• Pure random signal: Random excitation gives good coverage of phase plane. A pure random signal is typically generated in time domain by a random number. The bandwidth and spectrum can be shaped using digital filters. In frequency-domain, this signal has random amplitudes and random phases. Gatto et al. (2010) declared that this pure random signal provides a very good linear approximation in the presence of nonlinearities and is characterized by a good signal-to-noise-ratio (SNR). It is known that FRF data are strongly affected by leakage effect and the use of windows is necessary. By applying a Hanning window, FRF data tends to remove the non-periodic effect within the observation time, and hence removing the leakage effect. However, averaging is needed to cancel out non-coherent noise. Figure 2.4 shows an example of pure random signal.

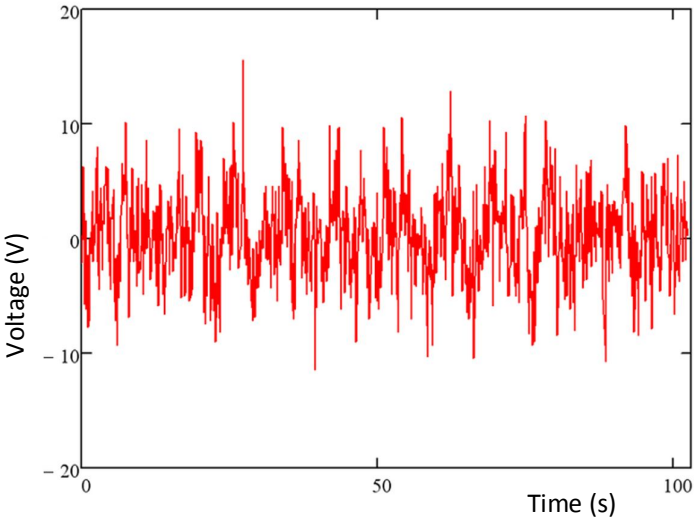


Figure 2.4: Pure Random Signal

• Burst random signal: This is a random signal that is only active for a user defined percentage of the acquisition block, and with no excitation during the remaining time. In the presence of nonlinearities, a very good linear approximation is obtained with burst random signal and no windowing is needed because leakage is minimized, provided that the response of the structure has died out in the observation

window. An example of burst random signal is shown in Figure 2.5. A small percentage of the time block is used to excite the structure effectively, so that the SNR of burst random is lower than in the random case.

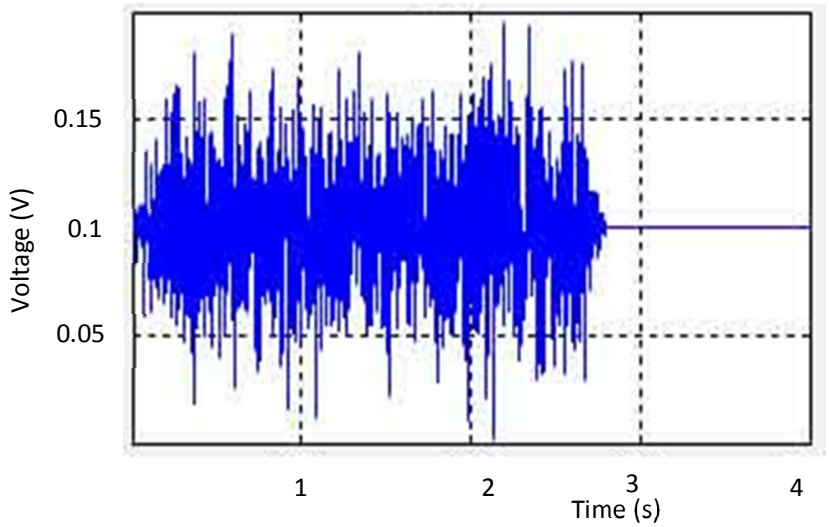


Figure 2.5: Burst Random Signal

• Sine sweep excitation or chirp signal: The sine sweep excitation signal excites the structure with sine signal - generated by an analogue signal generator - which varies the frequency slowly and continuously. Figure 2.6 shows an example of the excitation signal for a continuous sweep-sine measurement. This method has the best peak-to-root mean square (RMS) and SNR. This method is ideally suitable for characterising nonlinearity because higher excitation level can be applied. Meanwhile, it is extremely slow because the structure needs to be stabilized in the current excitation frequency in order to avoid frequency distortion. In the case of a lightly damped structure, a rather slow sweep rate should be applied.

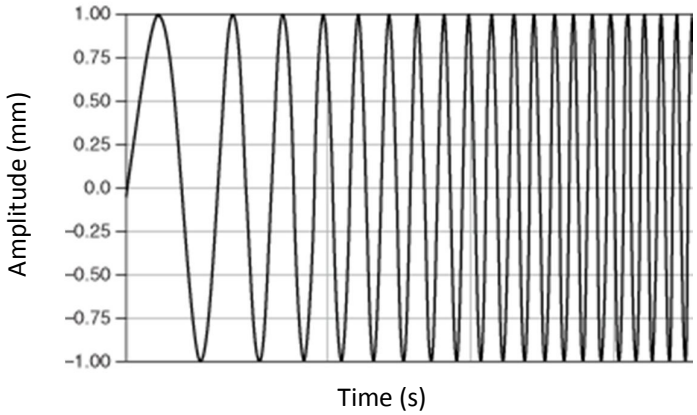


Figure 2.6: Sine Sweep Excitation (Source: National Instrument)

• Stepped sine excitation: The stepped sine excitation excites the structure at a stepwise frequency. The frequency, amplitude and phase are controlled in real time and result in long test time. Similarly to the sweep sine excitation, it provides the best peak-to-RMS and SNR. During the stepped sine measurement, the time of online correction of the signal is reduced. Besides, the wait periods and time can be defined with respect to the excitation frequency in order to avoid frequency distortion. Figure 2.7 shows an example of stepped sine excitation signal.

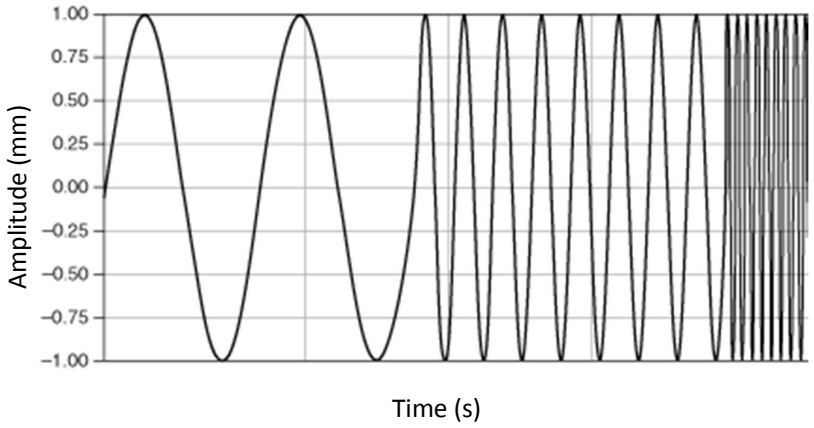


Figure 2.7: Stepped Sine Excitation (Source: National Instrument)

• Multi-sine: A source signal $u(t)$ that is the sum of multiple sine waves (Schoukens et.al, 2000), as shown in Figure 2.8:

$$u(t) = \sum_{k=1}^{N_s} A_k \cos(2\pi k f_o t + \emptyset_k) \quad (2.37)$$

where $N_s$ is the total number of sine components, $A_k$ and $\emptyset_k$ are the amplitude and phase of sine component $k$ and $f_o$ is the fundamental frequency. It is important that the sine components lie on a "Fourier grid" for discrete Fourier transform (DFT) processing, which produces a multi-sine periodic with respect to the observation period. All components can have arbitrary amplitudes and phases. A multi-sine signal is repeated at different times to allow the transient response to decay. The main advantage of using multi-sine as excitation signal is that the vibration phenomenon is periodic and it does not suffer from leakage when using DFT processing. Multi-sine makes it possible to reduce the measurement time, while maintaining good SNRs (Guillaume et.al, 2001).

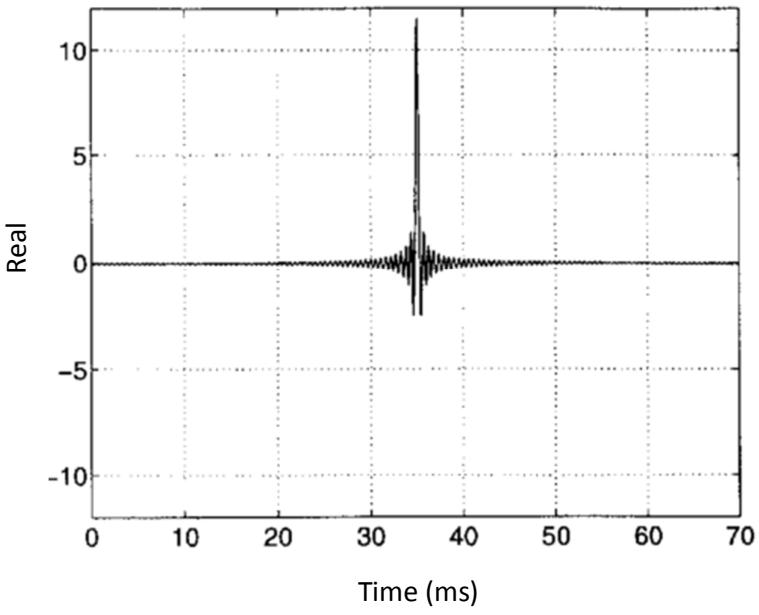


Figure 2.8: Zero-Phase Multi-Sine Excitation
with Crest Factor (CF) =16.00 (Guillaume et.al, 2001)

• Pseudo random signal: this is a special case of a multi-sine , with constant amplitudes of all components and phases randomly selected from a uniform distribution between –180° and 180° (Gatto et al., 2010). The time series of a pseudo random signal is obtained by applying inverse DFT to the generated frequency-domain representation of the signal. Transient effects are very light if one or more delay blocks (i.e. block during which the structure is excited, but actual acquisition only starts after repeating the same block a number of times) are used. FRF is not distorted by leakage or windowing and due to continuous excitation, the signal has high SNR. An example scheme of pseudo random excitation is shown in Figure 2.9.

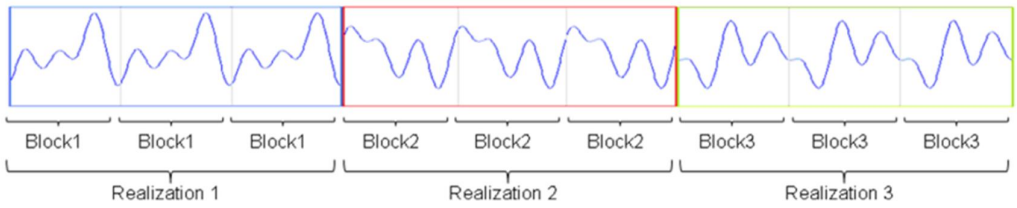


Figure 2.9: Example scheme of a pseudo random signal (the number of realizations is user defined as well as the number of blocks for each realization) (Gatto et al., 2010).

• Periodic random signal: this is another special case of a multi-sine, of which the frequency spectrum has random amplitude and random phase distribution. Historically, this signal is generated in the time domain and consists of a pure random time block which is sent out repeatedly. When the transient response has decayed, the input and response time histories become periodic and only frequency components at the spectral lines exist. Figure 2.10 shows the example of periodic random signal.

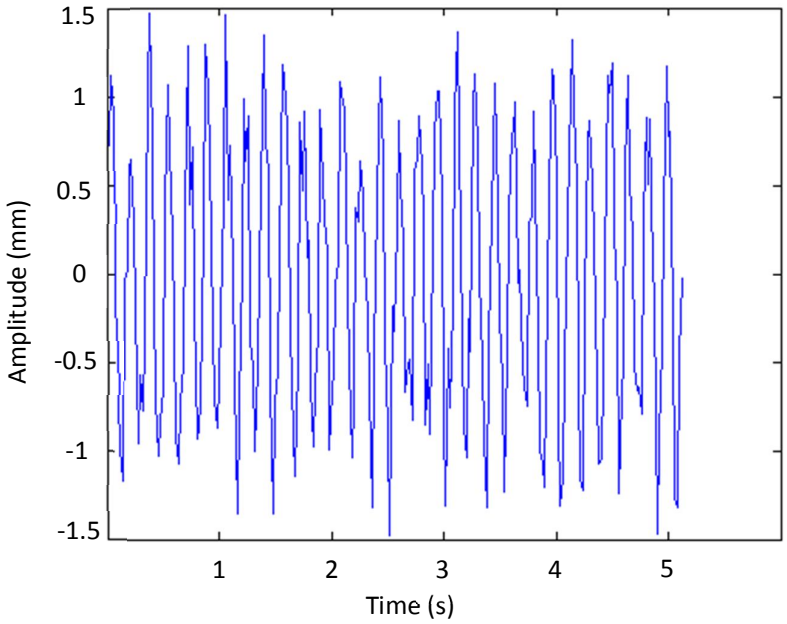


Figure 2.10: Periodic Random Signal

• Schröder multi-sine signal: For a broadband signal (such as a multi-sine), it can be important to have a low crest factor (ratio of peak amplitude to RMS value) to optimise the use of shaker/amplifier combination and to improve SNR (Guillaume et al., 2001). A pseudo random signal has a crest factor of 3-4. One particular method to decrease the crest factor is using Schröder phases (instead of random phases) of the different sine waves:

$$\emptyset_k = \emptyset_1 - \frac{\pi k(k-1)}{N_s} \tag{2.38}$$

This equation is valid for a multi-sine signal with constant amplitudes. Other more general methods exist for optimizing the crest factor such as the swapping method or more complex optimization methods (Guillaume et al., 1991). A Schröder multi-sine signal has the aspect of a sine sweep signal that sweeps through all frequencies within one acquisition block. No window is needed, but the structure is always excited in the same way and, therefore, stochastic nonlinearities are not

averaged. An example of Schröder Multi-Sine Excitation with Crest Factor (CF) =1.68 is shown in Figure 2.11.

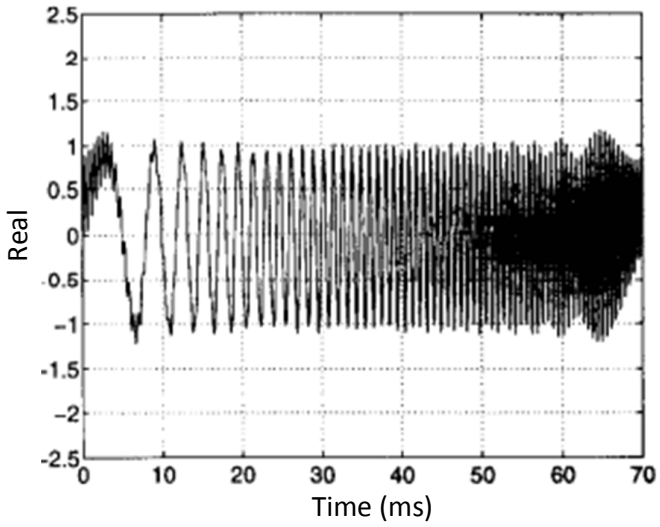


Figure 2.11: Schröder Multi-Sine Excitation
with Crest Factor (CF) =1.68 (Guillaume et.al, 2001)

Different excitation methods have different advantages and disadvantages. In order to obtain accurate results in a reasonable time, it is very important to use different excitation signals. Lau et al. (2011) concluded that burst random excitation provides the best compromise on broadband excitation, gives an indication of all the modes within the frequency range of interest in a very short time. However, it cannot characterize nonlinear behaviour. Sine excitation is very good for nonlinearity characterization. Sweep sine is less time consuming than stepped sine. For a lightly damped structure, the sweep rate influences the quality of the data and the test time. For more detailed nonlinear characterization, stepped sine is the most suitable. Normal mode testing depends on the shaker position, where the mode cannot be tuned for non-appropriate and insufficient number of shakers.

## 2.10 Summary

Since the last three decades, numerous methods have been developed for nonlinear vibration identification. At the beginning, most of these methods were targeted at SDOF systems, but significant progress in the identification of MDOF lumped parameter systems has been realized recently. Currently, most researchers deal with continuous structures with localized nonlinearity. It is reasonable to estimate all the model parameters for simple structures or approximate models of more complex structures.

However, resorting to multi-parameter complex structural models is crucial in order to analyze structures with a large number of DOFs and with a high modal density in a broad frequency range. This critical issue begins to be resolved by several recent approaches as follows:

a) Frequency domain approaches such as Hilbert Transform, CRP, nonlinear identification through feedback of the output (NIFO) – in principle, are capable of identifying the dynamics of large structures. In order to identify the nonlinear coefficients, these approaches are used an FRF-based model of the underlying linear structure directly from the experimental data, this facilitates the identification process.

b) The NLRDM proposes to classify the modes into different categories (i.e., influenced or not by nonlinear effects, coupled or uncoupled in damping nonlinearity), which enables the treatment of modes individually or in small groups. This method does not decrease the number of parameters to be estimated, but it simplifies the parameter estimation process by targeting a multi-stage identification.

c) Structural model updating techniques utilize the knowledge of the geometric and mechanical properties to determine an initial model of the structure,

many parameters of which are usually accurately computed and do not have to be identified from experimental data.

In this chapter, structural dynamics and nonlinear dynamics identification methods have been reviewed. This nonlinear approach is described in order to determine which modes are not nonlinear. This method is in the form of a combination of force appropriation method and restoring force method. The advantage of this approach is it identifies practical systems with a large number of modes and the modes are treated individually or in groups. Furthermore, this method allows a multi-stage identification of high order continuous systems. In this study, the combined force appropriation and restoring forces methods is applied to the experimental structure of a wing with two engine pylons of a rectangular wing with two stores suspended underneath.

# Chapter 3

# Theories of Force Appropriation and Restoring Forces Method

## 3.1 Introduction

In this chapter, the details on the theories of force appropriation and restoring forces methods are presented. The development of the force appropriation method including the Asher method, modified Asher method, Trail-Nash method, extended Asher method, multivariate mode indicator function (MMIF) and Juang-Wright method will be explained in next sub-chapter. Furthermore, the theory of the restoring forces method to identify nonlinearities of a system will be covered. Implementation types of excitation, integration of measured time data, and estimation of mass and modal matrices are explored.

## 3.2 Force Appropriation Theory

Consider $\mathbf{H}(\omega)$ as the ($r$ x $e$) measured frequency response function (FRF) matrix for a linear system, where $r$ is number of responses and $e$ is number of excitations or shakers. Then, the vector of response, $\mathbf{x}$ is ($r$ x 1) can be expressed as

$$\mathbf{x} = \mathbf{H}(\omega)\,\mathbf{f} \tag{3.1}$$

where $\mathbf{f}$ is the force vector ($e$ x 1) applied at excitation points. The FRF matrix for a system can be written as

$$\mathbf{H}(\omega) = \mathbf{A}(\omega) + \mathrm{i}\mathbf{B}(\omega) \tag{3.2}$$

where **A** and **B** are the real and imaginary parts. Thus, the response can be given as

$$\mathbf{x} = [\mathbf{A}(\omega) + i\mathbf{B}(\omega)]\mathbf{f} \tag{3.3}$$

In order to excite a normal or pure mode, the response in mono-phase and the excitation must be in quadrature (90° phase) with each other. In this condition, the real part of the response is zero, while the imaginary part corresponds to the undamped normal-mode shape, $\mathbf{\Phi}_k$. Therefore, for undamped normal mode:

$$\mathrm{Re}\,(\mathbf{x}) = \mathbf{A}\,\mathbf{f}_k = 0 \tag{3.4}$$

$$\mathrm{Im}\,(\mathbf{x}) = \mathbf{B}\,\mathbf{f}_k = \mathbf{\Phi}_k \tag{3.5}$$

where $\mathbf{f}_k$ is the appropriated force vector for mode *k*. A non-trivial solution of equation (3.4) occurs when determinant **A** is zero, which will occur at each undamped natural frequency. Solving $\mathbf{f}_k$ then will yield the appropriate force vectors. Taylor et.al (1967) stated that appropriated force vectors are determined iteratively by adjusting force amplitudes, phase and frequency until the phase resonance condition is satisfied.

According to Wright et al. (1999), the force vector derived for a corresponding normal mode will only excite that interested mode. The force vector of proportionality damped systems is derived from a modal force input to mode of interest and receives no contribution from other modes. However, for non-proportionally damped system, modal force contributions are included for any coupled modes in order to cancel unnecessary modal responses because of the modal cross-damping terms.

Wright et al. (1999) stated that the force appropriation method can be divided into three categories, namely square FRF matrices ($r = e$), rectangular FRF matrices ($r > e$) and combination rectangular FRF and rank reduction technique.

### 3.2.1 Square FRF Matrix Methods

Hamilton (1993) carried out a review of the Asher method, modified Asher method and Traill-Nash method operated on square FRF matrices measured at coincident excitation and response measurement points. These methods tend to be limited in their use to relatively simple structures, as the phase resonance condition is only sought at the excitation points.

Asher (1958) put forward a method to solve natural frequencies from the determinant of $A$ and then solve equation (3.5) directly using adjoint of $\mathbf{A}$. However, according to Alexiou and Wright (1993), this Asher formulation is sensitive and not ideal as the force vector, $\mathbf{f}_k$ would appear to be trivial if $\mathbf{A}(\omega)$ is not perfectly singular. Hence, an eigenvalue solution is a better option. The modified Asher method solves

$$\mathbf{A}\,\mathbf{f} = \lambda\,\mathbf{f} \tag{3.6}$$

This approach is possible since the determinant $\mathbf{A}(\omega)$ is in fact the product of eigenvalues of $\mathbf{A}(\omega)$, so then the determinant of $\mathbf{A}(\omega) = 0$, one or more of the eigenvalues are zero. Nash (1961) used the Traill-Nash method as an alternative approach to solve general eigenvalues of the form

$$\mathbf{A}\,\mathbf{f} = \lambda\,\mathbf{B}\,\mathbf{f} \tag{3.7}$$

Undamped natural frequencies would be identified at zero crossings of eigenvalues λ. Note that eigenvalues λ behave differently for each of the method discussed. The related eigenvectors give the appropriation force vectors for each mode of interest.

Alexiou (1990) concluded that the modified Asher method has the added benefit of providing a good approximation of $n^*$ (effective degree of freedom). The presence of missing modes, which occurs when $e < n^*$, can be identified through the significant fluctuations of $\lambda_k$ between crossings of the frequency axis. Similarly rank deficiency (i.e. $e > n^*$ if) is identified by $(e - n^*)$ zero or near zero eigenvalues; while non-zero eigenvalues can yield sensible results. When $e = n^*$, each eigenvalue crosses the frequency axis only once in the vicinity of a mode. However, rapidly changing eigenvalues and eigenvectors are sometimes obtained with this method, and this means that the author has encountered problems in implementing it because of inadequate resolution.

Alexiou (1990) also successfully applied the Traill-Nash method, but faced difficulties in interpolating eigenvalues curve due to measurement noise in FRF data. He concluded that the same limitations apply to the Asher and Modified Asher methods. In principle, if the number of exciters used is greater than $n^*$, the eigenvalue problem should break down because both $\mathbf{A}(\omega)$ and $\mathbf{B}(\omega)$ are singular. However, since $n^*$ is an imprecise value in practice, the quality of the result will simply deteriorate as $e$ increases.

### 3.2.2 Rectangular FRF Matrix Methods

In the case of rectangular FRF matrices, where the number of response points is more than the number of excitation points ($r > e$), an exact solution is not obtainable. In practice, the real part of the response can be minimised across all of the response

measurements with different specific cost functions for each method. Juang and Wright (1991) stated that this method uses eigen-properties, but has different expressions. Ibanez (1976) used the extended Asher method to minimise the sum of squares of the real part of the response with respect to the force vector, leading to the eigenvalue problem in equation (3.8).

$$\mathbf{A}^T\mathbf{A}\,\mathbf{f} = \lambda\,\mathbf{f} \tag{3.8}$$

In this formulation, it is defined that the eigenvalues $\lambda$ drop to zero at undamped natural frequencies. In addition, zero eigenvalues will only be produced if a quadrature response is recognized on all *r* responses simultaneously. Instead, minima in the Extended Asher eigenvalue trace should be sought.

The MMIF method was developed by Williams et al. (1986) which minimises the real part of the response compared to the total response. The cost function, $\lambda$ can be expressed as

$$\lambda = \frac{\left\|\mathbf{x}^{\mathrm{Re}}\right\|^2}{\left\|\mathbf{x}^{\mathrm{Re}} + \mathbf{x}^{\mathrm{Im}}\right\|^2} \tag{3.9}$$

where subscripts Re and Im refer to the real and imaginary parts of complex structural response vector, respectively. The norm of the real part of the response, $\|\mathbf{x}^{\mathrm{Re}}\|$ is defined as

$$\|\mathbf{x}^{\mathrm{Re}}\|^2 = [\mathbf{x}^{\mathrm{Re}}]^{\mathbf{T}}\,\mathbf{W}\,\mathbf{x}^{\mathrm{Re}} \tag{3.10}$$

where $\mathbf{W}$ is a weighting matrix. The authors used weighting matrix as the mass matrix such that the norm is proportional to the kinetic energy of the in-phase (real) part of the response. In this condition, the above cost function is based on minimising the kinetic energy of the in-phase response to the total response. Generally, an estimate of the mass matrix is not known and so, the weighting matrix

is usually taken as the identity matrix. The norm of the total response can be expressed as

$$\|\mathbf{x}^{\mathrm{Re}} + \mathrm{i}\mathbf{x}^{\mathrm{Im}}\|^2 = [\mathbf{x}^{\mathrm{Re}}]^{\mathbf{T}}\,\mathbf{W}\,\mathbf{x}^{\mathrm{Re}} + [\mathbf{x}^{\mathrm{Im}}]^{\mathbf{T}}\,\mathbf{W}\,\mathbf{x}^{\mathrm{Im}} \tag{3.11}$$

Referring to equation (3.3), the response may also be defined as a function of the real and the imaginary parts of the FRF matrix as

$$\mathbf{x} = [\mathbf{A}(\omega) + \mathrm{i}\mathbf{B}(\omega)]\mathbf{f} = \mathbf{x}^{\mathrm{Re}} + \mathrm{i}\mathbf{x}^{\mathrm{Im}} \tag{3.12}$$

where the subscripts have been dropped for clarity as has the dependency on frequency. Hence, substituting equations (3.10), (3.11) and (3.12) into equation (3.9) using an identity weighting matrix gives

$$\lambda = \frac{\mathbf{f}^{\mathrm{T}}[\mathbf{A}(\omega)]^{\mathrm{T}}\mathbf{W}\,[\mathbf{A}(\omega)]\mathbf{f}}{\mathbf{f}^{\mathrm{T}}[\mathbf{A}(\omega)]^{\mathrm{T}}\mathbf{W}\,[\mathbf{A}(\omega)]\mathbf{f} + \mathbf{f}^{\mathrm{T}}[\mathbf{B}(\omega)]^{\mathrm{T}}\mathbf{W}\,[\mathbf{B}(\omega)]\mathbf{f}} \tag{3.13}$$

Then, equation (3.13) is differentiated with respect to $\mathbf{f}$ and set as zero to correspond to a minimum, yielding

$$\mathbf{A}^{\mathrm{T}}\mathbf{A}\,\mathbf{f} = \lambda(\mathbf{A}^{\mathrm{T}}\mathbf{A} + \mathbf{B}^{\mathrm{T}}\mathbf{B})\,\mathbf{f} \tag{3.14}$$

The above equation is in the standard eigenvalue problem form, whereby eigen solutions for each frequency point resulting in $e$ eigenvalues $\lambda_j$ and corresponding eigenvectors, $\mathbf{f}_j$ .

An estimated mass matrix or potentially a weighting matrix may also be included in MMIF formulation. Minima of eigenvalues $\lambda$ can be identified through undamped natural frequencies.

Williams et al. (1986) also applied MMIF on three physical structures; a circular plate, a car body- in-white and an aerospace type structure. The circular plate was tested in order to evaluate MMIF on a structure with coincident modes. MMIF successfully identified the natural frequencies of three pairs of coincident modes. Unfortunately, the multiple input FRF matrices were constructed from single input impact tests (assuming reciprocity), and therefore, the corresponding appropriated force vectors were not applied in order to isolate any of the mode. FRF matrices for the car body-in-white were obtained from two simultaneous exciter inputs. Although no close or coincident mode was present, MMIF was used to identify the natural frequencies of a structure with a high modal density. Finally, MMIF was evaluated on FRF data obtained from an aerospace type structure.

Rades (1992) evaluated various types of mode indicator functions on theoretical FRF matrices. Discussions were limited to the identification of close modes and the method's ability to indicate the presence of localised modes produced by weak coupling effects. The determination and subsequent application of the appropriated force vectors were not discussed. Rades' conclusions for the MMIF were favourable.

Brillhart et al. (1992) conducted a multiple input ground vibration test (GVT) on a C-17 transport aircraft. Excitation was provided by eight simultaneous exciter inputs, four of which were attached to the airframe and one to each of the four engines. FRF matrices were constructed using both burst random and stepped sine excitation. Singularity of FRF matrices was not considered to be a problem as four of the exciters were employed to excite only the engine modes. MMIF proved successful in identifying all modes in the chosen frequency band. No noticeable difference between stepped sine or burst random excitation was reported. The authors successfully tuned several undamped normal modes. In these methods, resonances occur at minima of the eigenvalues and the corresponding eigenvectors yield the appropriated force distributions. The rectangular FRF

matrix approaches permit the phase resonance condition to be sought approximately at many points on the test structure and are not limited to coincident exciter and response positions. A significant advantage of this method is that when excitation point, $e$ is equal to effective degree of freedom, $n^*$, the appropriate force vector for each of two close modes can be obtained from the same eigenvalues solution. Nevertheless, Nash (1991) found out that when the number of exciters exceeds the number of effective degree of freedom, these methods will tend to fail due to rank deficiency of the FRF matrices.

### 3.2.3 Rectangular FRF Matrix Methods with Rank Reductions

The force appropriation methods described in the previous sections are relatively simple to implement, provided that the number of exciters to excite the structure does not exceed the effective number of degree of freedom $n^*$ of the system. The problem then arises in choosing the number of exciters needed to isolate a normal mode, which is a difficult task since it is not normally known before the structure is tested. If an insufficient number of exciters is used, it might not be possible to excite a normal mode, whilst an excess number of exciters may cause the methods described previously to degrade due to ill-conditioning of FRF matrices.

Two methods, namely the Juang-Wright (Juang and Wright,1991) and the modified MMIF (Nash,1991) methods were developed for rectangular FRF matrix with rank reduction. Unlike the force appropriation methods discussed in sections 3.2.1 and 3.2.2, these methods overcome the problems associated with ill-conditioned FRF matrices. Both the Juang-Wright and modified MMIF methods include the rank reduction feature, which yield appropriated force vectors from ill-conditioned FRF matrices, allowing the full set of exciters to be used.

A multipoint force appropriation method based upon Singular Value Decomposition (SVD) was developed by Juang and Wright (1991). The method aims to minimise the real part of the response vector via the function,

$$J_1 = f^T [A(\omega)^T A(\omega)]\{f\} \tag{3.15}$$

while the quadrature part is maximised via the function:

$$J_2 = f^T [B(\omega)^T B(\omega)]\{f\} \tag{3.16}$$

according to a fixed norm for the force vector (i.e. $|f| = 1$). Note that the norm ensures that the optimum force vector occurs at the relevant undamped natural frequency. At each frequency, the real part of the FRF matrix can be decomposed into a diagonal matrix of singular values [$D$], and matrices of left- and right-hand singular vectors [$P$] and [$Q$] are respectively,

$$[A(\omega)] = [P_a \quad P_o] \begin{bmatrix} D_a & 0 \\ 0 & D_o \end{bmatrix} \begin{bmatrix} Q_a{}^T \\ Q_o{}^T \end{bmatrix} \tag{3.17}$$

Ideally, if [$A$ ($\omega$)] is of dimension ($m$*$e$) but of rank $r$, then the decomposition may be partitioned as above into $r$ non-zero (or significant) singular values [$D_a$] and $q$ = ($e$ - $r$) zero (or small) singular values [$D_o$], with the corresponding singular vectors (note that the singular values ($d$) of the [D] matrix are written in descending order of magnitude) so that ($d_1 \geq d_2 \geq d_3 \ldots \geq d_e$). Thus the decomposition of [$A$ ($\omega$)] into its singular values can provide an estimate of rank, and hence the effective number of modes by comparing significant singular values to insignificant ones. That is to say that at each natural frequency, the effective rank is;

$$r = n^* - 1 \tag{3.18}$$

because [$A$ ($\omega$)] decreases the rank by 1 at each natural frequency. But elsewhere away from each natural frequency,

$$r = n^* \tag{3.19}$$

Using equations (3.4) and (3.17), it is possible to show the real component as below:

$$z_r = [P_a D_a Q_a{}^T + P_o D_o Q_o{}^T] \tag{3.20}$$

In order for $J_1$ to be a minimum, then $z_r$ must be small. Thus, $f$ must be chosen as some combinations of the singular vectors corresponding to the null space (i.e. the insignificant singular values) in order to eliminate the first term in equation (3.20). Then,

$$f = [Q_o]c \tag{3.21}$$

where $c$ is a ($q$ * 1) vector which needs to be determined in order to maximise $J_2$ . As the singular vectors are orthonormal (i.e. $[Q_a]^T[Q_o] = [0]$, $[Q_o]^T[Q_o] = [I]$), it is possible to show from equations (3.20) and (3.21) that the in-phase component of the complex response is small and given by,

$$z_r = [P_o][D_o]\, c \tag{3.22}$$

Thus $J_1$ becomes

$$J_1 = c^T[D_o]^2\, c \tag{3.23}$$

where $c^T = (c_1\, c_2\, c_3\, c_4 \ldots\ldots\, c_q)$ and $[D_o]$ = Diagonal $[(d_{o1}\ d_{o2}\ \ldots.\ d_{oq})]$. In order for $|f| = 1$, the constraints and $|\ Q_o\ | = 1$ are imposed. Note that $J_1$ will always be small since $[D_o]$ is taken from the insignificant singular values.

Now $c$ needs to be chosen to maximise $J_2$. Consider the imaginary component of the response is,

$$z_i = [B(\omega)]\, f \tag{3.24}$$

and substitute equation (41) into the above equation,

$$z_i = [B]\,[Q_o]c \tag{3.25}$$

if matrix $[BQ_o]_{m*q}$ is decomposed into its singular values, then

$$[BQ_o] = [U][[S][V]^T = [u_1 \quad u_2 \quad \dots \quad u_q] \begin{bmatrix} s_1 & 0 & \dots & 0 \\ 0 & s_2 & \dots & 0 \\ 0 & 0 & \dots & 0 \\ 0 & 0 & \dots & s_q \end{bmatrix} \begin{bmatrix} v_1^T \\ v_2^T \\ \dots \\ v_q^T \end{bmatrix} \tag{3.26}$$

where $[U]$ and $[V]$ are the matrices of left and right singular vectors, respectively and $[S]$ is the diagonal matrix of singular values. If $c$ is chosen to be a linear combination of the right hand singular vectors of $[BQ_o]$ then,

$$c = [V]g \tag{3.27}$$

and

$$z_i = [BQ_o]c = [U][S]\mathrm{g} \tag{3.28}$$

which leads to

$$J_2 = g^T[S]^2\, g \tag{3.29}$$

Thus, cost function $J_2$ will be maximised if $g^T = [1\ 0\ \ldots.\ 0]$ because $s_1 \geq s_2 \geq \ldots \geq s_q$ and $c$ can be found using equation (3.27). It can be shown from equations (3.21) and (3.28) that the appropriated force vector can be expressed as,

$$f = [Q_o]v_1 \tag{3.30}$$

## 3.3 Modal Purity Indicator (MPI)

Cooper et al. (1995) used the modal purity indicator (MPI) for evaluating the degree to which a normal mode has been appropriated numerically. A similar concept was proposed by Wright et al. (1999) and Desforges et al. (2004) to judge the quality of a tuned normal mode by calculating the normal mode purity. If $Y(x)$ is the response of a system at the $x$th measurement position, then MPI is defined as:

$$\text{MPI} = 1 - \frac{\sum_1^{no} |Y_R(x)||Y(x)|}{\sum_1^{no} |Y(x)|^2} \tag{3.31}$$

where $Y_R(x)$ is the real part of response $Y(x)$ and the excitation of the system is purely real. If MPI is equal to 1, it indicates a perfect appropriated normal mode such that all points on the mode shape will be in quadrature. Naylor (1998) stated that MPI $\geq$ 0.9 is considered as good, MPI $\geq$ 0.95 is very good and MPI $\geq$ 0.99 is excellent.

## 3.4 Force Appropriation and MMIF for Two Degree of Freedom System.

The force appropriation and MMIF method were applied on a simulated two degree of freedom system as shown in Figure 3.1, with the following properties:

$$m_1 = 2\ \text{kg};\ m_2 = 1\ \text{kg}\ ; k_1 = 2000\ \frac{\text{N}}{\text{m}}, k_2 = 1000\frac{\text{N}}{\text{m}} = \ ;\ c_1 = 2\frac{\text{Ns}}{\text{m}}\ ; c_1 = 1\frac{\text{Ns}}{\text{m}}$$

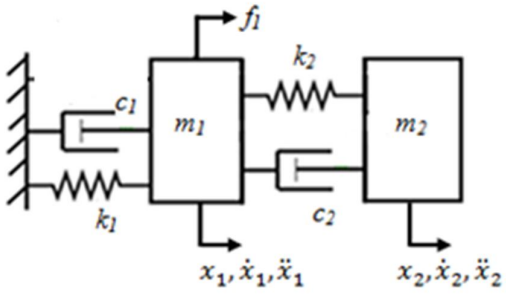


Figure 3.1: A Two Degree of Freedom System

Matlab coding for force appropriation was developed to run eigenvalues problem of two degrees of freedom with different frequency steps. Table 3.1 shows the force appropriation and MMIF result for two degree of freedom. A forward analysis for the normal mode test of this system gave the natural frequency for mode 1 as 22.3607 rad/s (3.5588 Hz) and mode 2 as 44.7214 rad/s (7.117 Hz). A higher frequency step (0.1 rad/s) provides a satisfactory result for natural frequencies and mode shapes, but not for force vector and minimum eigenvalue. Force vector for 0.1 rad/s frequency step is not accurate compare with 0.01 and 0.001 frequency steps. Minimum eigenvalue for 0.01 and 0.001 rad/s frequency steps are near zero compare with 0.1 rad/s frequency step. A smaller frequency step (0.001 rad/s) gives more accurate results for natural frequencies, mode shapes and force vector, but has longer

computational time. The target of this method is to determine the monophase force vector, $f_1$ and $f_2$ when applied at undamped natural frequencies and excite the corresponding undamped pure mode. Modal assurance criteria (MAC) and modal purity indicator (MPI) shows good correlation between each other. The function of the modal assurance criterion (MAC) is to provide a measure of consistency (degree of linearity) between estimates of a modal vector, which provides an additional confidence factor in the evaluation of a modal vector from different excitation (reference) locations or different modal parameter estimation algorithms. Perfect purity (MPI=1) of the mode shape is obtained when two degree of freedoms are applied at effective natural frequencies.

Table 3.1: Force Appropriation and MMIF Result for a system of Two Degree of Freedom

| | Frequency Step (rad/s) | | | | | |
|---|---|---|---|---|---|---|
| | 0.1 | | 0.01 | | 0.001 | |
| | Mode 1 | Mode 2 | Mode 1 | Mode 2 | Mode 1 | Mode 2 |
| Frequencies, ω (Hz) | 3.5651 | 7.1142 | 3.5587 | 7.1174 | 3.5589 | 7.1176 |
| Minimum Eigenvalue | 0.0217 | 0.0004 | $6.65\text{x}10^{-6}$ | $1.66\text{x}10^{-6}$ | $1.48\text{x}10^{-6}$ | $1.16\text{x}10^{-7}$ |
| $f_1$(N) | 94.95 | -117.33 | -11.90 | -125.89 | -8.53 | -126.42 |
| $f_2$(N) | -62.70 | 72.35 | -9.05 | 63.84 | -10.74 | 63.31 |
| Computational Time (s) | 0.355 | 0.348 | 0.710 | 0.700 | 36.18 | 36.41 |
| MAC | 1 | | 1 | | 1 | |
| MPI | 1 | | 1 | | 1 | |

Figure 3.2 and 3.3 shows the FRF graph and result for this system of two degree of freedom. This FRF has been divided into four divisions: H11, H12, H21 and H22. Furthermore, Figures 3.4 to 3.6 shows the MMIF graphs of eigenvalues, λ versus frequency, ω for different frequency steps.

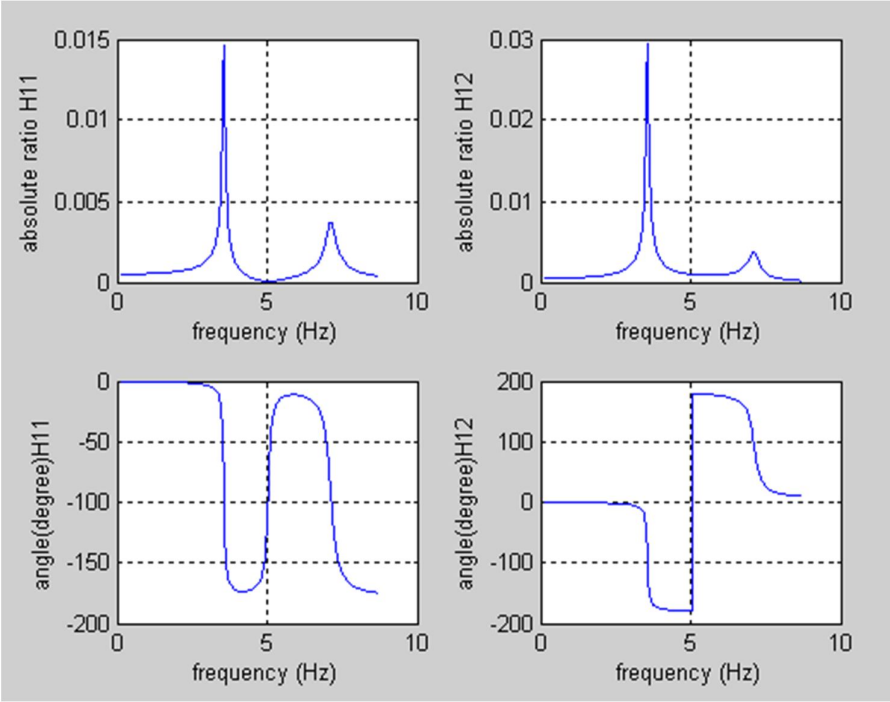


Figure 3.2: FRF result (H11 and H12) of a two degree of freedom system

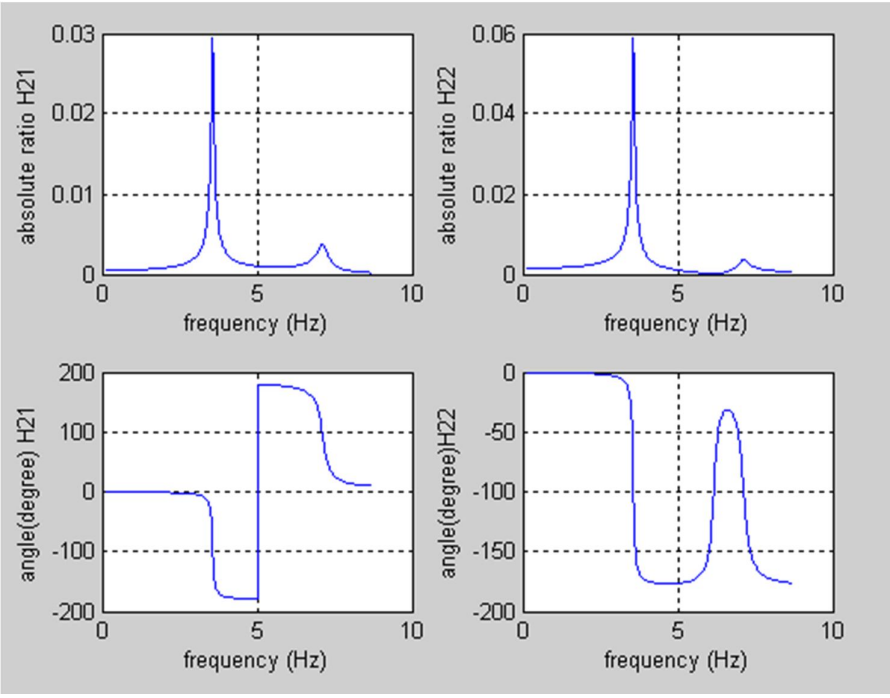


Figure 3.3: FRF result (H21 and H22) of a two degree of freedom system

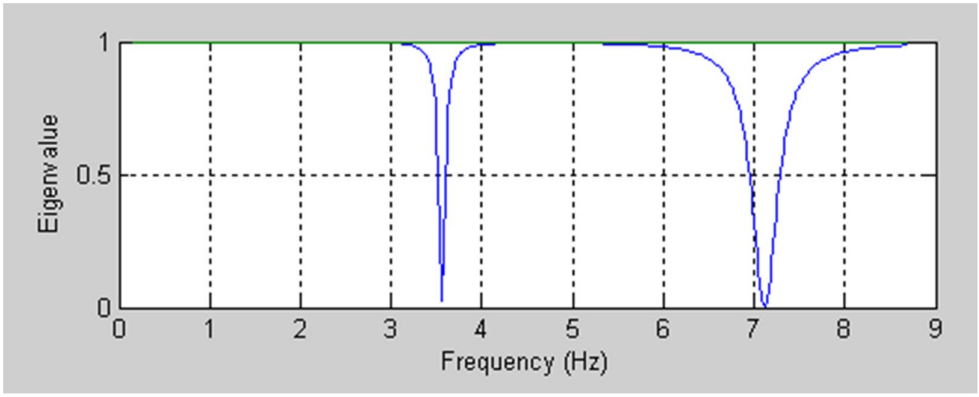


Figure 3.4: MMIF: Eigenvalue, λ versus Frequency, ω (0.1 rad/s frequency step)

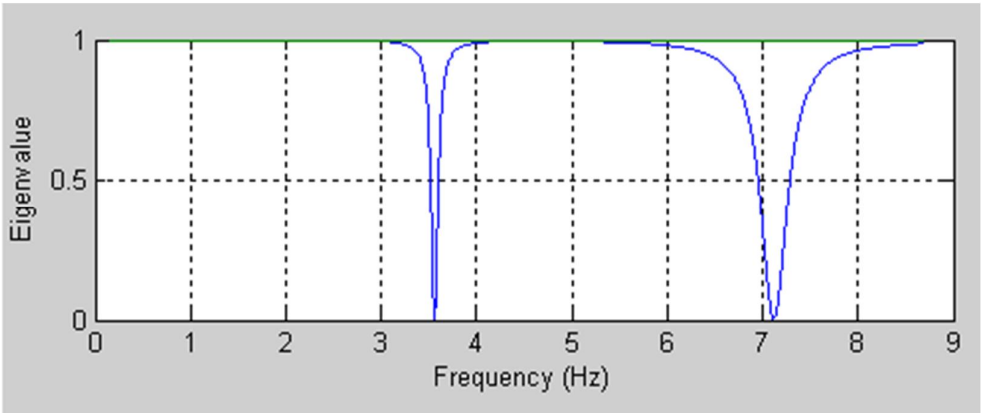


Figure 3.5: MMIF: Eigenvalue, λ versus Frequency, ω (0.01 rad/s frequency step)

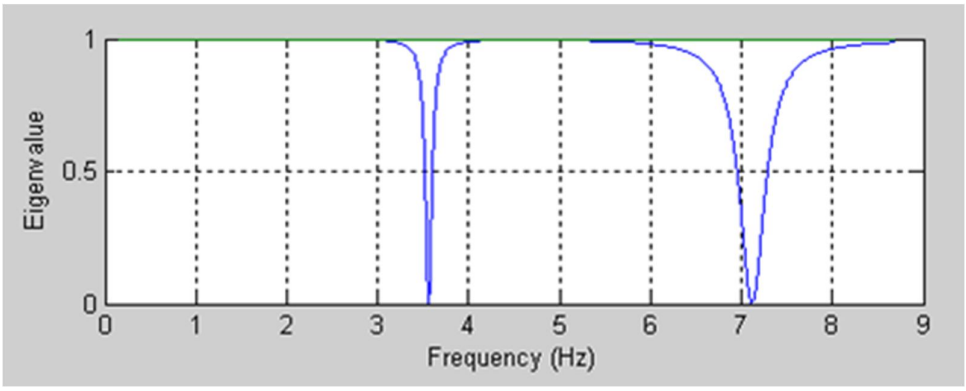


Figure 3.6: MMIF: Eigenvalue, λ versus Frequency, ω (0.001 rad/s frequency step)

## 3.5 Restoring Force Method

The equation of motion for SDOF system, can be written as

$$m\ddot{x} + g(\dot{x}, x) = f(t) \tag{3.32}$$

where $m$ is the mass, $\ddot{x}$ is the acceleration, $f(t)$ is any applied force and $g(\dot{x}, x)$ is the restoring force, which is a function of velocity, $\dot{x}$ and displacement, $x$. Equation (3.32) can be rewritten for the restoring force as follows:

$$g(\dot{x}, x) = f(t) - m\ddot{x} \tag{3.33}$$

The restoring force surface method offers an efficient and reliable identification of nonlinear SDOF (Platten et al., 2002). (Masri et al., 1979) described how the restoring force method could be extended to multi-degree of freedom (MDOF) systems. Equations of motion can be transformed from physical coordinates to modal coordinates by means of modal matrix of the linear part of the system. Velocity and displacement can be obtained through integration of acceleration or separate measurements and then curve fitting to form the restoring force surface (Kerschen et al., 2006).

## 3.6 Nonlinear Modal Model

The equations of motion of discretised structures in the physical space can be expressed as

$$\mathbf{M}\ddot{\mathbf{x}} + \mathbf{C}\dot{\mathbf{x}} + \mathbf{K}\mathbf{x} + \mathbf{g}_{nl}(\dot{\mathbf{x}}, \mathbf{x}) = \mathbf{f}(t) \tag{3.34}$$

where **M**, **C** and **K** are $n \times n$ mass, damping and stiffness matrices, respectively, $\mathbf{g}_{nl}$ is an $n \times n$ nonlinear stiffness matrix, $\mathbf{f}(t)$ is applied nodal force vector and $\mathbf{x}(t)$ is the vector of physical displacement. The equations can be obtained for example, from the finite element modelling of a structure. Transformation by $\mathbf{x} = \mathbf{\Phi p}$ leads to

$$\mathbf{\Phi}^{\mathrm{T}}\mathbf{M}\mathbf{\Phi}\ddot{\mathbf{p}} + \mathbf{\Phi}^{\mathrm{T}}\mathbf{C}\mathbf{\Phi}\dot{\mathbf{p}} + \mathbf{\Phi}^{\mathrm{T}}\mathbf{K}\mathbf{\Phi}\mathbf{p} + \mathbf{\Phi}^{\mathrm{T}}\mathbf{g}_{nl}(\mathbf{\Phi p}) = \mathbf{\Phi}^{\mathrm{T}}\mathbf{f}(t) \tag{3.35}$$

where $\mathbf{\Phi}$ is the modal vector matrix. Using the orthogonality of the modes, equation (3.35) becomes

$$\bar{\mathbf{M}}\ddot{\mathbf{p}} + \bar{\mathbf{C}}\dot{\mathbf{p}} + \bar{\mathbf{K}}\mathbf{p} + \bar{\mathbf{g}}_{nl} = \bar{\mathbf{f}} \tag{3.36}$$

where $\bar{\mathbf{M}} = \mathbf{\Phi}^{\mathrm{T}}\mathbf{M}\mathbf{\Phi} = [\bar{\mathrm{M}}_{rr}]$ and $\bar{\mathbf{K}} = \mathbf{\Phi}^{\mathrm{T}}\mathbf{K}\mathbf{\Phi} = [\bar{\mathrm{K}}_{rr}]$ are diagonal matrices, and $\bar{\mathbf{g}}_{nl} = \mathbf{\Phi}^{\mathrm{T}}\mathbf{g}_{nl}$. If the structure has proportional damping, $\bar{\mathbf{C}} = \mathbf{\Phi}^{\mathrm{T}}\mathbf{C}\mathbf{\Phi} = [\bar{\mathrm{C}}_{rr}]$, which is also a diagonal matrix, then equation (3.36) reduces to

$$\bar{\mathrm{M}}_{rr}\ddot{p}_r + \bar{\mathrm{C}}_{rr}\dot{p}_r + \bar{\mathrm{K}}_{rr}p_r + \bar{\mathrm{g}}_{nl,r} = \bar{\mathrm{f}}_r \tag{3.37}$$

where $p_r$ is the $r$th modal displacement and other parameters in the modal expression. Nonlinear terms, $\bar{\mathrm{g}}_{nl,r}$ refer to $r$th mode nonlinear restoring force and other modes allow for nonlinear cross-coupling terms.

Figure 3.7 shows the flow chart for the methodology of nonlinear identification. From equation (3.37), the nonlinear stiffness terms can be expressed as:

$$\bar{\mathrm{g}}_{nl,r} = \bar{\mathrm{f}}_r - \bar{\mathrm{M}}_{rr}\ddot{p}_r - \bar{\mathrm{C}}_{rr}\dot{p}_r - \bar{\mathrm{K}}_{rr}p_r \tag{3.38}$$

a) Choose the number of degree of freedom and the modes to represent the system.
b) Choose a suitable input and ‘measure’ the response.

c) Assume a suitable type of nonlinearity with coefficients to be determined in step f.
d) Set the time step, d*t*.
e) Compute the right-hand side of equation (3.38).
f) Curve fit the coefficients in step c. If the error between the two sides of equation (3.38) is big, return to step c and try a different type of nonlinearity. If the error is small enough, the identification is considered as completed and successful.

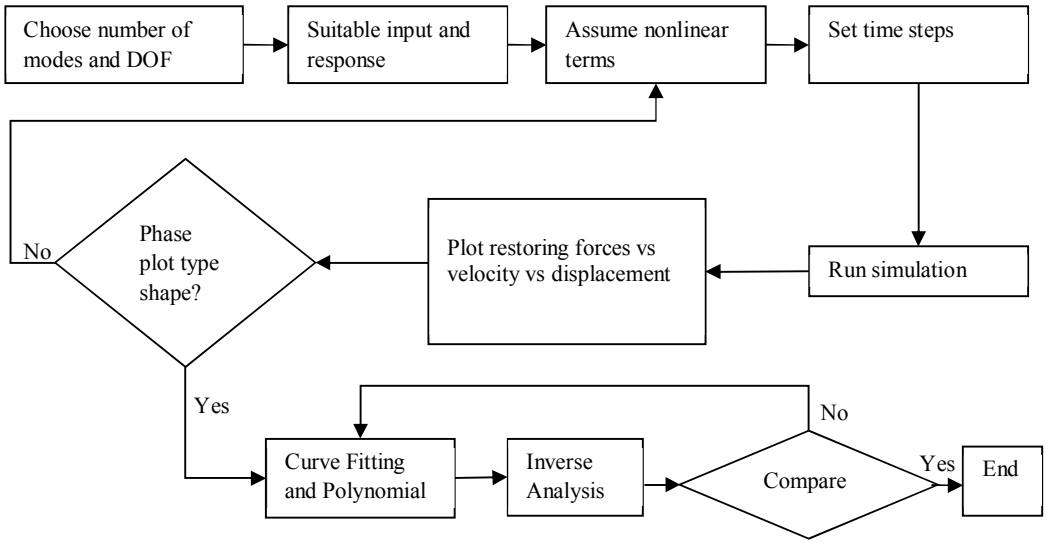


Figure 3.7: Methodology of nonlinear identification

## 3.7 Curve Fitting the Restoring Forces

A mathematical model of the restoring force can be obtained from the curve fit to the restoring forces expressed as some functions of the displacement and velocity data, typically a polynomial or orthogonal series. Displacement and velocity can always be calculated at the same instant of acceleration. During a modal test, acceleration is

usually measured. Velocity and displacement time histories can be obtained through integration. The acceleration data may be integrated in the time or frequency domain. Al-Hadid (1989) and Worden (1990) carried out detailed assessment and comparison of these methods.

The orthogonal approach employs the Chebyshev polynomial series. Chebyshev polynomials are used to form a two dimensional orthogonal series of polynomial terms. Orthogonality means that in the series expansion for the restoring forces may be added without re-computing the entire series, which can lead to a faster solution. However, there are several disadvantages with the Chebyshev polynomials (Al-Hadid, 1989), as follows:

- The normalisation step is required to compile data into the required range of (+1,-1) where the orthogonality conditions are satisfied (Worden and Tomlinson, 2001). It means that any odd or even behaviour of the function may not be utilised, yielding larger series.

- The integration of Chebyshev coefficients requires that the data points are equally spaced in the phase plane over the range of interest. Both interpolations can give equally spaced points in the region covered by data and interpolations into the empty corner regions are necessary. These processes are time consuming and give more opportunity for error.

Significant disadvantages associated with the Chebyshev polynomial approach caused some researchers according to Al-Hadid (1989) to abandon it in favour of using an ordinary polynomial series.

The ordinary polynomial series representation of the restoring forces involves a power series expansion of the form

$$g(x,\dot{x}) = \sum_{i=1}^{p}\sum_{j=1}^{p} C_{ij}T_{ij}(x_k,\dot{x}_k) \tag{3.39}$$

where $p$ is the model order or the series of order, and $i$ and $j$ are truncation of the sum of order. Each polynomial term is represented by a coefficient $C_{ij}$ and a function for Chebyshev polynomial order, $T_{ij}(x_k,\dot{x}_k)$. The functions form a series of polynomial terms, an example may be expressed as

$$T_{ij} = \sum_{i=1}^{p}\sum_{j=1}^{p} x_k^i\,\dot{x}_k^j \tag{3.40}$$

The least squares method may be used to curve fit this polynomial to obtain coefficient $C_{ij}$.

The ordinary polynomial approach has been found to be significantly faster than the Chebyshev polynomial approach. Singular Value Decomposition can be applied to eliminate ill conditioning of least square problem through decomposing the design matrix into a form that can be inverted.

### 3.7.1 Least Squares of Ordinary Polynomial Series

The least square method is a common approach to approximate the solution of over determined systems. The idea of this method is about overall solution by minimizing the sum of the squares of the errors made in the results of every single equation.

In order to solve ill conditioning least square problems, the basis and special functions form the ($q \times p$) design matrix $\mathbf{D}$. Each column represents a special function, while each row represents a data point. It is important that there are more rows than columns in this matrix. If there are less rows than columns, then insufficient data is presented for curve fitting of the model. If the number of rows is equal to the number of columns, then the problem will simply be a set of simultaneous equations, so more rows than columns are necessary to give the best fit solution. The unknown coefficients form a ($p \times 1$) vector $\mathbf{C}$ and the restoring force time history forms an ($q \times 1$) vector $\mathbf{G}$**.** The least square problem can be expressed as

$$\mathbf{G} = \mathbf{D}\,\mathbf{C} + \Delta\mathbf{E} \tag{3.41}$$

where $\Delta\mathbf{E}$ is the error vector. The least square cost function can be written as

$$\mathrm{J} = \sum_{\mathrm{k}=1}^{\mathrm{q}} (\Delta\mathbf{E}_k)^2 = \sum_{\mathrm{k}=1}^{\mathrm{q}} \left(\mathbf{G}_k - \widehat{\mathbf{G}}_k\right)^2 \tag{3.42}$$

where $\widehat{\mathbf{G}}_k$ is the estimated restoring force at data point $k$. This cost function indicates how good the model fits the data. The smallest cost function will occur when the derivatives of $\mathrm{J}$ toward $\mathbf{C}$, the unknown coefficients are zero. Expand equation 3.42

$$\begin{aligned} \mathrm{J} = \sum_{\mathrm{k}=1}^{\mathrm{q}} \left(\mathbf{G}_k - \widehat{\mathbf{G}}_k\right)^2 &= \left(\mathbf{G}_k - \widehat{\mathbf{G}}_k\right)^{\mathrm{T}} \left(\mathbf{G}_k - \widehat{\mathbf{G}}_k\right) \\ &= (\mathbf{G}_k - \mathbf{DC})^{\mathrm{T}} (\mathbf{G}_k - \mathbf{DC}) \\ &= (\mathbf{G}_k)^{\mathrm{T}} (\mathbf{G}_k) - (\mathbf{G}_k)^{\mathrm{T}}\,\mathbf{DC} - \mathbf{D}^{\mathrm{T}}\mathbf{C}^{\mathrm{T}}\mathbf{G}_k + \mathbf{D}^{\mathrm{T}}\mathbf{D}\,\mathbf{C}^{\mathrm{T}}\mathbf{C} \end{aligned} \tag{3.43}$$

Differentiating the cost function (equation 3.43) will give the following expression at the minimum

$$\frac{\delta \mathbf{J}}{\delta \mathbf{C}} = -2\mathbf{D}^{\mathrm{T}}\mathbf{G}_k + 2\mathbf{D}^{\mathrm{T}}\mathbf{D}\mathbf{C} = \mathbf{0} \tag{3.44}$$

Then,

$$\mathbf{D}^{\mathrm{T}}\mathbf{D}\mathbf{C} = \mathbf{D}^{\mathrm{T}}\mathbf{G}_k \tag{3.45}$$

which is known as the normal equation of the least square method. Rearranging this equation gives

$$\mathbf{C} = (\mathbf{D}^{\mathrm{T}}\mathbf{D})^{-1}\mathbf{D}^{\mathrm{T}}\mathbf{G}_k \tag{3.46}$$

where the inverse may be calculated using a conventional numerical method. It can be shown that the diagonal of matrix $(\mathbf{D}^{\mathrm{T}}\mathbf{D})^{-1}$ are the variances of the fitted coefficients $\mathbf{C}$ and the covariance between the elements of this vector. This matrix is known as the covariance matrix.

## 3.8 Nonlinear Identification for a SDOF SYSTEM

### 3.8.1 Cubic Stiffness

Consider a SDOF system with cubic nonlinearity as shown in Figure 3.8, with the following properties: $m$=5kg, $c$=10 Ns/m, $k$=5000 N/m, $g_{nl}$= 3x10$^5$ N/m$^3$, $f(t)$=100 N with chirp signal. A chirp is a signal in which the frequency increases ('up-chirp') or decreases ('down-chirp') with time (Masri et al., 1982). The equation of motion cubic stiffness nonlinearity system is called Duffing's equation, as follows:

$$M\ddot{x} + C\dot{x} + Kx + g_{nl}x^3 = f(t) \tag{3.47}$$

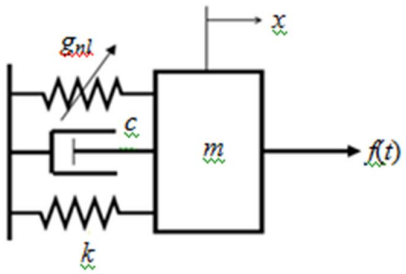


Figure 3.8: A nonlinear SDOF System

Figure 3.9 shows the input and output of cubic stiffness nonlinear SDOF system. Figure 3.10 shows the phase diagram for cubic stiffness nonlinearity of SDOF system excited by a chirp signal. Parameter estimation of 250,000 points centred around the jump region where the nonlinearity is most evidence. This data allowed the construction of the force surface as shown in Figure 3.11 (restoring forces vs. displacement) and Figure 3.12 (restoring forces vs. velocity vs. displacement). The surface is very smooth and clearly shows the cubic nature of nonlinearity.

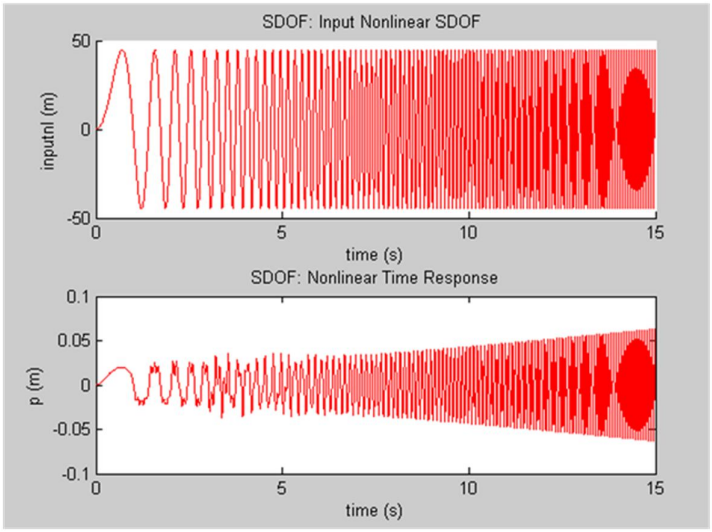


Figure 3.9: Input and Output of Cubic Stiffness Nonlinear SDOF System

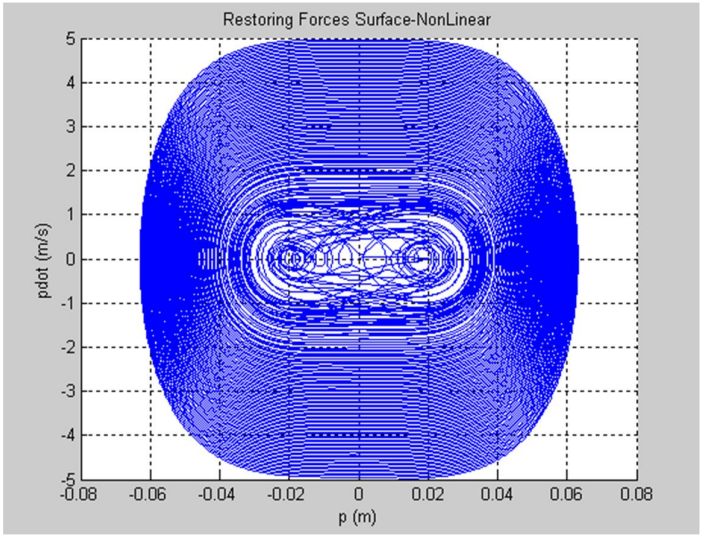


Figure 3.10: Phase Diagram of Cubic Stiffness Nonlinear SDOF System

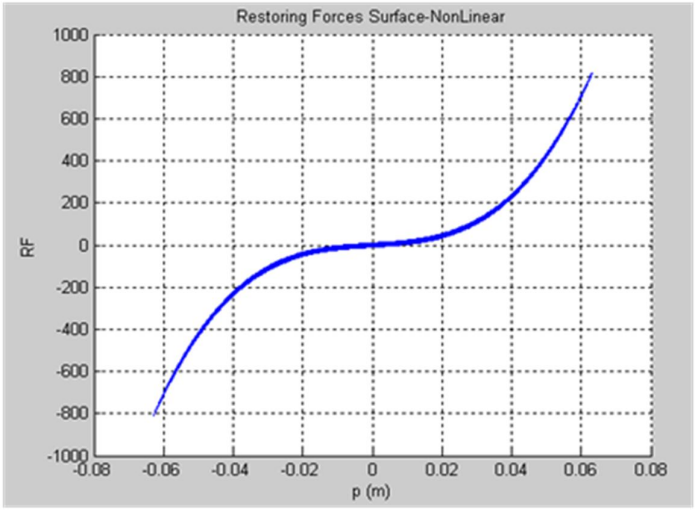


Figure 3.11: Restoring Forces vs. Displacement for Cubic Stiffness Nonlinear SDOF System

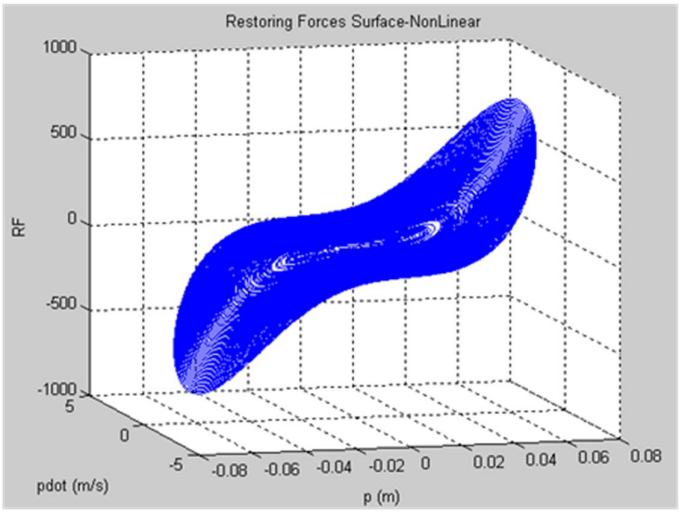


Figure 3.12: Restoring Forces vs. Velocity vs. Displacement for Cubic Stiffness Nonlinear SDOF System

The polynomial expression for this cubic nonlinear stiffness SDOF can be investigated through inverse analysis on the output from forward analysis. Polynomial expression for this cubic nonlinear SDOF can be defined as follows:

$$g_{nl,r} = A_1\dot{p}_r^3 + B_1\dot{p}_r^2 p_r + C_1\dot{p}_r p_r^2 + D_1 p_r^3 \tag{3.48}$$

Table 3.2 shows the value of each coefficient from the polynomial expression in equation (3.4) in physical and modal coordinates. Nonlinear cubic stiffness coefficient for an SDOF system can be compared with $g_{nl}$ forward analysis and $D_1$ inverse analysis. Others nonlinearities can be modelled using suitable basic functions. (Göge et al., 2004) explored an extension of nonlinear coefficients and functions in their model. (Dimitriadis et al., 1998) applied the restoring force surface to identify MDOF using a simple least square computation. The percentage of error between forward and inverse analyses of cubic nonlinear SDOF is highlighted in Table 3.3.

Table 3.2: Coefficient from Inverse Analysis Cubic Nonlinear SDOF

| Coefficient | Inverse Analysis (Physical Coordinate) | Inverse Analysis (Modal Coordinate) |
|---|---|---|
| $A_1$ | 0 | $4.06 \times 10^{-18}$ |
| $B_1$ | 0 | $2.44 \times 10^{-13}$ |
| $C_1$ | 0 | $1.65 \times 10^{-19}$ |
| $D_1$ | $2.966 \times 10^{5}$ | $3 \times 10^{5}$ |

Table 3.3: Percentage of Error for Forward and Inverse Analyses Cubic Nonlinear SDOF

| $g_{nl}$ Forward Analysis | $D_1$ Coefficient Inverse Analysis (Physical Coordinate) | $D_1$ Coefficient Inverse Analysis (Modal Coordinate) | % of Error |
|---|---|---|---|
| $3 \times 10^{5}$ | $2.966 \times 10^{5}$ | | 1.13 |
| $3 \times 10^{5}$ | | $3 \times 10^{5}$ | 0 |

### 3.8.2 Bilinear Stiffness

Consider a SDOF system with a bilinear stiffness shown in Figure 3.8, with properties as follows: $m$=5kg, $c$=10 Ns/m, $k_1$=5000 N/m, $k_2$= $3\text{x}10^5$ N/m, $f$(t)=100 N with chirp signal. The force displacement characteristics bilinear stiffness nonlinearity system is:

$$g_{nl}(x) = \begin{cases} k_1 x, & x > 0 \\ k_2 x, & x < 0 \end{cases} \tag{3.49}$$

Figure 3.13 shows the input and output of bilinear stiffness nonlinearity SDOF system. Figure 3.14 shows the phase diagram for bilinear stiffness nonlinearity of SDOF system excited by a chirp signal. This data allows the constructions of the force surface as shown in Figure 3.15 (restoring forces vs. displacement) and Figure

3.16 (restoring forces vs. velocity vs. displacement). The surface is very smooth and is clearly showing the bilinear nature of nonlinearity.

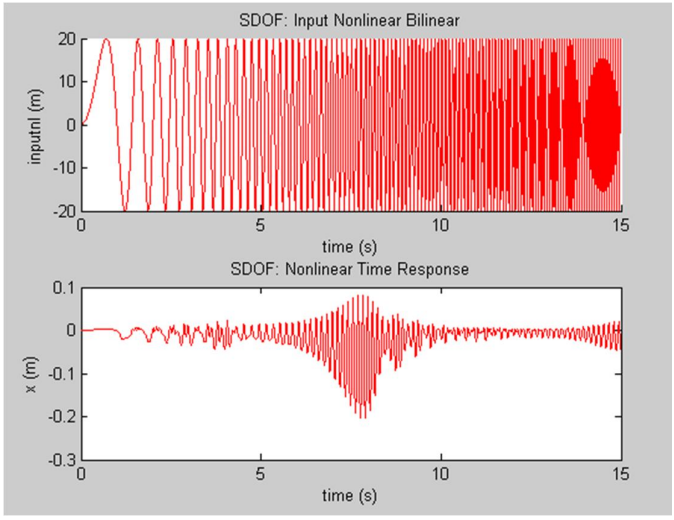


Figure 3.13: Input and Output of Bilinear Stiffness Nonlinearity SDOF System

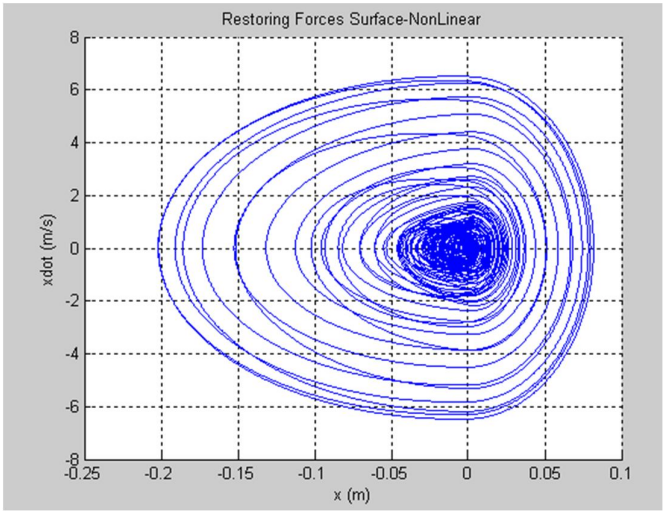


Figure 3.14: Phase Diagram of Bilinear Stiffness Nonlinearity SDOF System

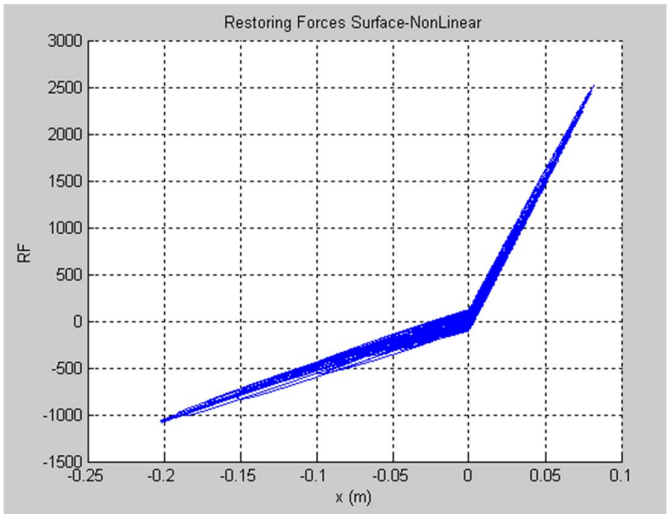


Figure 3.15: Restoring Forces vs Displacement for Bilinear Stiffness Nonlinearity SDOF System

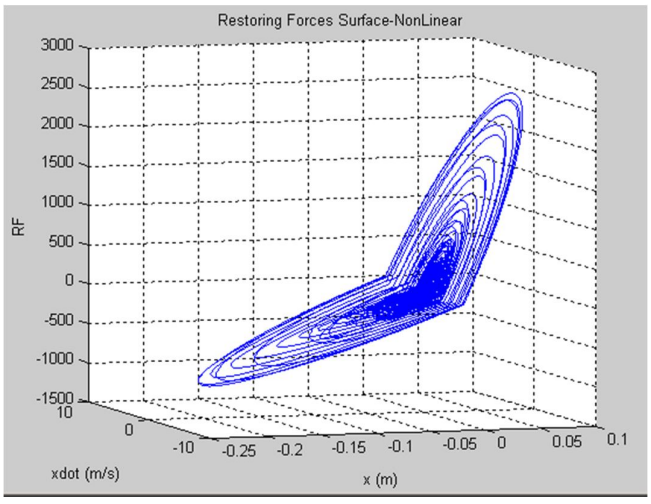


Figure 3.16: Restoring Forces vs. Velocity vs. Displacement for Bilinear Stiffness Nonlinearity SDOF System

### 3.8.3 Piecewise Stiffness

Consider a SDOF system with a piecewise or backlash nonlinear stiffness shown in Figure 3.8, with properties as below: $m$=5kg, $c$=10 Ns/m, $k_1$=5000 N/m, $k_2$= 3x10$^5$ N/m, $f(t)$=100 N with chirp signal. The force displacement characteristics for a piecewise stiffness nonlinearity system are as follows:

$$g_{nl}(x) = \begin{cases} k_2 x + (k_1 - k_2)d, & x > d \\ k_1 x, & |x| < d \\ k_2 x - (k_1 - k_2)d, & x < -d \end{cases} \tag{3.50}$$

Figure 3.17 shows the input and output of a piecewise stiffness nonlinearity SDOF system. Figure 3.18 shows the phase diagram for a piecewise stiffness nonlinearity of SDOF system excited by a chirp signal. This data allows the constructions of the force surface as shown in Figure 3.19 (restoring forces vs. displacement) and Figure 3.20 (restoring forces vs. velocity vs. displacement). The surface is very smooth and is clearly showing the piecewise nature of the nonlinearity.

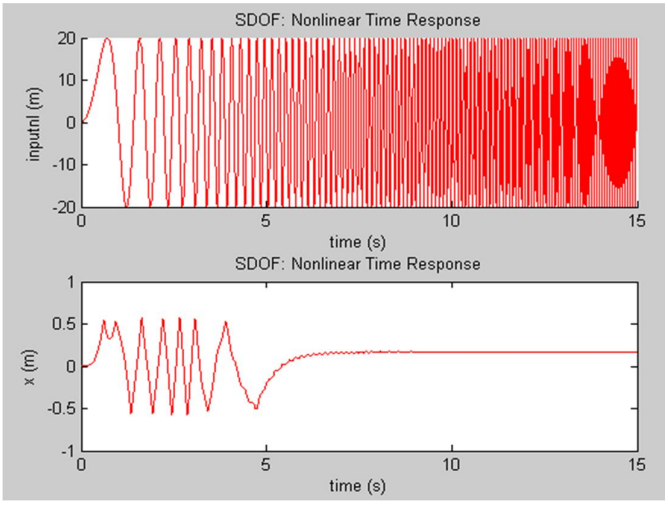


Figure 3.17: Input and Output of Piecewise Stiffness Nonlinear SDOF System

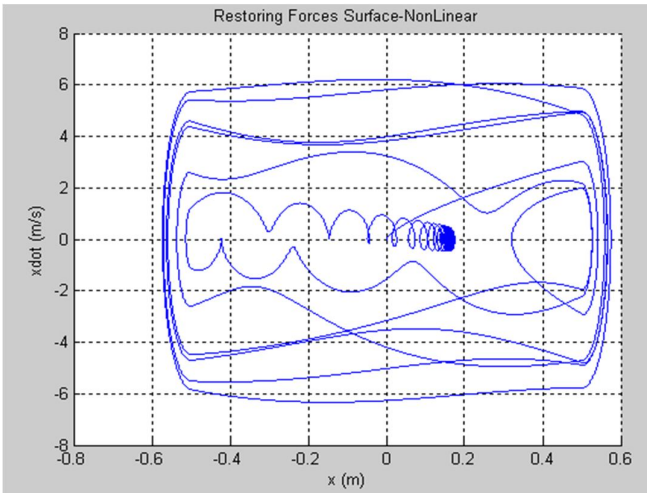


Figure 3.18: Phase Diagram of Piecewise Stiffness Nonlinear SDOF System

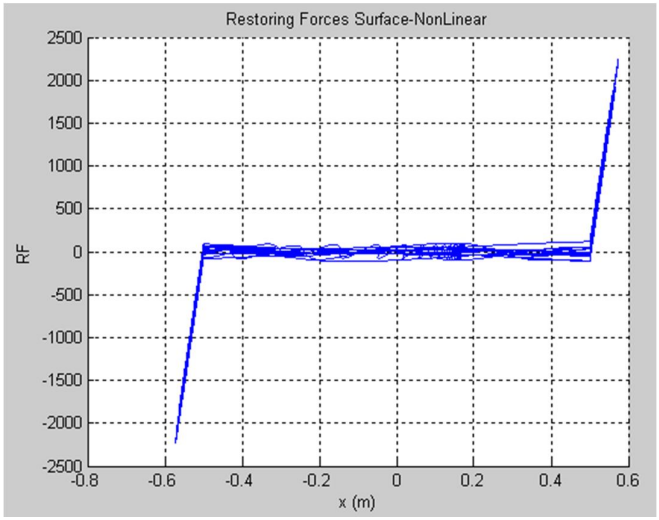


Figure 3.19: Restoring Forces vs. Displacement for Piecewise Stiffness Nonlinear SDOF System

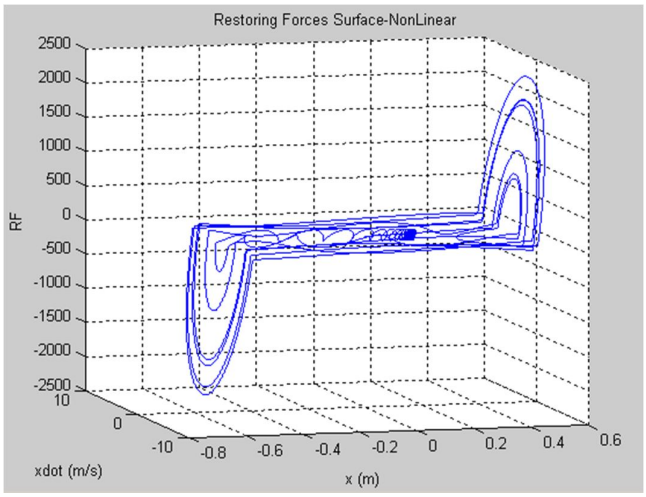


Figure 3.20: Restoring Forces vs. Velocity vs. Displacement for Piecewise Stiffness Nonlinear SDOF System

## 3.9 Nonlinear Identification of a TWO-DOF SYSTEM

Consider a two degree of freedom nonlinear system as shown in Figure 3.21, with the following properties:

$$m_1 = 2\ \text{kg};\ m_2 = 2\ \text{kg}\ ; k_1 = 2000\ \frac{\text{N}}{\text{m}}, k_2 = 2000\frac{\text{N}}{\text{m}} = \ ;\ c_1 = 2\frac{\text{Ns}}{\text{m}}\ ;$$
$$c_2 = 1\frac{\text{Ns}}{\text{m}}\ ;\ g_{nl} = 100000\frac{\text{N}}{\text{m}^3}; f_1 = 100\ \text{N}.$$

Figure 3.22 shows the input and output of the system. The equations of motion in physical coordinates are:

$$\begin{bmatrix}2 & 0\\ 0 & 1\end{bmatrix}\begin{bmatrix}\ddot{x}_1\\ \ddot{x}_2\end{bmatrix} + \begin{bmatrix}3000 & -1000\\ -1000 & 1000\end{bmatrix}\begin{bmatrix}\dot{x}_1\\ \dot{x}_2\end{bmatrix} + \begin{bmatrix}3 & -1\\ -1 & 1\end{bmatrix}\begin{bmatrix}x_1\\ x_2\end{bmatrix} + \begin{bmatrix}100000 & 0\\ 0 & 0\end{bmatrix}\begin{bmatrix}x_1^3\\ x_2^3\end{bmatrix} = \begin{bmatrix}100\sin\omega t\\ 0\end{bmatrix} \quad (3.51)$$

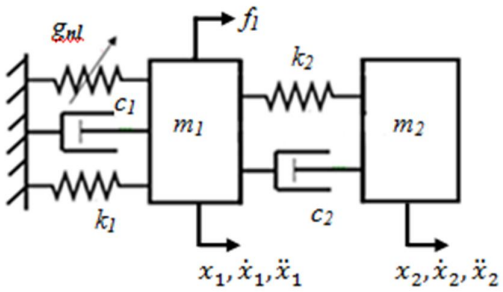


Figure 3.21: A nonlinear TWO-DOF System

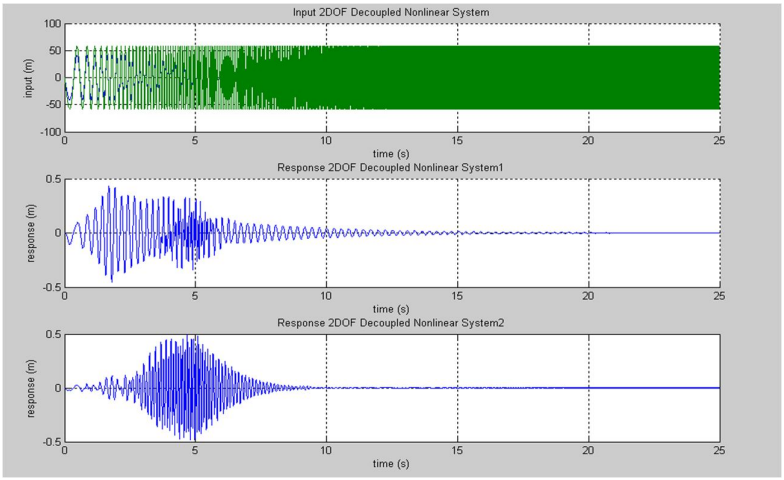


Figure 3.22: Input and Output of the Nonlinear TWO-DOF System

The transformation of equation (3.50) into modal coordinates as follows:

$$\ddot{p}_1 + 0.5\dot{p}_1 + 500p_1 + 2776.5p_1^3 + 11782p_1^2p_2 + 16666p_1p_2^2 + 7858p_2^3 = -40.83 \quad (3.52)$$

$$\ddot{p}_2 + 2\dot{p}_2 + 2000p_2 + 3927.3p_1^3 + 16666p_1^2p_2 + 23574p_1p_2^2 + 11115p_2^3 = -57.74 \quad (3.53)$$

The polynomial expression for this cubic nonlinear stiffness TWO-DOF can be investigated when performing an inverse analysis based on the output from a forward analysis. The polynomial expression for stiffness cubic nonlinear TWO-DOF is as follows:

$$g_{nl1,r} = A_{11}\dot{p}_1^3 + B_{11}\dot{p}_1^2 p_1 + C_{11}\dot{p}_1 p_1^2 + D_{11}p_1^3 + A_{12}\dot{p}_2^3 + B_{12}\dot{p}_2^2 p_2 + C_{12}\dot{p}_2 p_2^2 + D_{12}p_2^3 + E_{11}p_1^2 p_2 + F_{11}p_1 p_2^2 \quad (3.54)$$

$$g_{nl2,r} = A_{21}\dot{p}_1^3 + B_{21}\dot{p}_1^2 p_1 + C_{21}\dot{p}_1 p_1^2 + D_{21}p_1^3 + A_{22}\dot{p}_2^3 + B_{22}\dot{p}_2^2 p_2 + C_{22}\dot{p}_2 p_2^2 + D_{22}p_2^3 + E_{21}p_1^2 p_2 + F_{21}p_1 p_2^2 \quad (3.55)$$

Both polynomial equations (3.47) and (3.48) had ignored the damping coefficient. Table 3.4 shows the percentage of error in the forward and backward analyses from the coefficients of polynomial expression in equations (3.54) and (3.55). In the forward analysis, the value for nonlinear cubic stiffness, $g_{nl}$ is 100000 N/m$^3$ and from the inverse analysis was, $g_{nl}$ = 99997.96 N/m$^3$. The percentage of error between forward and inverse analyses was 0.02%.

As seen in Table 3.4, those coefficients associated with the nonlinear stiffness terms were identified very accurately (within 0.3%) and all coefficients of zero value were identified to be extremely small. So the identification of this simulated example is successful.

Table 3.4: Percentage of Error in Forward and Inverse Analyses for Cubic Nonlinear TWO-DOF

| Coefficient | Forward Analysis | Inverse Analysis | % of Error |
|---|---|---|---|
| $A_{11}$ | 0 | $-5.1\times10^{-16}$ | very small |
| $B_{11}$ | 0 | $-5.53\times10^{-13}$ | very small |
| $C_{11}$ | 0 | $-1.32\times10^{-12}$ | very small |
| $D_{11}$ | 2776.50 | 2776.46 | 0.144 |
| $A_{12}$ | 0 | $4.82\times10^{-17}$ | very small |
| $B_{12}$ | 0 | $1.09\times10^{-13}$ | very small |
| $C_{12}$ | 0 | $5.65\times10^{-13}$ | very small |
| $D_{12}$ | 7858 | 7857.84 | 0.204 |
| $E_{11}$ | 11782 | 11781.95 | 0.042 |
| $F_{11}$ | 16666 | 16665.59 | 0.025 |
| $A_{21}$ | 0 | $-9.23\times10^{-16}$ | very small |
| $B_{21}$ | 0 | $-3.53\times10^{-13}$ | very small |
| $C_{21}$ | 0 | $-1.32\times10^{-12}$ | very small |
| $D_{21}$ | 3927.30 | 3929.63 | 0.059 |
| $A_{22}$ | 0 | $1.05\times10^{-16}$ | very small |
| $B_{22}$ | 0 | $6.66\times10^{-14}$ | very small |
| $C_{22}$ | 0 | $9.58\times10^{-13}$ | very small |
| $D_{22}$ | 11115 | 11121.48 | 0.058 |
| $E_{21}$ | 16666 | 16675.41 | 0.056 |
| $F_{21}$ | 23574 | 23587.41 | 0.057 |

A simple and quick methodology for nonlinear identification based on the restoring force method is presented. This method was demonstrated on a nonlinear system with one or two degree-of-freedom. Furthermore, it can be used to identify nonlinear systems, which have a large number of degree-of-freedom.

## 3.10 Summary

In this chapter, the theories of force appropriation and restoring forces methods were presented. Simulated results were demonstrated and validated for both methods. The combination of these methods is proven for multi-stage identification of high degree of freedom continuous systems.

# Chapter 4

# Experimental Modal Analysis of Structure

## 4.1 Introduction

Experimental study of structural dynamics plays an important role in design and analysis of structures. This method has grown steadily since the late 1970's and spread very fast in parallel with development of FFT spectrum analysers from analogue to digital. Basically, a modal test consists of an acquisition phase and an analysis phase. The main objective of modal testing is to determine dynamic characteristics of structures. However, validation of numerical models can be used to further detail analysis.

In this chapter, an overview of experimental modal analysis is presented. It is important to understand this background information before modal testing is conducted on any structures. Impact hammer and shaker tests are common methods used to perform modal tests. Information about these methods is provided in this chapter.

Furthermore, for nonlinear structures, Multi-Input Multi-Output (MIMO) tests are implemented such as MIMO sine testing and MIMO normal mode tests. MIMO sine testing is an excitation of the structure with a shaker input with slowly sweeping sine signal over an interested frequency range. Moreover, experimental work through MIMO normal mode test is carried out on the wing structure based on force appropriation method. Details about these particular nonlinear testing methods are given in this chapter.

## 4.2 Experimental Modal Analysis (EMA)

The dynamic behaviour of a structure in a particular frequency range can be modelled as a set of individual modes of vibration. Normally, the structure is assumed to behave as a linear and time-invariant system. Modal properties that describe each vibration mode are:

- Natural frequency
- Modal damping
- Mode shape

A mathematical model based on these parameters is a linear model of a dynamic description of linear behaviour of the structure. Thus, EMA is the process of obtaining modal properties that permits a dynamic mathematical model to be formed. Figure 4.1 (next page) shows the theoretical route to vibration analysis, which includes three stages: spatial model, modal model and response model (Ewins, 2000). Basically, a mathematical model is formulated to describe the structure's physical characteristics, generally in term of mass, damping and stiffness properties. This level of model is referred to as spatial model. The spatial model is then used to define the modal model. Then, the modal model expresses the normal modes of structures, by which the structure vibrates in free vibration (without external excitations). In the final stage, a response model is built in order to describe how the structure will responds under given excitations by developing a set of FRF's within the frequency of range interest.

As a summary, the purposes of EMA tests are as follows:

- to determine frequencies of the structure
- to obtain mode shapes and modal damping for the structure
- to correlate EMA results with analytical models (FEM) of the structure

- to acquire a dynamic model that can be used for FE model updating
- to gain a dynamic model of the structure that can be used for further nonlinear analysis.

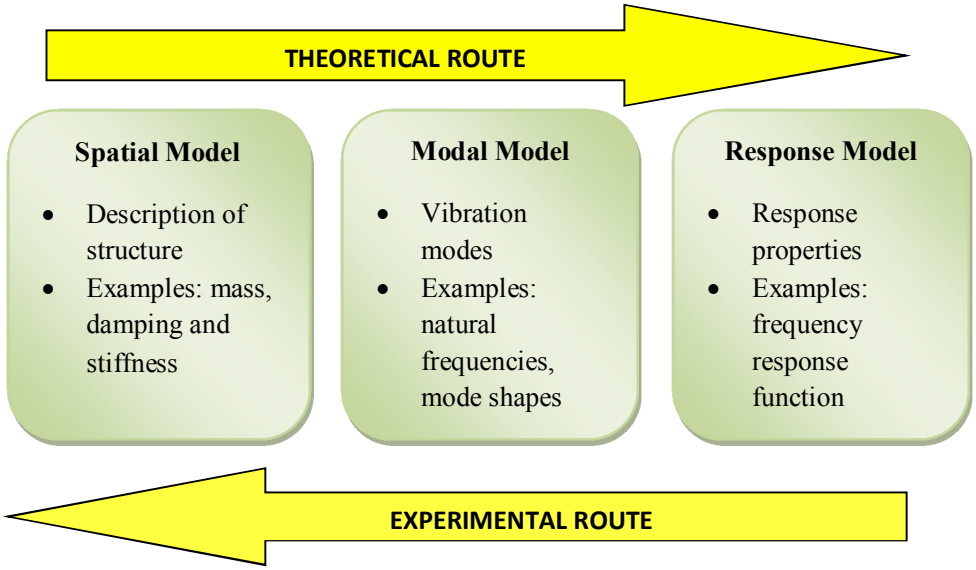


Figure 4.1: Vibration Analysis Routes

The experimental route of vibration analysis is in the inverse direction of the theoretical route, in which the FRF's are measured to form the response and modal model consisting of natural frequencies, modal damping and where the mode shape can be defined. Finally, the spatial model can be determined providing enough measurements are made in order to describe the physical structure. It is very important to make sure that enough DOFs in the measurement and also to cover most of the vibration modes within a frequency range. Equation (4.1) and (4.2) shows relationships between response model $\mathbf{H}(\omega)$ and the spatial and modal models which can be established (Ewins, 2000) as follows:

$$\mathbf{H}(\omega) = [\mathbf{K} + \mathrm{i}\omega\mathbf{C} - \omega^2\mathbf{M}]^{-1} \tag{4.1}$$

$$\mathbf{H}(\omega) = \boldsymbol{\phi}\left[\omega^2 - \omega_n^2 - 2\mathrm{i}\omega_n\,\zeta_n\right]^{-1}\boldsymbol{\phi}^{\mathrm{T}} \tag{4.2}$$

where **M**, **C** and **K** represent mass, damping and stiffness matrices. While $\omega_n$, $\boldsymbol{\phi}$ and $\zeta_n$ correspond to natural frequency, mode shape vector and modal damping to form be modal model, where $\omega$ is the excitation frequency of the system.

## 4.3 Basic Components of EMA

This section describes basic components of EMA. Figure 4.2 illustrates a typical layout for a measurement system used for single excitation which includes the three main elements of EMA (Ewins, 2000; Maia and Silva, 1997). These are excitation of structure method, sensing mechanism and data acquisition and processing mechanism.

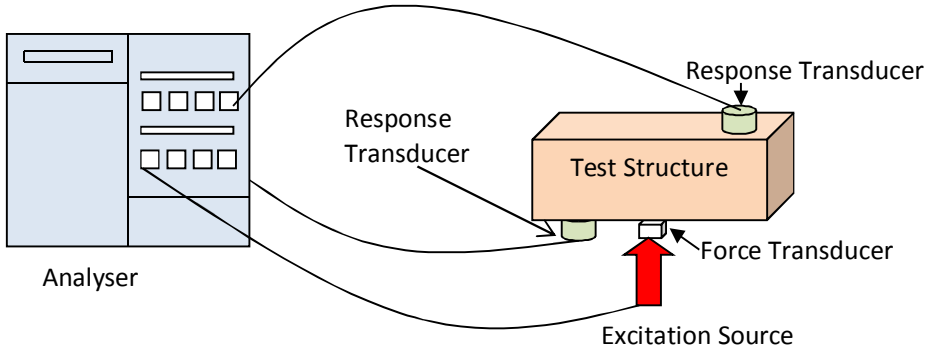


Figure 4.2: General Diagram of EMA

The excitation mechanism is set-up by a system which provides the input to the structure under analysis. There are various types of structure excitation which can be

generally classified into contacting and non-contacting categories. Contacting mechanism involve connecting an exciter that remains attached to the structure such as electromagnetic or electro-hydraulic shakers. This type of excitation mechanism is easily to be controlled both in frequency and amplitude, thus providing overall accuracy. Anyhow, this type also has disadvantages such as the need to have the exciter connected to the structure and also the mass loading effect of the structures.

A connecting excitation mechanism also known as a shaker is constituted by a system that applies the excitation, normally in the form of a driving force $\mathbf{f}(t)$ applied at a given coordinates. Figure 4.3 shows an electromagnetic shaker that is used in modal testing. There are wide varieties of signal excitation forms such as random, harmonic, stepped-sine, transient etc. which must be chosen to match the requirements of the test. Furthermore, a signal generator and a power amplifier are needed in order to provide sufficient input for measurement. A force transducer is used and located at the end of the exciter to measure the force applied to the structure.

Figure 4.3: Shaker

Non-contacting types of excitation mechanisms mean that the excitation device either in contact for a short period (example: impact hammer) or totally no contact (example: electromagnetic device) to the structure. The impact hammer is a popular device which consists of a hammer with force transducer attached to its head. Hence, there is no need for a connection between excitation device and test structure, therefore mass loading effects can be avoided. In addition, this device does not need a signal generator and a power amplifier, which are essential for the shakers.

Figure 4.4 shows the impact hammer that used to hit the test structure in order to excite a wide range of frequencies. However, the excitation and frequency range depends on the properties of the hammer head and tip. The magnitude of the impact is determined by the mass of the hammer head and the velocity of the impact that is introduced by the operator. In addition, the frequency range is defined by the stiffness of the contacting surfaces and the mass of the hammer head. Consequently, the stiffer the materials, the higher the effective frequency range covered by the impact. Therefore, the impact hammer should be supplied with different sets of tips and heads that are interchangeable to obtain suitable impact magnitudes and frequency ranges.

Figure 4.4: Impact Hammer

Sensing is established by sensing devices known as transducers. Most commonly used in modal test are piezoelectric transducers either used force transducers to measure force excitation or accelerometers to measure acceleration response. Figure 4.5 shows accelerometer that is commonly used in EMA. This sensor generates electric signals that are proportional to the physical parameter needs to measure. A conditioning amplifier may be needed if the electric signals are weak to boost the signals to be measured by the analyser.

There are two main criteria to be considered when mounting and locating the transducers on the test structure. Initially, there are several way of mounting the accelerometers to the surface of test structure; using stud, wax, magnet and hand-held during the test. However, wax is simplest, easiest and applied widely in modal testing. Secondly, it is very important to locate the accelerometers at the correct location. Normally, we need to avoid locating accelerometers too close to a node of vibration modes. This is important in order to capture actual mode shapes of the structure. Heylen et al. (1998) proposed that the accelerometers used in modal testing should not exceed 10 per cent of the weight of the structure to be measured to avoid mass loading effects.

Figure 4.5: Accelerometer

The basic objective data acquisition and processing system is to measure the signals developed by the excitation and sensing mechanisms using a sophisticated device called analyser. Figure 4.6 shows a 12 channels LMS signal analyser that can be

used in dynamics lab, University of Liverpool. A spectrum analyser or FFT analyser is commonly used and provides direct measurement of FRF's. Basically, this is done by converting the analogue time domain signals generated by the transducer into digital frequency domain information that can be processed by the digital computer afterwards.

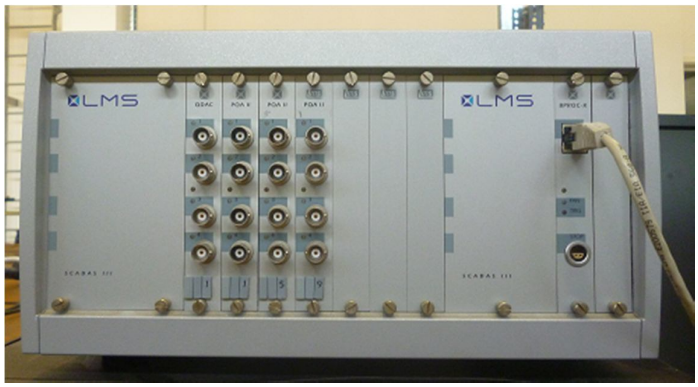


Figure 4.6: LMS Signal Analyser

## 4.4 Experimental Modal Analysis of Substructures of Engine Pylon

The structure under investigation is an engine pylon model which consists of pylon plates in a variable-profile clamp as shown in Figure 4.7. In this clamp, the pylon plates become shorter and stiffer as this substructure deflected laterally. Figure 4.8 shows an engine pylon model clamped with fixed-free boundary configuration.

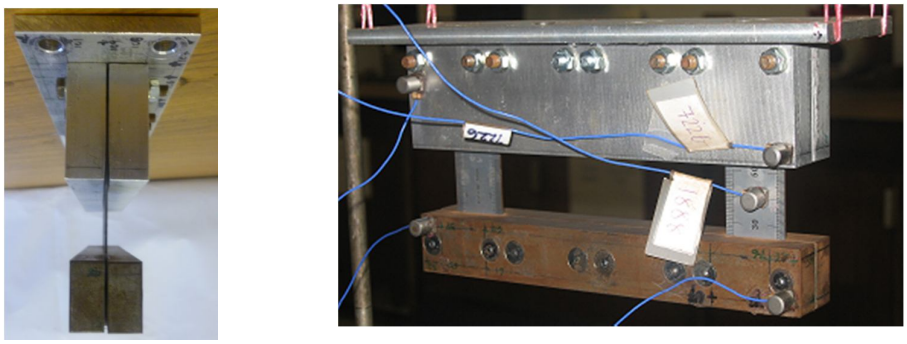

a) Front View b) Side View

Figure 4.7: Variable-Profile Clamp Arrangement of Engine Pylon Model

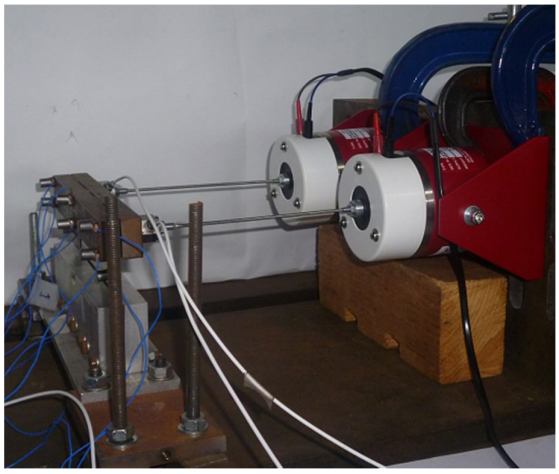

Figure 4.8: Fixed-Free Boundary Condition of Engine Pylon Model

The engine pylon model in the LMS data acquisition system is shown in Figure 4.9. Eight accelerometers are used to get the response from excitation force. Impact hammer and shakers are used to excite in (-Y) direction. In this project, impact hammer (impact testing), single and double shakers (spectral testing) are used in order to perform modal testing. In order to get the quality and correct FRF's, averages of five the responses excited by the impact hammer are set in the LMS system. In addition for the shaker, averages of 20 of the excitations are set in the LMS system to get better FRF's measured from modal test.

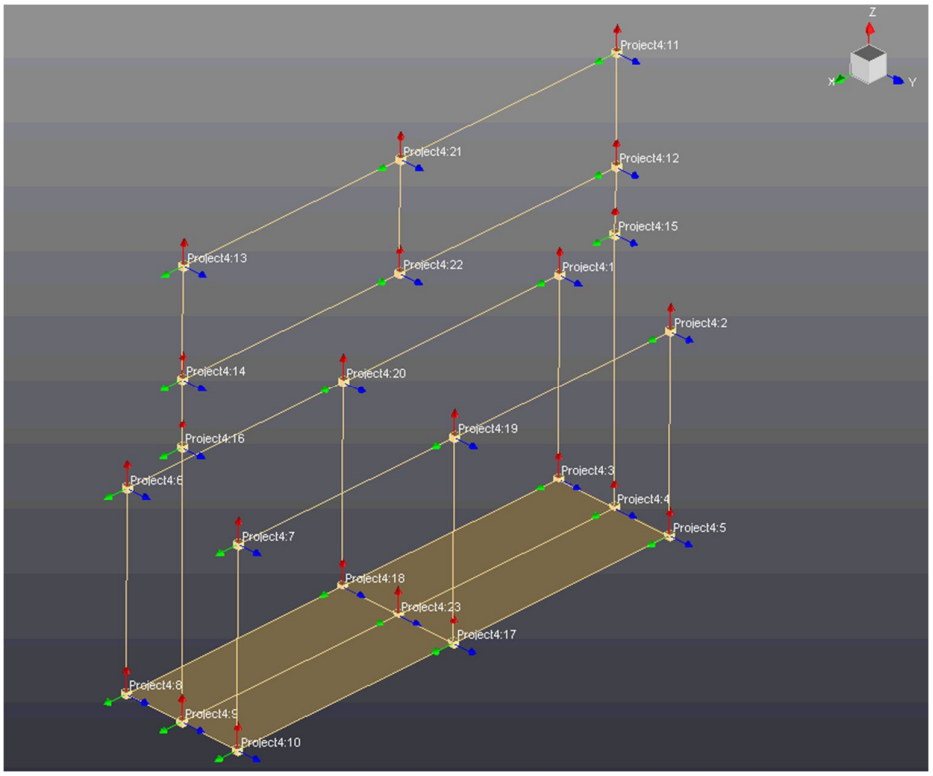


Figure 4.9: Engine Pylon Model in LMS Data Acquisition System.

The details of the accelerometers arranged over this substructure are depicted in Table 4.1 in which the test run column represents the number of FRF measurements at every measuring point when performing modal test by using the shaker. Force from the shaker can be controlled by adjusting the voltage supplied to the shaker through the amplifier.

Table 4.1: Number of measuring points and measuring direction with different voltage of engine pylon model

| Series No. Accelerometers (Kistler) | Test Run (Shaker) | | | | | | |
|---|---|---|---|---|---|---|---|
| | Run 1 (0.01V) | Run 2 (0.05V) | Run 3 (0.1V) | Run 4 (0.15V) | Run 5 (0.2V) | Run 6 (0.25V) | Run 7 (0.3V) |
| 2008887 | Point 11 in (-Y) | Point 11 in (-Y) | Point 11 in (-Y) | Point 11 in (-Y) | Point 11 in (-Y) | Point 11 in (-Y) | Point 11 in (-Y) |
| 2007226 | Point 21 in (-Y) | Point 21 in (-Y) | Point 21 in (-Y) | Point 21 in (-Y) | Point 21 in (-Y) | Point 21 in (-Y) | Point 21 in (-Y) |
| 2008890 | Point 13 in (-Y) | Point 13 in (-Y) | Point 13 in (-Y) | Point 13 in (-Y) | Point 13 in (-Y) | Point 13 in (-Y) | Point 13 in (-Y) |
| 2008893 | Point 15 in (-Y) | Point 15 in (-Y) | Point 15 in (-Y) | Point 15 in (-Y) | Point 15 in (-Y) | Point 15 in (-Y) | Point 15 in (-Y) |
| 2007224 | Point 16 in (-Y) | Point 16 in (-Y) | Point 16 in (-Y) | Point 16 in (-Y) | Point 16 in (-Y) | Point 16 in (-Y) | Point 16 in (-Y) |
| 2008895 | Point 12 in (-Y) | Point 12 in (-Y) | Point 12 in (-Y) | Point 12 in (-Y) | Point 12 in (-Y) | Point 12 in (-Y) | Point 12 in (-Y) |
| 2008888 | Point 22 in (-Y) | Point 22 in (-Y) | Point 22 in (-Y) | Point 22 in (-Y) | Point 22 in (-Y) | Point 22 in (-Y) | Point 22 in (-Y) |
| 2008881 | Point 14 in (-Y) | Point 14 in (-Y) | Point 14 in (-Y) | Point 14 in (-Y) | Point 14 in (-Y) | Point 14 in (-Y) | Point 14 in (-Y) |

Table 4.2 shows the experimental frequencies obtained from the LMS PolyMAX curve-fitting procedure which is used to extract the responses calculated from the measuring points by using impact hammer test. Furthermore Tables 4.3 and 4.4 show experimental frequencies of engine pylon model obtained by performing single and double shaker tests at different levels of force. Both tests (single and double shaker) are using spectral test LMS data acquisition to acquire dynamic data of excitation. Apparently, there are big differences in frequencies from the three methods (impact hammer, single shaker and double shaker). Obviously, double shaker method is more accurate compared to single shaker and impact hammer test.

This is because of the energy from double shakers allows the structure to be more uniformly excited throughout the entire structure and thus allows for the better extraction of frequency response functions (FRF). When only using a single shaker, the measurements obtained are generally not as good as those obtained from double shaker excitations, especially when considering larger structures. On the other hands, an impact hammer test is less accurate compared with a shaker test as it is difficult to get consistent hammer hits to the structure, and he energy imparted to the structure may be too low and does not sufficiently excite enough number of modes of a test structure. However, there are such a big difference on first frequency of engine pylon between impact hammer, single shaker and double shaker tests. Application of the shaker could be crucial in this case, while with impact testing the response time is limited. Moreover, shakers are often used for modal testing of big structures because of uniform excitation. It seems that the shaker test will give more reliable FRF than impact hammer test because the excitation is well defined and controlled, but this also depends on the reliability of the shaker.

Table 4.2: Experimental frequencies of engine pylon model by performing impact hammer test.

| Mode | Experimental Natural Frequencies (Hz) |
|---|---|
| 1 | 14.6 |
| 2 | 54.27 |
| 3 | 129.95 |
| 4 | 170.82 |
| 5 | 182.42 |

Table 4.3: Experimental frequencies of engine pylon model by performing single shaker test (spectral test) with different level of forces.

| Run | Experimental Natural Frequencies (Hz) | | | | |
|---|---|---|---|---|---|
| | Mode 1 | Mode 2 | Mode 3 | Mode 4 | Mode 5 |
| R1(0.01V) | 20.31 | 58.59 | 135.96 | 175.39 | 190.02 |
| R2(0.05V) | 20.45 | 58.52 | 135.51 | 175.39 | 188.95 |
| R3(0.10V) | 20.24 | 58.24 | 135.34 | 174.66 | 188.21 |
| R4(0.15V) | 20.58 | 58.04 | 135.06 | 173.83 | 188.16 |
| R5(0.20V) | 20.50 | 57.95 | 134.86 | 173.26 | 187.49 |
| R6(0.25V) | 20.52 | 57.89 | 134.79 | 173.09 | 187.29 |
| R7(0.30V) | 20.19 | 57.82 | 134.63 | 173.21 | 186.33 |

Table 4.4: Experimental frequencies of engine pylon model by performing double shakers test (spectral test) with different level of forces.

| Run | Experimental Natural Frequencies (Hz) | | | | |
|---|---|---|---|---|---|
| | Mode 1 | Mode 2 | Mode 3 | Mode 4 | Mode 5 |
| R1(0.01V) | 23.10 | 59.82 | 149.32 | 175.49 | 203.25 |
| R2(0.05V) | 23.05 | 59.52 | 148.73 | 174.82 | 201.91 |
| R3(0.10V) | 22.99 | 59.26 | 148.27 | 174.04 | 201.06 |
| R4(0.15V) | 22.89 | 59.05 | 147.84 | 173.57 | 201.15 |
| R5(0.20V) | 22.87 | 58.94 | 147.82 | 173.29 | 200.82 |
| R6(0.25V) | 22.87 | 58.88 | 147.13 | 172.93 | 200.51 |
| R7(0.30V) | 22.83 | 58.85 | 146.52 | 172.75 | 200.17 |

Experimental mode shapes of the engine pylon substructure are depicted in Figure 4.10 to 4.13. The first mode shape of the engine pylon is a bending mode which is similar to a fixed-free cantilever beam mode. However, the second mode shape is a twisting mode. Then, the third and fourth modes are higher bending modes having different frequencies. It was found that the mode shapes from third mode and fourth mode are not the same shape in this modal test. This result was contradicted by the mode shape shown in Figure 4.12 and Figure 4.13 due to not enough or sufficient points of response to distinguish these two mode shapes.

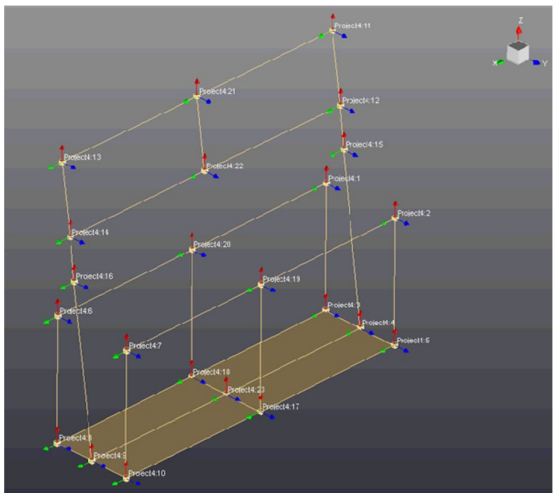

Figure 4.10: Mode Shape 1 Substructure of Engine Pylon – Bending Mode (Fixed-Free Boundary Condition)

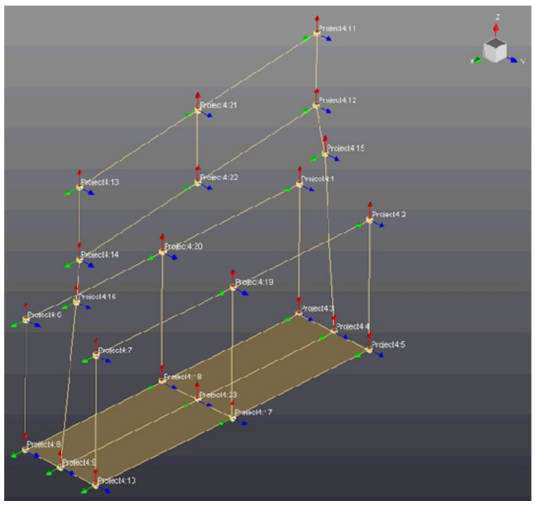

Figure 4.11: Mode Shape 2 Substructure of Engine Pylon – Twisting Mode (Fixed-Free Boundary Condition)

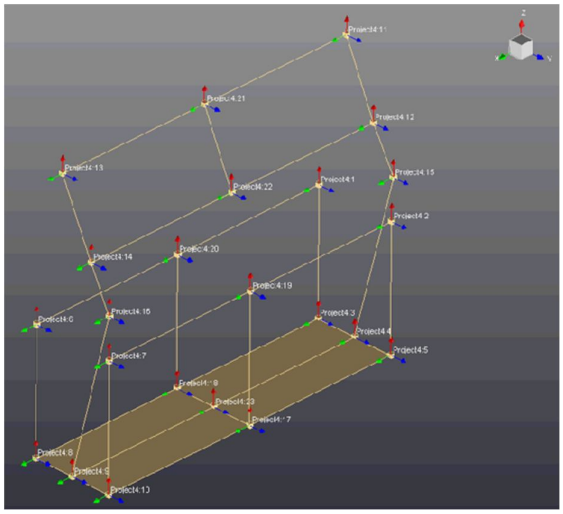

Figure 4.12: Mode Shape 3 Substructure of Engine Pylon – Bending Mode (Fixed-Free Boundary Condition)

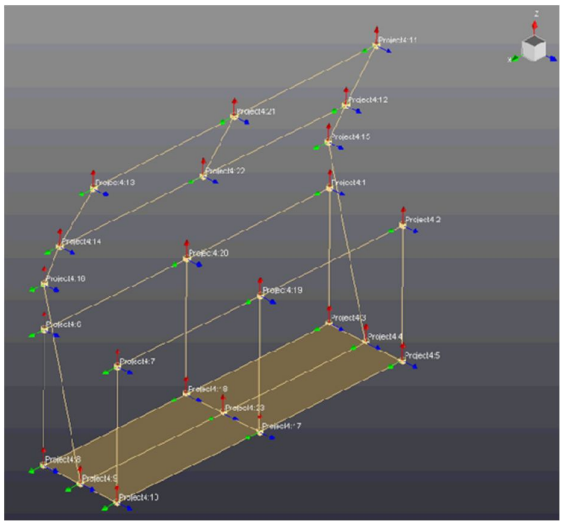

Figure 4.13: Mode Shape 4 Substructure of Engine Pylon – Bending Mode (Fixed-Free Boundary Condition)

## 4.5 Experimental Modal Analysis of Wing Structure

In this section, the procedures used to process experimental data of vibration responses of the wing substructure and the associated results are presented. This wing substructure is a plate without 2 pylons. Modal tests are conducted in order to predict the modal properties of the overall wing with pylons substructure. It would be very useful to be able to predict the modal properties of an assembled structure from those of its components. Figure 4.14 shows the wing model with free-free boundary configuration. The modal testing procedure by using an impact hammer test is applied.

Figure 4.14: Free-Free Boundary Condition of Substructure Wing Model

Figure 4.15 shows the wing substructure model in the LMS Data Acquisition System. In this modal test, roving accelerometers are used. Nine sets of accelerometers are used to measure the vibration responses at 33 points. These 33 points had been chosen in this experiment to ensure smooth mode shapes of the wing substructure can be obtained. If fewer locations are measured, the mode shapes of the substructure are difficult to depict. The aspect ratio of element this wing structure

is nearly 1:1. An aspect ratio is simply a figure that represents the width-to-length ratio of an element. The details of the accelerometer arrangements are highlighted in Table 4.5. All the accelerometers are roving over the plate and point 29 is the fixed excitation point of impact hammer (SN 12377) in the (-Z) direction.

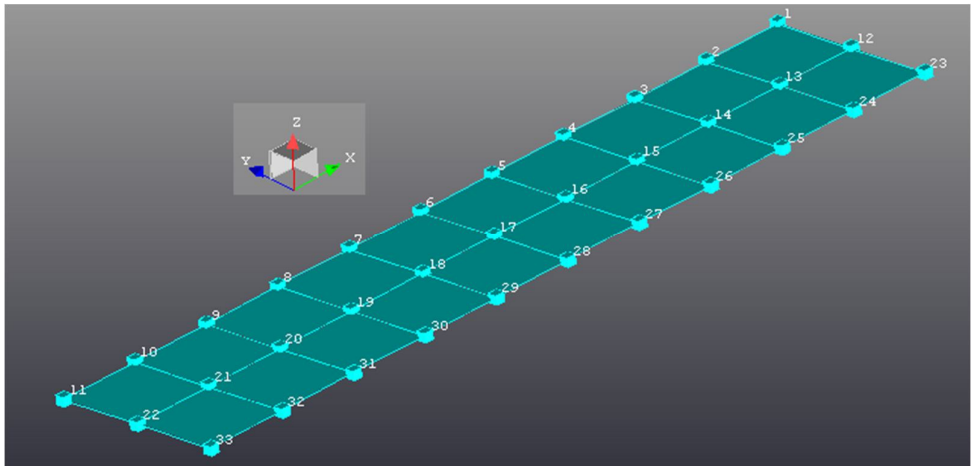


Figure 4.15: Substructure of Wing Model in LMS Data Acquisition System

Table 4.5: Id numbers of measuring points and measuring direction of wing substructure with roving accelerometers

| Series No. Accelerometers (Kistler) | Run | | | |
|---|---|---|---|---|
| | R1 | R2 | R3 | R4 |
| 2008887 | Point 1 in (-Z) | Point 4 in (-Z) | Point 7 in (-Z) | Point 10 in (-Z) |
| 2007226 | Point 23 in (-Z) | Point 15 in (-Z) | Point 18 in (-Z) | Point 21 in (-Z) |
| 2008890 | Point 12 in (-Z) | Point 26 in (-Z) | Point 29 in (-Z) | Point 32 in (-Z) |
| 2008893 | Point 2 in (-Z) | Point 5 in (-Z) | Point 8 in (-Z) | Point 11 in (-Z) |
| 2007224 | Point 13 in (-Z) | Point 16 in (-Z) | Point 19 in (-Z) | Point 22 in (-Z) |
| | Point 24 | Point 27 | Point 30 | Point 33 |

| | | | | |
|---|---|---|---|---|
| 2008895 | in (-Z) | in (-Z) | in (-Z) | in (-Z) |
| 2008888 | Point 3 in (-Z) | Point 6 in (-Z) | Point 9 in (-Z) | |
| 2008881 | Point 14 in (-Z) | Point 17 in (-Z) | Point 20 in (-Z) | |
| 2008891 | Point 25 in (-Z) | Point 28 in (-Z) | Point 31 in (-Z) | |

The frequency range of interest in this modal test is from 0 to 200 Hz. The first five measured natural frequencies of wing structure are shown in Table 4.6. Mode shapes of substructure wing are depicted in Figure 4.16 to 4.20

Table 4.6: Experimental frequencies of substructure of wing model by performing impact hammer test (roving accelerometer).

| Mode | Experimental Natural Frequencies (Hz) |
|---|---|
| 1 | 31.28 |
| 2 | 84.38 |
| 3 | 86.58 |
| 4 | 101.94 |
| 5 | 171.04 |

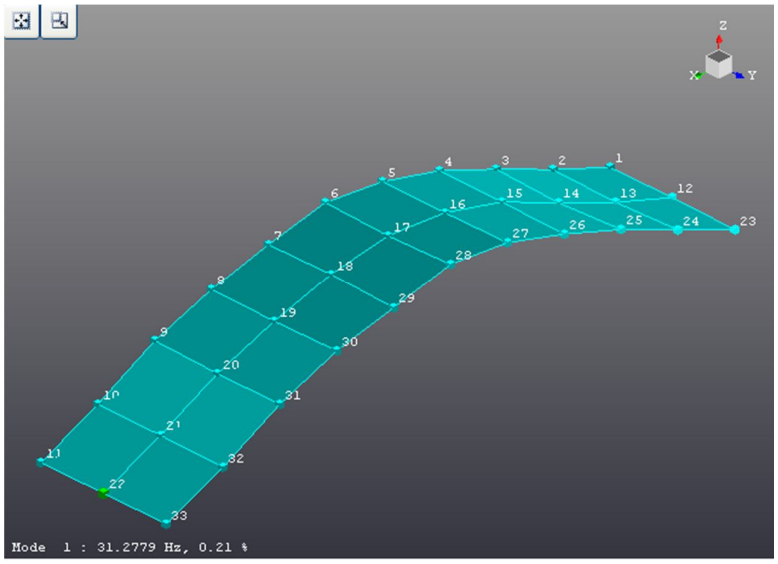


Figure 4.16: Mode Shape 1 Substructure of Wing – Bending Mode (Free-Free Boundary Condition)

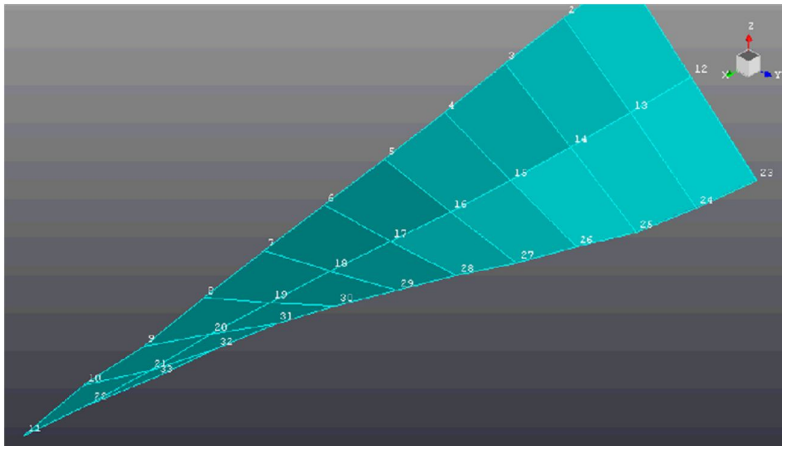

Figure 4.17: Mode Shape 2 Substructure of Wing – Twisting Mode
(Free-Free Boundary Condition)

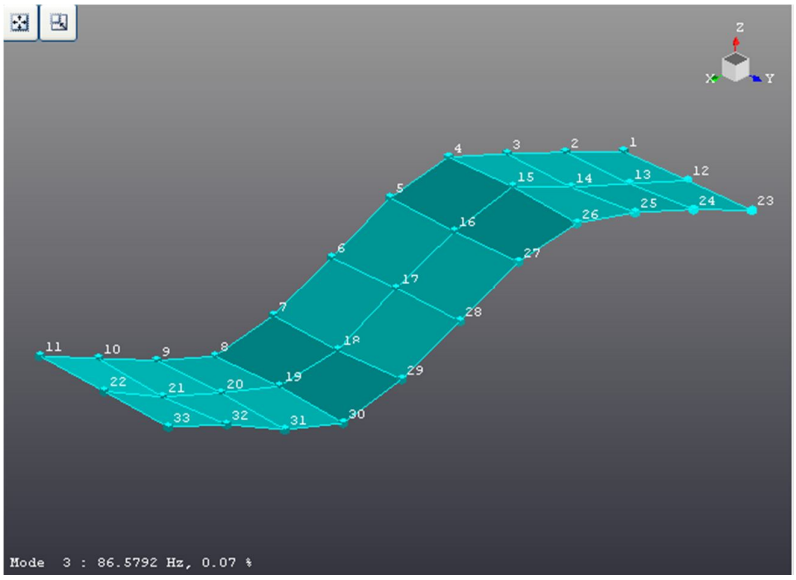


Figure 4.18: Mode Shape 3 Substructure of Wing – 2nd Bending Mode
(Free-Free Boundary Condition)

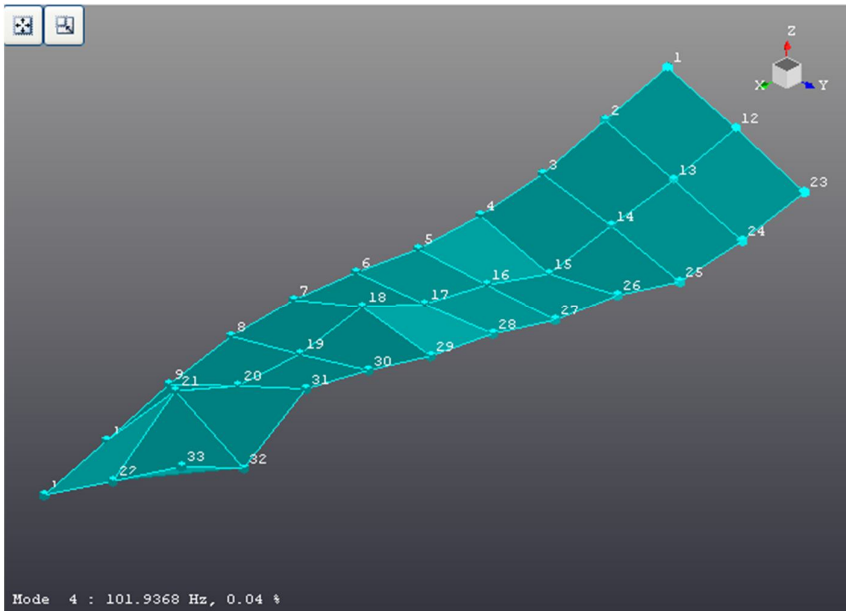


Figure 4.19: Mode Shape 4 Substructure of Wing – 2nd Twisting Mode (Free-Free Boundary Condition)

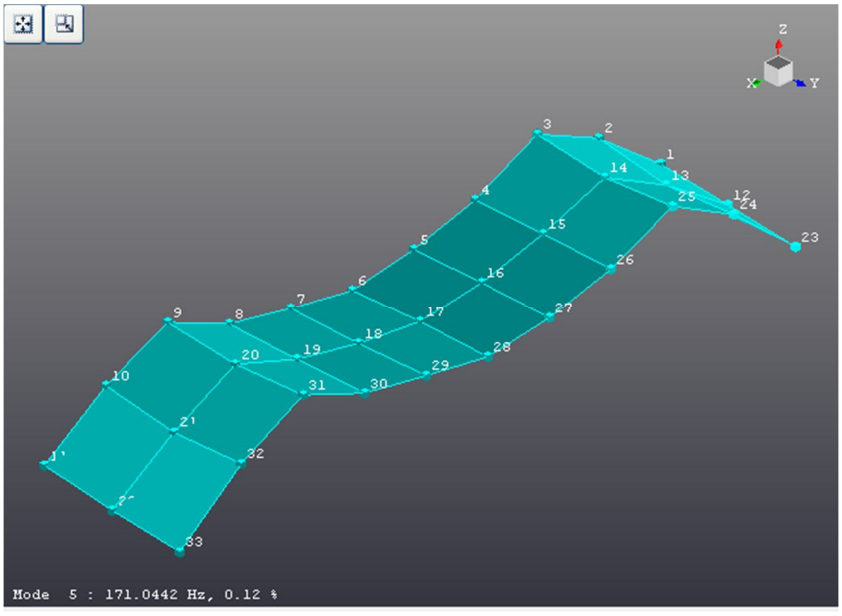


Figure 4.20: Mode Shape 5 Substructure of Wing – 3rd Bending Mode (Free-Free Boundary Condition)

## 4.6 Experimental Modal Analysis of Overall Wing Structure

The overall test structure used in this project is intended to represent roughly the configuration of an aircraft wing having two under-wing stores (for example: engine, fuel tanks etc.) with nonlinear pylon connection between them. Breitbach (1978) proposed that under-wing stores were able to introduce nonlinearities. The presence of an attached pylon brings in nonlinear kinematical terms in equation of motions of a cantilever wing (Brenan et al., 2004). Furthermore, Göge et al. (2005) presented Ground Vehicle Test (GVT) results showing that under-wing mounted-on pylons can exhibit free play in the yaw mode. Figure 4.21 shows the arrangement of the wing model, supported from a frame through bungee cords in a free-free boundary configuration. Two Data Physics V4 shakers were attached to the centerline of the wing via force transducers and driven by Data Physics power amplifiers. The objective of placing shaker below the structure is to excite and measure bending modes.

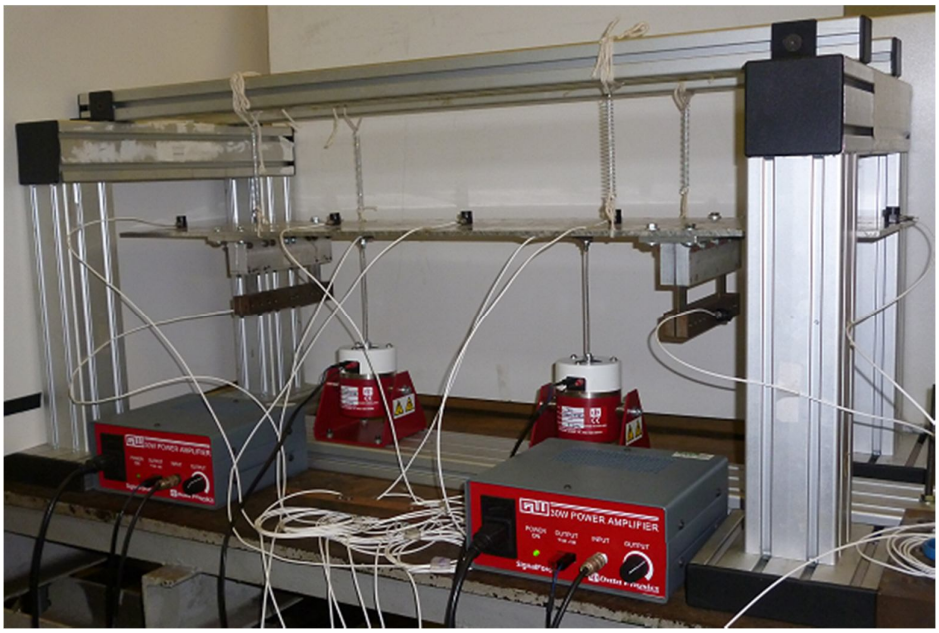


Figure 4.21: Overall Wing Structure Arrangement

Figure 4.22 shows the overall wing structure model in the LMS Data Acquisition System. In this modal test, double shaker using LMS Spectral testing is implemented. Two Data Physics V4 shakers are attached with stinger and force transducers which are located at point 21 and 25 of overall structure. Force transducer SN 20390 will excite at point 21 and another force transducer SN 10900 will excite at point 25. Both are excited in the Z direction. Nine accelerometers are roving to measure the vibration response at 72 points in (+Z) and X direction. The details of the accelerometer set up are presented in Table 4.7

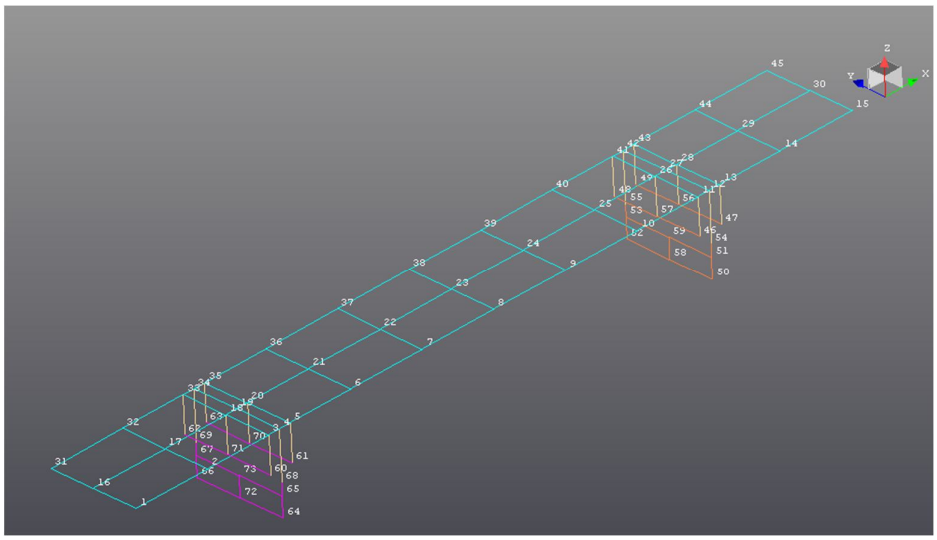

Figure 4.22: Overall Wing Structure Model in LMS Data Acquisition System

Table 4.7: Id numbers of measuring points and measuring direction of overall structure with roving accelerometers

| Series No. Accelerometers (Kistler) | Run | | | |
|---|---|---|---|---|
| | R1 | R2 | R3 | R4 |
| 2007026 | Point 1 in (+Z) | Point 4 in (+Z) | Point 7 in (+Z) | Point 10 in (+Z) |
| 2008868 | Point 16 in (+Z) | Point 19 in (+Z) | Point 22 in (+Z) | Point 25 in (+Z) |
| 2008871 | Point 31 in (+Z) | Point 34 in (+Z) | Point 37 in (+Z) | Point 40 in (+Z) |
| 2007015 | Point 2 in (+Z) | Point 5 in (+Z) | Point 8 in (+Z) | Point 11 in (+Z) |
| 2008866 | Point 17 in (+Z) | Point 20 in (+Z) | Point 23 in (+Z) | Point 26 in (+Z) |
| 2002825 | Point 32 in (+Z) | Point 35 in (+Z) | Point 38 in (+Z) | Point 41 in (+Z) |
| 2008864 | Point 3 in (+Z) | Point 6 in (+Z) | Point 9 in (+Z) | Point 12 in (+Z) |
| 2008888 | Point 18 in (+Z) | Point 21 in (+Z) | Point 24 in (+Z) | Point 27 in (+Z) |
| 2008881 | Point 33 in (+Z) | Point 36 in (+Z) | Point 39 in (+Z) | Point 42 in (+Z) |
| Series No. Accelerometers (Kistler) | R5 | R6 | R7 | R8 |
| 2007026 | Point 13 in (+Z) | Point 64 in (-Z) | Point 50 in ((-X)) | Point 51 in (-X) |
| 2008868 | Point 28 in (+Z) | Point 72 in (-X) | Point 58 in (-X) | Point 53 in (-X) |
| 2008871 | Point 43 in (+Z) | Point 66 in (-X) | Point 52 in (-X) | Point 54 in (-X) |
| 2007015 | Point 14 in (+Z) | Point 60 in (-X) | Point 46 in (-X) | Point 55 in (-X) |
| 2008866 | Point 29 in (+Z) | Point 71 in (-X) | Point 57 in (-X) | Point 59 in (-X) |
| 2002825 | Point 44 in (+Z) | Point 62 in (-X) | Point 48 in (-X) | Point 65 in (-X) |
| 2008864 | Point 15 in (+Z) | Point 61 in (-X) | Point 47 in (-X) | Point 67 in (-X) |
| 2008888 | Point 30 in (+Z) | Point 70 in (-X) | Point 56 in (-X) | Point 68 in (-X) |
| 2008881 | Point 45 in (+Z) | Point 63 in (-X) | Point 49 in (-X) | Point 69 in (-X) |

This double shaker modal test can lead to an estimate of the modal parameters of the underlying linear model. The natural frequencies, damping ratios, modal masses for the first five modes, extracted from FRF matrix using PolyMAX parameter estimation method are shown in Table 4.8. Figure 4.23 to 4.27 show the corresponding mode shapes. It can be concluded that the modes shapes are reasonably independent of excitation level. It turns out that modes 1, 3, and 5 are symmetric but modes 2 and 4 are anti-symmetric. Mode 1 shows that the wing displays bending in the Z direction of the wing and the two pylons moves in the opposite X direction. Mode 2 is most responsive to the difference in stiffness properties between two pylons which indicates levels of antisymmetric behaviour. Modes 1 and 2 characteristics display the highest level of bending between both pylons and give an indication of nonlinear behaviour. Mode 3 only shows large single bending on wing structure in the Z direction but medium displacement for both pylons in the X direction. In addition, mode 4 and 5 indicates double bending on the wing structure but a small displacement on both pylons in the X direction. It can be summarised that mode 3 shows less nonlinear behaviour for the force levels compared to mode 1 and 2. However, mode 4 and 5 shows that this mode only behaves with linear characteristics. The effective modal mass provides a way for determine the significance of a vibration mode. Modes with relatively high effective masses can be readily excited by base excitation. In contrast, modes with low effective masses cannot be readily excited in this manner. Total modal mass for first five modes of wing test structure is 8.18 kg. However overall mass for wing test structure is 8.55 kg. It is showed that the total effective modal mass of the wing structure is 95.7% of the actual overall mass.

Table 4.8: Experimental frequencies, damping ratio and modal mass of overall structure of wing model by performing double shaker test.

| Mode | Experimental Natural Frequencies (Hz) | Damping Ratio (%) | Modal Mass (kg) |
|---|---|---|---|
| 1 | 15.09 | 0.76 | 2.10 |
| 2 | 18.40 | 0.91 | 2.40 |
| 3 | 32.33 | 0.32 | 1.62 |
| 4 | 78.01 | 0.09 | 0.99 |
| 5 | 135.08 | 0.27 | 1.07 |

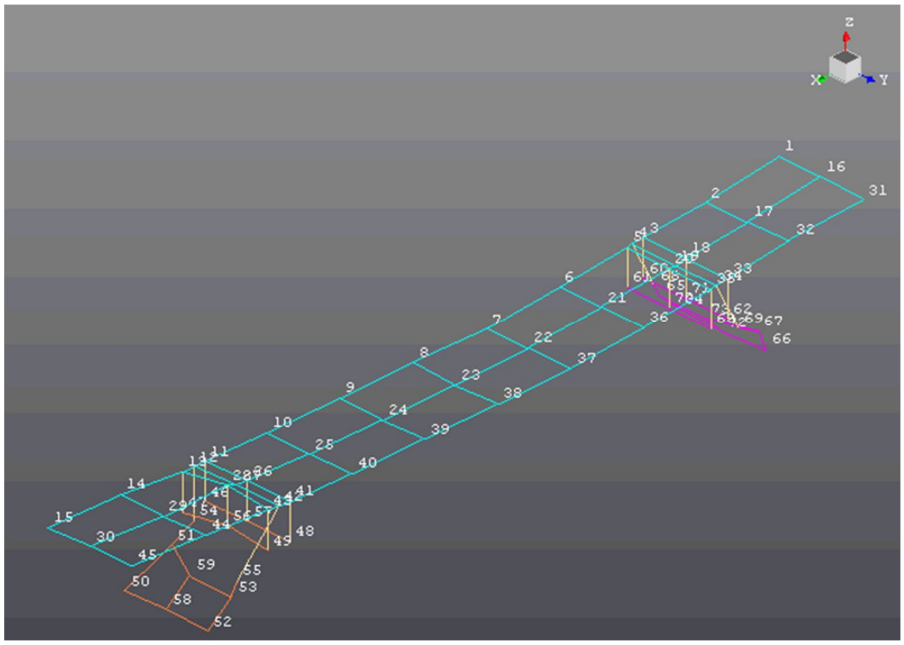


Figure 4.23: Mode Shape 1 Overall structure of Wing – Bending Mode at Z (wing) and X Direction on both pylons (Free-Free Boundary Condition)

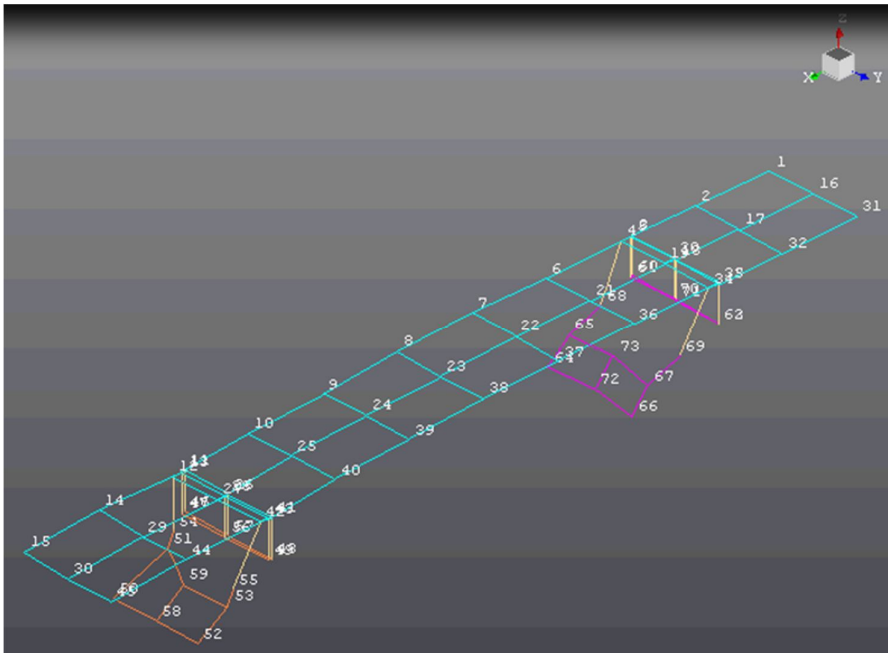

Figure 4.24: Mode Shape 2 Overall structure of Wing – Small Twisting Mode at Y (wing) and Bending mode at X Direction on both pylons (Free-Free Boundary Condition)

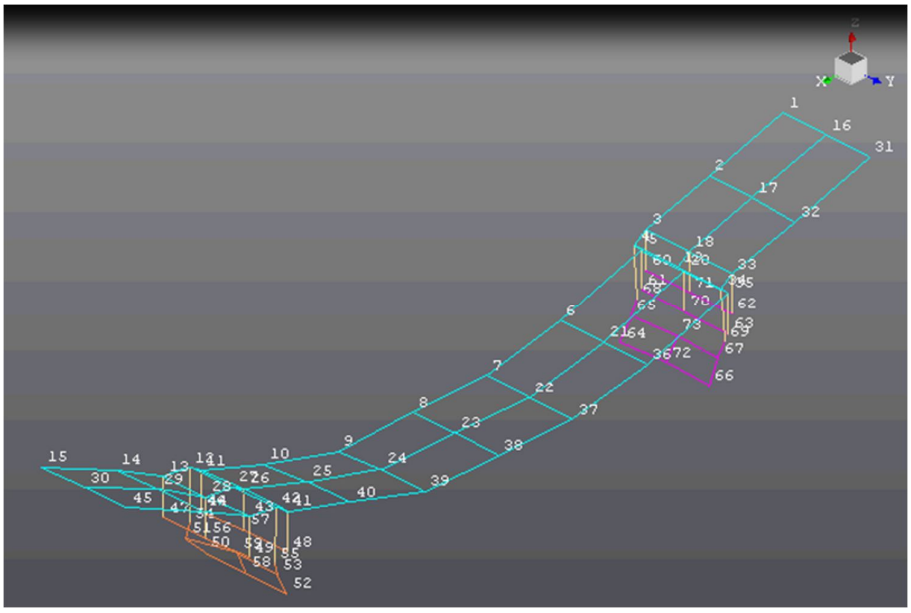

Figure 4.25: Mode Shape 3 Overall structure of Wing – Bending Mode at Z (wing) and X Direction on both pylons (Free-Free Boundary Condition)

Figure 4.26: Mode Shape 4 Overall structure of Wing – 2nd Bending Mode at Z (wing) and X Direction on both pylons (Free-Free Boundary Condition)

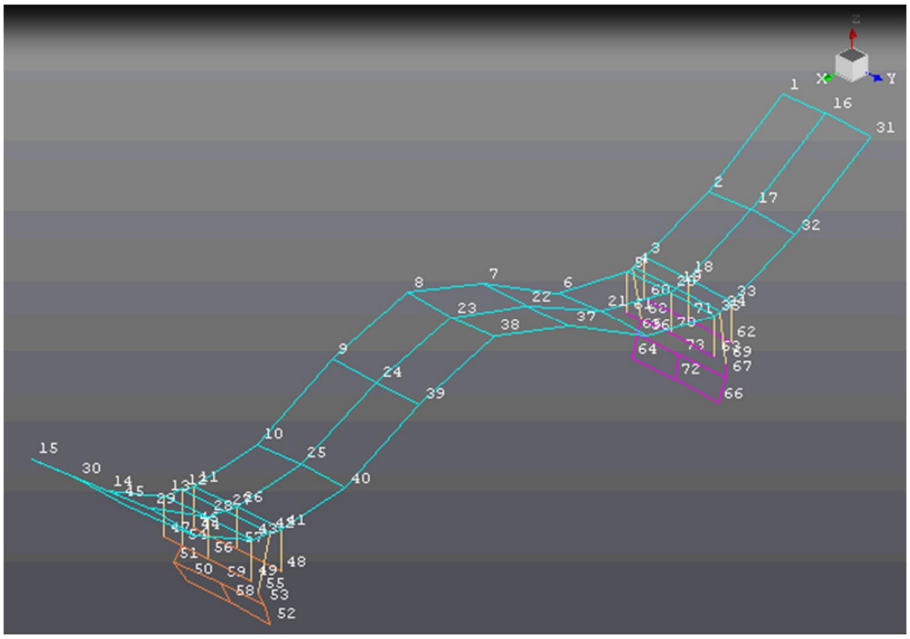

Figure 4.27: Mode Shape 5 Overall structure of Wing – 2nd Bending Mode at Z (wing) and X Direction on both pylons (Free-Free Boundary Condition)

## 4.7 MIMO Sine Sweep and Step Sine Testing

MIMO Sine Testing permits the measurement of data for use in modal analysis, operation deflection shapes and time animation. The excitation of the structure is a shaker input of a slowly sweeping sine tone a user defined frequency band. The data reduction uses a harmonic estimator to calculate FRF and coherence function. This FRF and coherence function data is needed when performing MIMO Normal Mode Test. However, the advantages of MIMO Sine Testing compared to random excitation in spectral acquisition are:

- Good signal to noise (S/N) ratio, leakage free acquisition which contributes high quality of FRF's.
- The possibility to excite highly damped structures.
- Fast acquisition procedure compared to using random excitation that requires a high number of averages.
- Ability to test nonlinear structures with precise control of force input levels.

MIMO sine sweep are performed on the single pylon and overall wing structure model using two shakers at several drive voltage levels. Natural frequencies at different levels of force for the first 5 modes are listed in Table 4.9 for engine pylon and Table 4.10 for overall structure.

Table 4.9: Experimental frequencies of engine pylon model by performing double shakers test (MIMO Sine Sweep and Step Sine) with different level of forces.

| Run | Experimental Natural Frequencies (Hz) | | | | |
|---|---|---|---|---|---|
| | Mode 1 | Mode 2 | Mode 3 | Mode 4 | Mode 5 |
| R1(0.01V) | 23.09 | 59.42 | 150.17 | 175.43 | 203.25 |
| R2(0.025V) | 22.92 | 58.95 | 149.34 | 174.09 | 202.04 |
| R3(0.05V) | 22.89 | 59.20 | 149.91 | 174.41 | 201.52 |
| R4(0.075V) | 22.88 | 59.06 | 149.15 | 173.24 | 200.05 |
| R5(0.10V) | 22.94 | 60.26 | 148.75 | 173.39 | 200.15 |
| R6(0.125V) | 22.96 | 61.13 | 147.78 | 172.99 | 199.22 |
| R7(0.15V) | 23.06 | 62.07 | 148.68 | 174.18 | 199.26 |

Table 4.10: Experimental frequencies of overall structure by performing double shakers test (MIMO Sine Sweep and Step Sine) with different level of forces.

| Run | Experimental Natural Frequencies (Hz) | | | | |
|---|---|---|---|---|---|
| | Mode 1 | Mode 2 | Mode 3 | Mode 4 | Mode 5 |
| R1(0.01V) | 14.62 | 17.39 | 31.94 | 77.82 | 134.83 |
| R2(0.025V) | 14.39 | 17.28 | 31.94 | 77.75 | 134.75 |
| R3(0.05V) | 14.74 | 17.50 | 31.92 | 77.72 | 134.66 |
| R4(0.075V) | 14.82 | 17.97 | 31.92 | 77.63 | 134.45 |
| R5(0.10V) | 14.88 | 17.09 | 31.89 | 77.57 | 134.40 |
| R6(0.125V) | 15.64 | 17.80 | 31.90 | 77.51 | 134.36 |
| R7(0.15V) | 15.88 | 18.53 | 31.94 | 77.45 | 134.29 |

## 4.8 MIMO Normal Mode Test

MIMO Normal Modes Testing presents multiple input and output phase appropriation techniques. It is designed to measure resonance frequency, damping and mode shapes of a structure. This testing automatically adjusts amplitude and phase of the forces injected into the structure to tune a single, normal vibration mode. The solution provides manual and automatic resonance tracking as well as force appropriation techniques. The frequency and forcing vector must be identified and applied in such a way that the complete structure vibrates only according to the desired mode and that all acceleration responses are in phase quadrature with the input force vector.

MIMO Normal Modes Testing also offers an intuitive way to define channel, acquisition, tuned modes and tuning parameters. In all stages, the user gets feedback on the parameters defined, so that the test setup can be maximally validated before the actual testing starts. Based on frequency response functions measured with either random or sine excitation, users can easily define the force ratio that needs to be applied for each mode. Manual tuning provides manual control of drive frequency and level. During actual measurements, all relevant information such as Lissajous

display, scatter diagram, mode indicator function, animated geometry and time data can be displayed and monitored online.

### 4.8.1 Result MIMO Normal Mode Test for Engine Pylon

MIMO normal mode test was performed on the single engine pylon using two shakers based on FRF measured data from MIMO sine testing. In this test, the experimental on arrangement of the engine pylon structure is the same as with the spectral testing as shown in Figure 4.8. This test drives at several levels of voltages. The excitation ratio and force ratio are shown mode by mode with different level of forces starting from Table 4.11 to Table 4.13. The results of MIMO normal mode test of engine pylon (refer to Table 4.11, 4.12 and 4.13) indicate that the force ratio is proportional to the excitation level (voltage value). It means that when higher level of excitation given, the value of force ratio also increase. Force ratio is important parameter in order to compute mathematical model in force appropriation method for each mode. Force realization is a special MIMO FRF-based control algorithm using singular value decomposition (SVD) for the FRF matrix inversions that provides high accuracy of the required force vector. The results also show the indication of all modes to show the status of the phase angle (excitation and force phase angle) with different level of excitation. This phase parameter is used for tuning iteration. When two shakers are used, the system can be programmed for the excitation to be in phase or 180° phase shifted (in opposition).

Table 4.11: Excitation and force ratio of engine pylon for first mode with different level of voltage.

| Mode 1 & 0.01 V | | | |
|---|---|---|---|
| Excitation Ratio | | Force Ratio | |
| Force (N) | 8.28E-03 | Channel ID | Project4:13:(-Y) |
| Phase (°) | 8.37E-16 | Ratio | 0.446 |
| Target Force (N) | 0.1 | Phase (°) | 84.24 |
| Target Phase (°) | 0 | Target Ratio | 1.48 |
| Mode 1 & 0.025 V | | | |
| Excitation Ratio | | Force Ratio | |
| Force (N) | 3.11E-02 | Channel ID | Project4:13:(-Y) |
| Phase (°) | -3.16E-15 | Ratio | 0.639 |
| Target Force (N) | 0.1 | Phase (°) | -176.12 |
| Target Phase (°) | 0 | Target Ratio | 1.43 |
| Mode 1 & 0.05 V | | | |
| Excitation Ratio | | Force Ratio | |
| Force (N) | 9.05E-03 | Channel ID | Project4:13:(-Y) |
| Phase (°) | -1.94E-15 | Ratio | 0.654 |
| Target Force (N) | 0.1 | Phase (°) | -171.04 |
| Target Phase (°) | 0 | Target Ratio | 1.12 |
| Mode 1 & 0.075 V | | | |
| Excitation Ratio | | Force Ratio | |
| Force (N) | 1.24E-02 | Channel ID | Project4:13:(-Y) |
| Phase (°) | 4.75E-15 | Ratio | 0.71 |
| Target Force (N) | 0.1 | Phase (°) | 146.30 |
| Target Phase (°) | 0 | Target Ratio | 1.12 |
| Mode 1 & 0.1 V | | | |
| Excitation Ratio | | Force Ratio | |
| Force (N) | 2.40E-02 | Channel ID | Project4:13:(-Y) |
| Phase (°) | 1.63E-15 | Ratio | 0.78 |

| | | | |
|---|---|---|---|
| Target Force (N) | 0.1 | Phase (°) | -169.34 |
| Target Phase (°) | 0 | Target Ratio | 1.11 |
| Mode 1 & 0.125 V | | | |
| Excitation Ratio | | Force Ratio | |
| Force (N) | 2.31E-02 | Channel ID | Project4:13:(-Y) |
| Phase (°) | -9.73E-15 | Ratio | 1.09 |
| Target Force (N) | 0.1 | Phase (°) | -174.34 |
| Target Phase (°) | 0 | Target Ratio | 1.11 |
| Mode 1 & 0.15 V | | | |
| Excitation Ratio | | Force Ratio | |
| Force (N) | 9.72E-03 | Channel ID | Project4:13:(-Y) |
| Phase (°) | 1.05E-14 | Ratio | 1.26 |
| Target Force (N) | 0.1 | Phase (°) | 171.36 |
| Target Phase (°) | 0 | Target Ratio | 1.10 |

Table 4.12: Excitation and force ratio of engine pylon for second mode with different level of voltage.

| | | | |
|---|---|---|---|
| Mode 2 & 0.01 V | | | |
| Excitation Ratio | | Force Ratio | |
| Force (N) | 8.62E-3 | Channel ID | Project4:13:(-Y) |
| Phase (°) | 6.68E-15 | Ratio | 0.90 |
| Target Force (N) | 0.1 | Phase (°) | -5.02 |
| Target Phase (°) | 0 | Target Ratio | -1.02 |
| Mode 2 & 0.025 V | | | |
| Excitation Ratio | | Force Ratio | |
| Force (N) | 1.55E-2 | Channel ID | Project4:13:(-Y) |
| Phase (°) | -3.70E-17 | Ratio | 1.01 |
| Target Force (N) | 0.1 | Phase (°) | -0.56 |
| Target Phase (°) | 0 | Target Ratio | -0.92 |

| Mode 2 & 0.05 V | | | |
|---|---|---|---|
| Excitation Ratio | | Force Ratio | |
| Force (N) | 1.02E-2 | Channel ID | Project4:13:(-Y) |
| Phase (°) | -2.03E-15 | Ratio | 1.18 |
| Target Force (N) | 0.1 | Phase (°) | -2.80 |
| Target Phase (°) | 0 | Target Ratio | -0.91 |
| Mode 2 & 0.075 V | | | |
| Excitation Ratio | | Force Ratio | |
| Force (N) | 9.10E-3 | Channel ID | Project4:13:(-Y) |
| Phase (°) | 1.74E-15 | Ratio | 1.23 |
| Target Force (N) | 0.1 | Phase (°) | -0.13 |
| Target Phase (°) | 0 | Target Ratio | -0.92 |
| Mode 2 & 0.1 V | | | |
| Excitation Ratio | | Force Ratio | |
| Force (N) | 1.48E-2 | Channel ID | Project4:13:(-Y) |
| Phase (°) | -1.69E-15 | Ratio | 1.29 |
| Target Force (N) | 0.1 | Phase (°) | -5.00 |
| Target Phase (°) | 0 | Target Ratio | -0.95 |
| Mode 2 & 0.125 V | | | |
| Excitation Ratio | | Force Ratio | |
| Force (N) | 1.25E-2 | Channel ID | Project4:13:(-Y) |
| Phase (°) | 1.15E-15 | Ratio | 1.32 |
| Target Force (N) | 0.1 | Phase (°) | -2.00 |
| Target Phase (°) | 0 | Target Ratio | -0.98 |
| Mode 2 & 0.15 V | | | |
| Excitation Ratio | | Force Ratio | |
| Force (N) | 1.72E-2 | Channel ID | Project4:13:(-Y) |
| Phase (°) | -1.47E-15 | Ratio | 1.35 |
| Target Force (N) | 0.1 | Phase (°) | 9.28 |
| Target Phase (°) | 0 | Target Ratio | 0.65 |

Table 4.13: Excitation and force ratio of engine pylon for third mode with different level of voltage.

| Mode 3 & 0.01 V | | | |
|---|---|---|---|
| Excitation Ratio | | Force Ratio | |
| Force (N) | 4.05E-3 | Channel ID | Project4:13:(-Y) |
| Phase (°) | 6.32E-16 | Ratio | 0.17 |
| Target Force (N) | 0.1 | Phase (°) | -147.17 |
| Target Phase (°) | 0 | Target Ratio | 1.62 |
| Mode 3 & 0.025 V | | | |
| Excitation Ratio | | Force Ratio | |
| Force (N) | 8.70E-3 | Channel ID | Project4:13:(-Y) |
| Phase (°) | 2.67E-16 | Ratio | 0.74 |
| Target Force (N) | 0.1 | Phase (°) | -102.85 |
| Target Phase (°) | 0 | Target Ratio | -0.92 |
| Mode 3 & 0.05 V | | | |
| Excitation Ratio | | Force Ratio | |
| Force (N) | 1.39E-2 | Channel ID | Project4:13:(-Y) |
| Phase (°) | 2.93E-15 | Ratio | 0.95 |
| Target Force (N) | 0.1 | Phase (°) | 159.30 |
| Target Phase (°) | 0 | Target Ratio | 1.13 |
| Mode 3 & 0.075 V | | | |
| Excitation Ratio | | Force Ratio | |
| Force (N) | 7.73E-2 | Channel ID | Project4:13:(-Y) |
| Phase (°) | 5.86E-15 | Ratio | 1.14 |
| Target Force (N) | 0.1 | Phase (°) | -171.87 |
| Target Phase (°) | 0 | Target Ratio | 0.72 |
| Mode 3 & 0.1 V | | | |
| Excitation Ratio | | Force Ratio | |
| Force (N) | 1.66E-2 | Channel ID | Project4:13:(-Y) |
| Phase (°) | 7.69E-15 | Ratio | 1.55 |

| | | | |
|---|---|---|---|
| Target Force (N) | 0.1 | Phase (°) | 37.75 |
| Target Phase (°) | 0 | Target Ratio | 0.67 |
| Mode 3 & 0.125 V | | | |
| Excitation Ratio | | Force Ratio | |
| Force (N) | 6.81E-3 | Channel ID | Project4:13:(-Y) |
| Phase (°) | 7.33E-15 | Ratio | 1.72 |
| Target Force (N) | 0.1 | Phase (°) | 159.23 |
| Target Phase (°) | 0 | Target Ratio | 0.65 |
| Mode 3 & 0.15 V | | | |
| Excitation Ratio | | Force Ratio | |
| Force (N) | 2.31E-3 | Channel ID | Project4:13:(-Y) |
| Phase (°) | -2.61E-15 | Ratio | 2.29 |
| Target Force (N) | 0.1 | Phase (°) | -48.43 |
| Target Phase (°) | 0 | Target Ratio | 0.66 |

### 4.8.2 Result MIMO Normal Mode Test for Overall Wing Structure

MIMO normal mode tests were performed on the single engine pylon using two shakers based on FRF measured data on MIMO sine testing. In this test, the experimental arrangement of the overall wing structure is the same as with the spectral testing as shown in Figure 4.21. This test drives at several levels of voltages. The excitation ratio and force ratio are shown mode by mode with different level of forces starting from Table 4.14 to Table 4.16. The results of MIMO normal mode test of overall wing structure (refer to Table 4.14, 4.15 and 4.16) point out that the force ratio is proportional to the excitation level (voltage value). It means that the higher level of excitation given, the value of force ratio also increases. Force ratio is key parameter in order to compute mathematical model in force appropriation method for each mode in matlab programming. This force realisation is a special MIMO FRF-based control algorithm using singular value decomposition (SVD) for the FRF matrix inversions that provides high accuracy of the required force vector.

The results also indicate the representation of all modes to show the status of the phase angle (excitation and force phase angle) with different level of excitation. This phase parameter is used for tuning iteration. When two shakers are used, the system can be programmed for the excitation to be in phase or 180° phase shifted (in opposition).

Table 4.14: Excitation and force ratio of overall wing structure for first mode with different level of voltage.

| Mode 1 & 0.01 V | | | |
|---|---|---|---|
| Excitation Ratio | | Force Ratio | |
| Force (N) | 3.42E-01 | Channel ID | Project8:47:(+Z) |
| Phase (°) | -1.58E-15 | Ratio | 0.82 |
| Target Force (N) | 0.1 | Phase (°) | -0.39 |
| Target Phase (°) | 0 | Target Ratio | 1.14 |
| Mode 1 & 0.025 V | | | |
| Excitation Ratio | | Force Ratio | |
| Force (N) | 2.83E-01 | Channel ID | Project8:47:(+Z) |
| Phase (°) | -3.80E-15 | Ratio | 0.83 |
| Target Force (N) | 0.1 | Phase (°) | -0.85 |
| Target Phase (°) | 0 | Target Ratio | 1.11 |
| Mode 1 & 0.05 V | | | |
| Excitation Ratio | | Force Ratio | |
| Force (N) | 3.71E-01 | Channel ID | Project8:47:(+Z) |
| Phase (°) | 3.55E-15 | Ratio | 0.87 |
| Target Force (N) | 0.1 | Phase (°) | -0.46 |
| Target Phase (°) | 0 | Target Ratio | 1.05 |
| Mode 1 & 0.075 V | | | |
| Excitation Ratio | | Force Ratio | |
| Force (N) | 2.12E-02 | Channel ID | Project8:47:(+Z) |
| Phase (°) | 7.79E-15 | Ratio | 0.95 |

| | | | |
|---|---|---|---|
| Target Force (N) | 0.1 | Phase (°) | -21.19 |
| Target Phase (°) | 0 | Target Ratio | 1.10 |
| Mode 1 & 0.1 V | | | |
| Excitation Ratio | | Force Ratio | |
| Force (N) | 1.50E-01 | Channel ID | Project8:47:(+Z) |
| Phase (°) | 1.29E-15 | Ratio | 0.91 |
| Target Force (N) | 0.1 | Phase (°) | -0.96 |
| Target Phase (°) | 0 | Target Ratio | 1.45 |
| Mode 1 & 0.125 V | | | |
| Excitation Ratio | | Force Ratio | |
| Force (N) | 6.99E-02 | Channel ID | Project8:47:(+Z) |
| Phase (°) | -5.24E-15 | Ratio | 0.96 |
| Target Force (N) | 0.1 | Phase (°) | 0.96 |
| Target Phase (°) | 0 | Target Ratio | 1.49 |
| Mode 1 & 0.15 V | | | |
| Excitation Ratio | | Force Ratio | |
| Force (N) | 7.88E-02 | Channel ID | Project8:47:(+Z) |
| Phase (°) | -1.84E-15 | Ratio | 0.99 |
| Target Force (N) | 0.1 | Phase (°) | 0.01 |
| Target Phase (°) | 0 | Target Ratio | 1.34 |

Table 4.15: Excitation and force ratio of overall wing structure for second mode with different level of voltage.

| | | | |
|---|---|---|---|
| Mode 2 & 0.01 V | | | |
| Excitation Ratio | | Force Ratio | |
| Force (N) | 1.81E-02 | Channel ID | Project8:47:(+Z) |
| Phase (°) | -2.78E-15 | Ratio | 0.73 |
| Target Force (N) | 0.1 | Phase (°) | -1.89 |
| Target Phase (°) | 0 | Target Ratio | -1.29 |

| Mode 2 & 0.025 V | | | |
|---|---|---|---|
| Excitation Ratio | | Force Ratio | |
| Force (N) | 1.21E-01 | Channel ID | Project8:47:(+Z) |
| Phase (°) | 6.87E-15 | Ratio | 0.77 |
| Target Force (N) | 0.1 | Phase (°) | -0.80 |
| Target Phase (°) | 0 | Target Ratio | -1.22 |
| Mode 2 & 0.05 V | | | |
| Excitation Ratio | | Force Ratio | |
| Force (N) | 9.56E-02 | Channel ID | Project8:47:(+Z) |
| Phase (°) | 1.11E-14 | Ratio | 0.79 |
| Target Force (N) | 0.1 | Phase (°) | 8.45 |
| Target Phase (°) | 0 | Target Ratio | -0.65 |
| Mode 2 & 0.075 V | | | |
| Excitation Ratio | | Force Ratio | |
| Force (N) | 1.63E-02 | Channel ID | Project8:47:(+Z) |
| Phase (°) | 5.72E-15 | Ratio | 0.89 |
| Target Force (N) | 0.1 | Phase (°) | 172.67 |
| Target Phase (°) | 0 | Target Ratio | -1.11 |
| Mode 2 & 0.1 V | | | |
| Excitation Ratio | | Force Ratio | |
| Force (N) | 8.85E-01 | Channel ID | Project8:47:(+Z) |
| Phase (°) | -1.07E-14 | Ratio | 0.95 |
| Target Force (N) | 0.1 | Phase (°) | -0.29 |
| Target Phase (°) | 0 | Target Ratio | 1.12 |
| Mode 2 & 0.125 V | | | |
| Excitation Ratio | | Force Ratio | |
| Force (N) | 3.32E-01 | Channel ID | Project8:47:(+Z) |
| Phase (°) | 2.98E-16 | Ratio | 0.990 |
| Target Force (N) | 0.1 | Phase (°) | -1.38 |
| Target Phase (°) | 0 | Target Ratio | 1.10 |

| Mode 2 & 0.15 V | | | |
|---|---|---|---|
| Excitation Ratio | | Force Ratio | |
| Force (N) | 3.73E-02 | Channel ID | Project8:47:(+Z) |
| Phase (°) | -5.57E-15 | Ratio | 1.08 |
| Target Force (N) | 0.1 | Phase (°) | -178.88 |
| Target Phase (°) | 0 | Target Ratio | -0.42 |

Table 4.16: Excitation and force ratio of overall wing structure for third mode with different level of voltage.

| Mode 3 & 0.01 V | | | |
|---|---|---|---|
| Excitation Ratio | | Force Ratio | |
| Force (N) | 6.07E-04 | Channel ID | Project8:47:(+Z) |
| Phase (°) | -3.06E-15 | Ratio | 0.853 |
| Target Force (N) | 0.1 | Phase (°) | 122.68 |
| Target Phase (°) | 0 | Target Ratio | 1.07 |
| Mode 3 & 0.025 V | | | |
| Excitation Ratio | | Force Ratio | |
| Force (N) | 5.95E-03 | Channel ID | Project8:47:(+Z) |
| Phase (°) | -7.58E-15 | Ratio | 0.89 |
| Target Force (N) | 0.1 | Phase (°) | -2.64 |
| Target Phase (°) | 0 | Target Ratio | 1.09 |
| Mode 3 & 0.05 V | | | |
| Excitation Ratio | | Force Ratio | |
| Force (N) | 8.88E-03 | Channel ID | Project8:47:(+Z) |
| Phase (°) | -6.86E-16 | Ratio | 0.98 |
| Target Force (N) | 0.1 | Phase (°) | 35.17 |
| Target Phase (°) | 0 | Target Ratio | 1.10 |
| Mode 3 & 0.075 V | | | |
| Excitation Ratio | | Force Ratio | |

| | | | |
|---|---|---|---|
| Force (N) | 1.94E-02 | Channel ID | Project8:47:(+Z) |
| Phase (°) | -8.14E-16 | Ratio | 1.07 |
| Target Force (N) | 0.1 | Phase (°) | -3.15 |
| Target Phase (°) | 0 | Target Ratio | 1.06 |
| Mode 3 & 0.1 V | | | |
| Excitation Ratio | | Force Ratio | |
| Force (N) | 7.07E-03 | Channel ID | Project8:47:(+Z) |
| Phase (°) | -1.45E-15 | Ratio | 1.09 |
| Target Force (N) | 0.1 | Phase (°) | -16.29 |
| Target Phase (°) | 0 | Target Ratio | 1.09 |
| Mode 3 & 0.125 V | | | |
| Excitation Ratio | | Force Ratio | |
| Force (N) | 1.46E-02 | Channel ID | Project8:47:(+Z) |
| Phase (°) | -3.15E-15 | Ratio | 1.13 |
| Target Force (N) | 0.1 | Phase (°) | -12.20 |
| Target Phase (°) | 0 | Target Ratio | 1.09 |
| Mode 3 & 0.15 V | | | |
| Excitation Ratio | | Force Ratio | |
| Force (N) | 5.88E-03 | Channel ID | Project8:47:(+Z) |
| Phase (°) | 1.26E-14 | Ratio | 1.18 |
| Target Force (N) | 0.1 | Phase (°) | -24.33 |
| Target Phase (°) | 0 | Target Ratio | 1.09 |

## 4.9 Summary

Experimental modal analysis (EMA) has been explained and discussed in this chapter. Impact hammer, single shaker (spectral test), double shaker (spectral test), MIMO sine sweep and step sine testing and MIMO normal mode testing are used in EMA to extract modal properties and other parameters. In linear analysis, it is sufficient to conduct EMA with impact hammer or single shaker (spectral) test of the structure. Meanwhile for nonlinear analysis, MIMO sine sweep and step sine testing and MIMO normal mode testing are used in modal test to determine the excitation ratio and force ratio mode by mode with different level of forces. Furthermore, in the time domains in the MIMO normal mode test it is vital to compute the coefficient in the restoring force method in order to identify nonlinearlities.

# Chapter 5

# Finite Element Analysis and Model Updating of Structures

## 5.1 Introduction

Finite Element (FE) methods are widely used in engineering analysis especially in structural dynamics. Therefore, development of FE methods has become more significant and parallel with growing capabilities of computing facilities. This effort can reduce or eliminate traditional design phases including testing product prototypes due to demands of a reduced time to market among product manufacturers. In order to meet the demands, increasing use of analysis in engineering problems has been accomplished. FE methods are largely employed for linear and nonlinear analyses, and the simulations of highly nonlinear events are of much interest (Bathe, 2007; Zienkiewicz and Taylor, 2005).

Validation of FE models are performed by carrying out experimental modal tests. This validation is very crucial in order to make sure that measured modal properties (i.e., natural frequencies and modes) are close to numerical results. The comparison between FE and modal test data usually reveals some discrepancies which normally stem from uncertainties in the governing equations of the system, mainly due to assumptions, nonlinearity and inaccurate boundary conditions applied to the structure. Ahmadian et al. (2006), Mottershead et al. (2006) and Palmonella (2003) found important differences between the initial numerical frequencies and their modal test results when investigating different types of joints. Most of these cases demonstrate that FE models have to be modified or updated in order to reduce the discrepancies.

Finite element updating has been intensively investigated by many researchers in the past decades to improve the accuracy and quality of finite element models of structures using modal test data. Most researchers who work on model updating methods use the experimental data as a reference for updating selected parameters for the purpose of minimize the differences between the experimental and numerical modal data. Nevertheless, the data measured from experiments are always incomplete since it is impossible to capture all the vibration modes and all points of a single mode during experiments, especially in large scale and complicated structures (Ewins, 2000; Friswell and Mottershead, 1995; Kenigsbuch and Halevi, 1998).

In this chapter, finite element result of engine pylon and overall structure are discussed in detail. Furthermore, model updating is performed to minimize the discrepancies between numerical and experimental results.

## 5.2 FE Modelling and Model Updating

The FE model is most suitable for analysing the behaviour of structures. In the FE analysis, structures are discretized into a finite number of elements such as beam, shells, membrane etc. that are defined by known material properties and boundary condition. Consequently, global mass and stiffness matrices of a model can be easily computed, irrespective of the complexity of the structure. These matrices can then be used to construct a set of second order differential equations in matrix form (Eq. (5.1), which may be solved for estimating dynamic response of the structure.

$$\mathbf{M}\ddot{\mathbf{x}} + \mathbf{C}\dot{\mathbf{x}} + \mathbf{K}\mathbf{x} = \boldsymbol{f}(\boldsymbol{t}) \tag{5.1}$$

with **M**, **C** and **K** represent the assembled *n*x*n* mass, damping and stiffness matrices of the structure, while $\ddot{\mathbf{x}}$ , $\dot{\mathbf{x}}$ and **x** are *n*x1 accelerations, velocities and displacements.

Many researchers have performed FE model updating on structural joints in mechanical structures. Kim et al. (1989), and Arruda and Santos (1993) conducted the FE model updating of structures with mechanical joints for identification of the joint properties (stiffness and damping). Mottershead et al. (2006) applied the model updating technique to converge a set of analytical models upon a set of nominally identical physical structures welded with spot weld joints. Another paper by Mottershead et al. (2000) investigated a three-storey aluminium space frame, using five model updating experiments with different sets of updating parameters in order to obtain a physical improvement to the modelling of the joints provided by standard Meroform aluminium nodes. Palmonella et al. (2003) updated three different FE models of spot weld joints to improve the accuracy of these models by searching for the optimum values of the parameters characterising the spot weld models using experimental data. There are also many other reported works on FE model updating applications in different types of structures.

## 5.3 FE Modelling and Normal Mode Analysis of Structures

The FE model of a single engine pylon is initially modelled by using MD NASTRAN which consists of 152 solid elements (CHEXA) and 20 plate/shell elements (CQUAD4) as shown in Figure 5.1.

CHEXA element is a brick element with six faces, and eight nodes each having three DOF's in translation. However, there are five DOF's at each node of the CQUAD4 elements, with zero stiffness for rotational DOF about the surface normal of the elements. There are 550 nodes in this model. A fixed boundary condition is applied at all nodes at the base of the model. Other nodes are in free-free boundary condition.

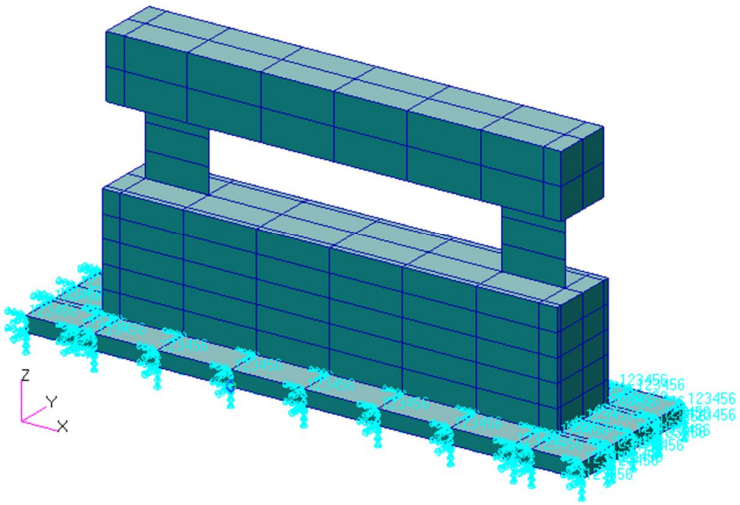


Figure 5.1: FE model of single pylon

In this project, the challenge is to model the gap of the pylon which contributes to nonlinear stiffness. The gap of the pylon is the space between two blocks of the engine pylon as shown in Figure 5.2. In this clamp, the pylon plates become shorter and stiffer as this structure is deflected laterally. This gap of the pylon is designed to exhibit nonlinear characteristics of the structure. Initially, Breitbach (1973) reported that the pylon can introduce nonlinearities and recently how the pylon introduces nonlinear kinematical terms in the equations of motion of a cantilever wings was investigated by Beran et al. (2004). Furthermore, Göge et al. (2005) presented the result from ground vehicle testing (GVT) that underwing engines mounted on pylons can exhibit free play nonlinearities type in yaw mode.

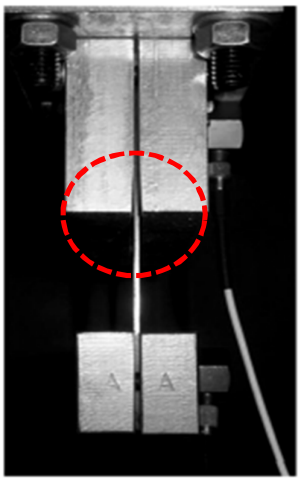

Figure 5.2: Gap design of pylon clamp arrangement.

Figure 5.3 shows a two dimensional view of the FE model of single pylon with fixed boundary condition at the bottom. It is very difficult to know exact location which the flat plates are in contact with the engine-pylon components or block. Equivalent nodes level by level is simulated through MSC NASTRAN/PATRAN to identify which ranges of natural frequencies from numerical results are close to experimental results. Level by level equivalent node models can be defined in the Table 5.1.

As the 'anchor' of the flat plates of the pylon is V-shaped (see the red circle in Fig. 5.2), the location (the z-coordinate) where the clamped boundary for the flat plates starts is not known. So different horizontal nodal lines (called levels in Fig. 5.3) are assumed to be the start of the clamped boundary respectively in the simulation and the predicted frequencies are compared experimental frequencies in the hope of locating the right location of the clamped boundary. In order to describe these results, the corresponding FE models are given different model numbers in Table 5.1.

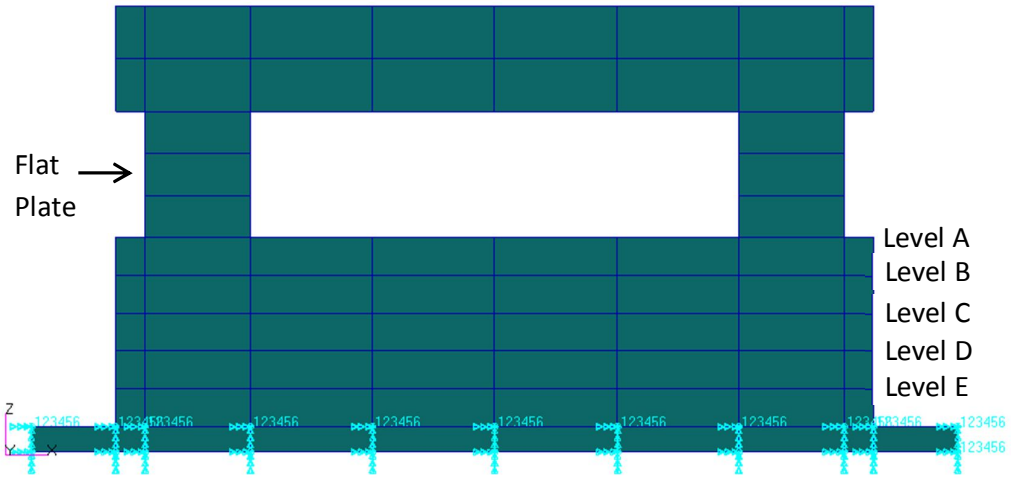


Figure 5.3: Two Dimensional FE model of single pylon

Table 5.1: Node equivalent level by level description

| Model | Description |
|---|---|
| Model 1 | All nodes are equivalent at all levels |
| Model 2 | All nodes are equivalent except nodes at Level A |
| Model 3 | All nodes are equivalent except nodes at Level A and B |
| Model 4 | All nodes are equivalent except nodes at Level A, B and C |
| Model 5 | All nodes are equivalent except nodes at Level A, B, C and D |

Two engine pylons are designed and attached to a rectangular wing structure. The FE model of the wing structure is shown in Figure 5.4 which consists of 852 solid elements (CHEXA) and 40 plate elements (CQUAD4). There are 1824 nodes and a free-free boundary condition is applied to this model. The materials of engine solid elements, pylon solid elements, and plate elements are respectively mild steel, aluminium and stainless steel and their nominal material properties values are used, as tabulated in Table 5.2, 5.3 and 5.4.

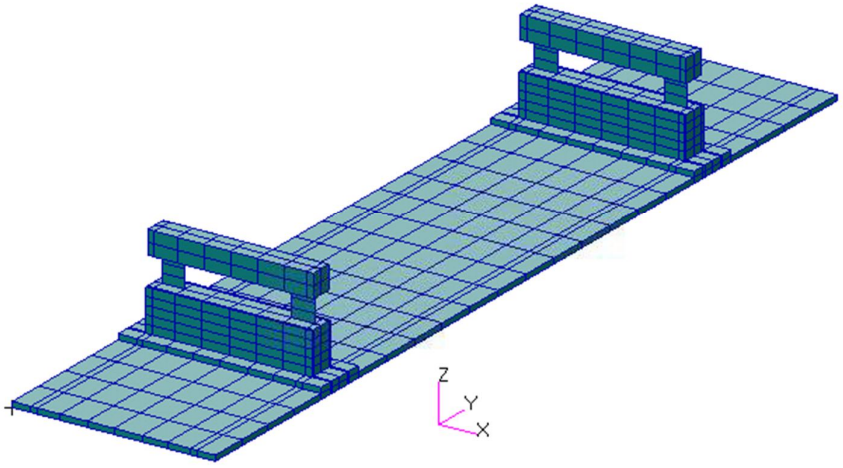


Figure 5.4: FE model of overall wing structure

Table 5.2: Nominal values of material properties of mild steel

| Material Properties | Nominal Values |
|---|---|
| Young's modulus ($E$) | 210 GPa |
| Poisson's ratio ($v$) | 0.3 |
| Mass density ($\rho$) | 7850 kg/m$^3$ |

Table 5.3: Nominal values of material properties of stainless steel

| Material Properties | Nominal Values |
|---|---|
| Young's modulus ($E$) | 190 GPa |
| Poisson's ratio ($v$) | 0.349 |
| Mass density ($\rho$) | 8000 kg/m$^3$ |

Table 5.4: Nominal values of material properties of aluminium

| Material Properties | Nominal Values |
|---|---|
| Young's modulus ($E$) | 70 GPa |
| Poisson's ratio ($v$) | 0.3 |
| Mass density ($\rho$) | 2700 kg/m$^3$ |

The MSC NASTRAN code for normal mode analysis (SOL 103) is developed and used to compute natural frequencies of the single engine pylon and the overall wing structure. The results are shown in Tables 5.5 and 5.6 respectively. The definition of the model is given by Table 5.1. However, the experimental natural frequencies (thefirst 3 modes) lie in between the theoretical natural frequencies of the corresponding modes) of Model 3 and Model 4 of the structures (engine pylon and overall wing structures). This means that the 'true' engine pylon finite element model should be in between Model 3 and Model 4. Mode shapes for the engine pylon and overall wing structure FE models are depicted in Figures 5.5 and 5.6. For single engine pylon with fixed boundary condition shows bending modes in mode shape 1, 3, 4 and 5. However, mode 2 of engine pylon exhibits torsion. For the overall structure, mode 1, 2 and 3 are bending modes. Then, mode 4 for the overall structure displays a torsion mode and mode 5 exhibits the second bending mode.

Table 5.5: FE natural frequencies model of single engine pylon.

| Mode | Natural Frequencies (Hz) : Finite Element | | | | | Natural Frequencies (Hz) |
|---|---|---|---|---|---|---|
| | Model 1 | Model 2 | Model 3 | Model 4 | Model 5 | Experimental Result |
| 1 | 26.0 | 19.67 | 15.8 | 13.04 | 11.05 | 14.6 |
| 2 | 108.9 | 75.40 | 57.42 | 45.87 | 38.13 | 54.27 |
| 3 | 236.9 | 160.84 | 137.32 | 121.14 | 109.5 | 129.95 |
| 4 | 1303.8 | 1065 | 872.50 | 725.75 | 613.8 | 170.82 |
| 5 | 2310.6 | 2132.6 | 1849.7 | 1338.50 | 1021.9 | 182.42 |

Table 5.6: FE natural frequencies model of overall wing structure.

| Mode | Natural Frequencies (Hz): Finite Element | | | | | Natural Frequencies (Hz) |
|---|---|---|---|---|---|---|
| | Model 1 | Model 2 | Model 3 | Model 4 | Model 5 | Experimental Result |
| 1 | 22.04 | 18.14 | 15.25 | 12.80 | 10.80 | 15.09 |
| 2 | 29.20 | 22.27 | 18.40 | 15.16 | 12.70 | 18.40 |
| 3 | 36.90 | 33.78 | 33.10 | 32.6 | 32.30 | 32.33 |
| 4 | 53.90 | 53.17 | 53.70 | 46.95 | 38.50 | 78.01 |
| 5 | 87.40 | 75.33 | 58.90 | 47.00 | 38.60 | 135.08 |

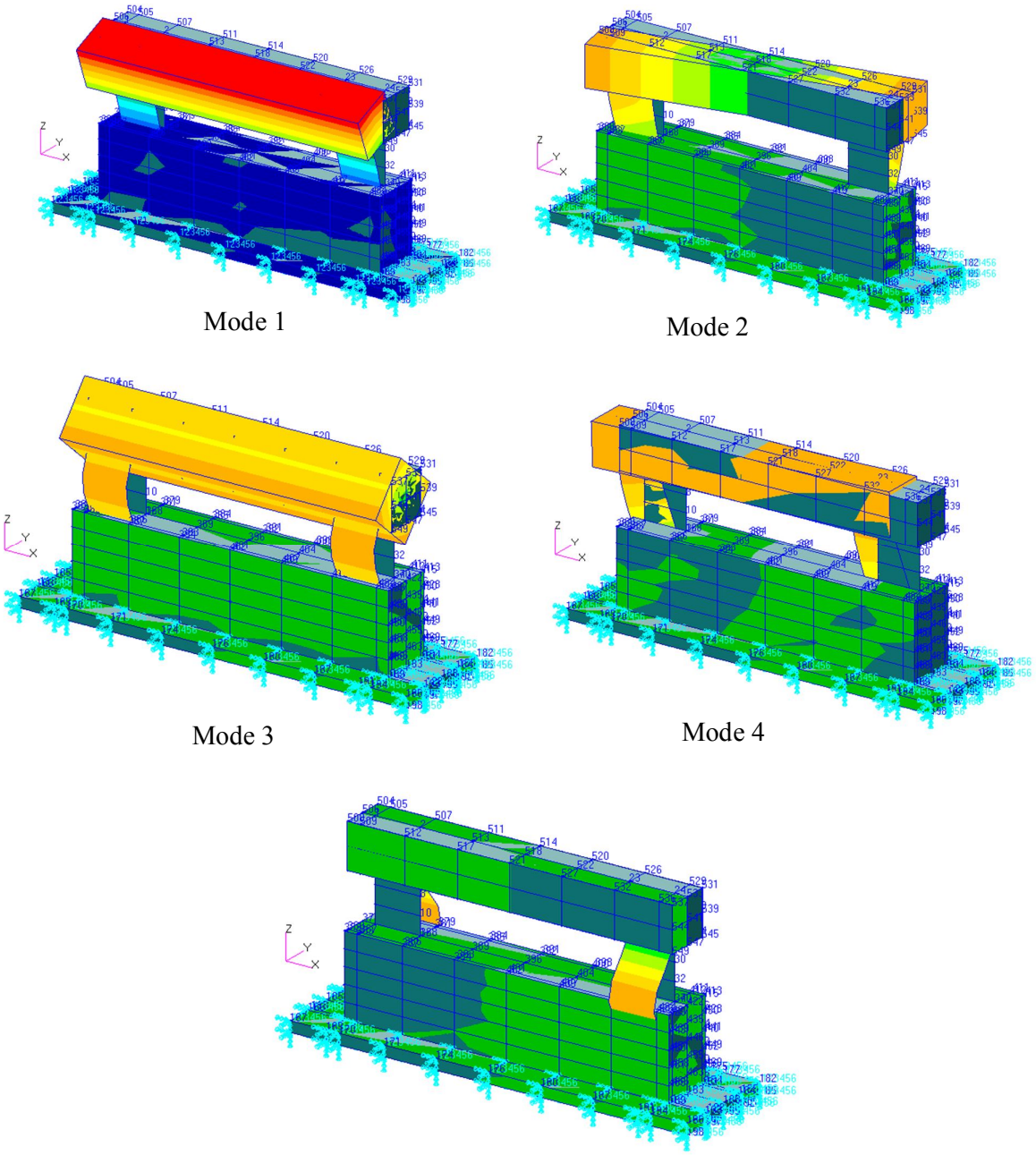


Figure 5.5: Mode shapes of single engine pylon

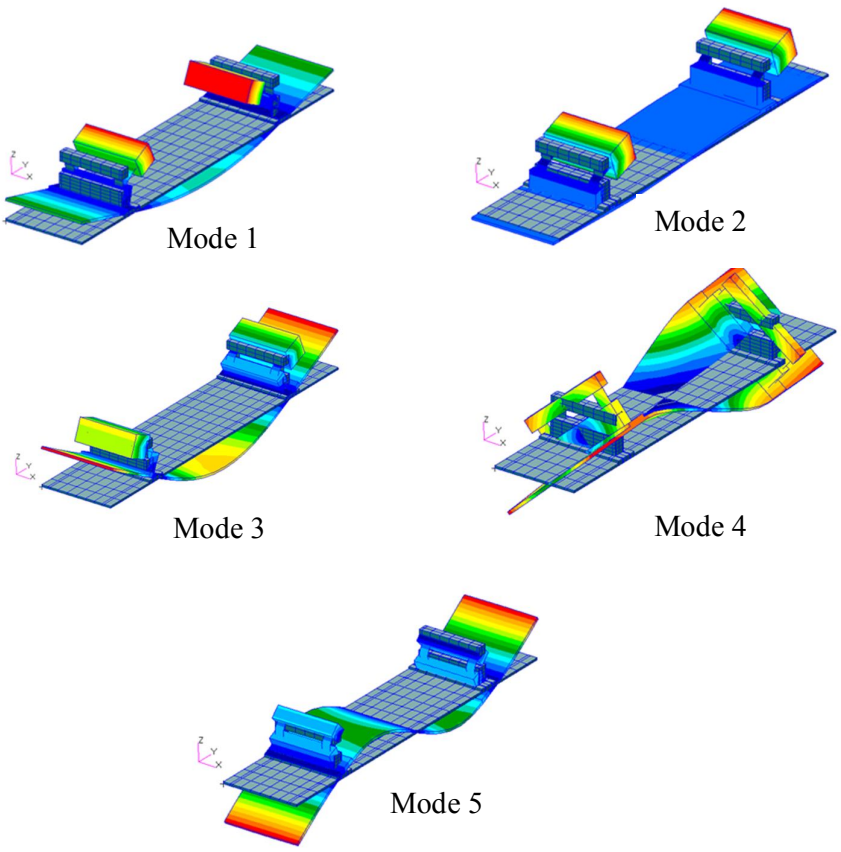


Figure 5.6: Mode shapes of the overall wing structure

## 5.4 FE Model Updating via MSC NASTRAN (SOL200)

Model updating can be performed in two ways minimise the error or discrepancies. The improvement process of updating can be implemented in an efficient or inefficient way. The inefficient manner is by trial and error method in which parameters are randomly changed, the normal mode analysis is re-run and the update numerical result is compared with the experimental result. A repeated process of changing parameters and rerunning the analysis is needed if the natural frequencies

are not close enough. This naive approach is very inefficient and time consuming for large structures with more parameters to update. However, an efficient way is using MSC NASTRAN SOL 200 to compute the response directly. This objective function is for model updating through the use of an optimization algorithm which uses partial derivatives of a function to assist in the numerical search for optimum results. In this work, the objective function is constructed based on frequencies to minimise the error between the numerical and experimental frequencies. It is defined by

$$R = \sum_{i=1}^{n} w_i \left( \frac{\lambda_i^{fe}}{\lambda_i^{exp}} - 1 \right)^2 \tag{5.1}$$

where $\lambda_i^{fe}$ is the $i^{\text{th}}$ numerical eigenvalue predicted from FE model and $\lambda_i^{exp}$ is the $i^{\text{th}}$ experimental eigenvalue obtained from experimental model. However, $w_i$ is a weighting coefficient implemented in the objective function to give more attention to certain modes. Nevertheless, $w_i$= 1 is used in this work to show that all the modes have the same level of interest. It should be noted that Equation (5.1) only holds if the measured and predicted complement are paired correctly and then it is important to make sure that the experimental and numerical data relate to the same mode. Only eigenvalue information is used for updating in this study, while the mode shapes data is only to check the pairing of the experimental and numerical modes. Mottershead et al. (1996) reported that the mode shapes are not considered in model updating because they normally contain more measurement errors and are rather less insensitive to parameters changes than the frequencies. Sensitivity analysis can be carried out by using existing FE codes (MSC Nastran) to compute the sensitivity coefficient of parameters.

### 5.4.1 FE Model Updating of Engine Pylon Structure

The comparison of FE natural frequencies with experimental natural frequencies of the engine pylon structure are tabulated in the Table 5.7. Percentage of error for engine pylon structure is below 10% for each mode. Average percentage of error for first three modes of engine pylon is 6.56%. In order to minimize the error, model updating should be performed to improve modal properties of the structure.

Table 5.7: Comparison FE natural frequencies (Model 3) with experimental natural frequencies of engine pylon structure.

| Mode | Natural Frequencies (Hz) | | Percentage of Error (%) |
|---|---|---|---|
| | Model 3 Numerical | Experimental | |
| 1 | 15.8 | 14.6 | 8.22 |
| 2 | 57.42 | 54.27 | 5.80 |
| 3 | 137.32 | 129.95 | 5.67 |
| Average Percentage of Error | | | 6.56 |

The parameterisation for model updating of the engine pylon structure is performed through a series of sensitivity analyses in which several potential parameters such as thickness of the flat plate in between two blocks at engine pylon, Young's Modulus, Poisson's ratio and shear modulus are listed in the data of NASTRAN SOL 200 code. The coefficients of design sensitivity of the engine pylon structure which are tabulated in Table 5.8 are defined as the rate of change of the frequencies with respect to a change in the parameters. The coefficient is proportional to the sensitivity of parameters. It means the higher the coefficient, the more sensitive to the parameter the frequencies are. From the table it is found that the highest coefficient is thickness of flat plate, which is then followed by Young's Modulus and Poisson ratio. The frequencies are shown to be much less sensitive to the shear modulus.

Table 5.8: Summarised results of the sensitivity analysis of engine pylon model.

| Mode | Natural Frequency | Parameters of engine pylon | | | |
|---|---|---|---|---|---|
| | | Thickness | Young's Modulus | Shear Modulus | Poisson's Ratio |
| 1 | 15.80 | 4.45E+01 | 2.55E-01 | 1.35E-02 | 1.00E-01 |
| 2 | 57.42 | 8.39E+01 | 3.37E-01 | 1.87E-02 | 1.07E-01 |
| 3 | 137.32 | 2.58E+01 | 5.47E-01 | 3.38E-02 | 1.85E-01 |

The updated values of the updating parameters used in the finite model of engine pylon model are given in Table 5.9. The initial value of the flat plate thickness has decreased by about 3.5 percent and two iterations are required to converge. Meanwhile the Young's Modulus has increased by about 1.69 percent with three iterations taken to converge.

Table 5.9: The updated values of the updating of the engine pylon

| Parameter | Initial Value | Updated Value | Unit |
|---|---|---|---|
| Flat Plate Thickness | 1 | 0.965 | mm |
| Young's Modulus | 210 | 213.55 | GPa |

The updating procedure of the engine pylon structure is performed by minimising the objective function as Equation (5.1) with the results tabulated in Table 5.10. Here the first three natural frequencies have improved significantly and reduced from 6.56% average percentage of error initially to 1.13% after the updating process. Each mode of the natural frequencies contributes less than 1.25% of error.

Table 5.10: Summarised results of the updating of engine pylon model.

| Mode | Natural Frequencies (Hz) | | Initial Percentage of Error (%) | Natural Frequencies (Hz) Updated Numerical | Updated Percentage of Error (%) | Initial Error – Updated Error |
|---|---|---|---|---|---|---|
| | Initial Numerical | Experimental | | | | |
| 1 | 15.80 | 14.6 | 8.22 | 14.74 | 0.96 | 7.26 |
| 2 | 57.42 | 54.27 | 5.80 | 54.95 | 1.25 | 4.55 |
| 3 | 137.32 | 129.95 | 5.67 | 131.50 | 1.19 | 4.48 |
| Average Percentage of Error | | | 6.56 | | 1.13 | 5.43 |

### 5.4.2 FE Model Updating of Overall Wing Structure

Table 5.11 shows the comparison FE natural frequencies (Model 3) with experimental natural frequencies for overall wing structure. Percentage of error for overall wing structure is below 5% each mode. Average percentage of error for the first three modes of overall wing structure is 1.15%. In order to reduce the percentage of error, model updating for overall wing structure should be performed.

Table 5.11: Comparison FE natural frequencies (Model 3) with experimental natural frequencies of overall wing structure.

| Mode | Natural Frequencies (Hz) | | Percentage of Error (%) |
|---|---|---|---|
| | Model 3 Numerical | Experimental | |
| 1 | 15.25 | 15.09 | 1.06 |
| 2 | 18.40 | 18.40 | 0 |
| 3 | 33.10 | 32.33 | 2.38 |
| Average Percentage of Error | | | 1.15 |

In order to identify the most sensitive parameters to frequencies, NASTRAN SOL 200 is used to compute the sensitivity based on the parameters of the overall wing structure. The coefficients giving high sensitivity for the overall wing structure which are tabulated in Table 5.12 are defined as these which give most rate of change of the frequencies with respect to a change in the parameters. The coefficient is proportional to the sensitivity of parameters. It means the higher the coefficient, the more sensitive to the parameter the frequencies are. From the table, it is found that the higher coefficient is thickness of flat plate, which is then followed by Young's Modulus and Poisson ratio. The frequencies are shown much less to the shear modulus.

Table 5.12: Summarised results of the sensitivity analysis of overall wing structure.

| Mode | Natural Frequency | Parameters of overall wing structure | | | |
|---|---|---|---|---|---|
| | | Thickness | Young's Modulus | Shear Modulus | Poisson's Ratio |
| 1 | 15.25 | 3.75E+01 | 2.45E-01 | 1.35E-02 | 1.00E-01 |
| 2 | 18.40 | 2.39E-01 | 1.37E-01 | 1.27E-02 | 1.01E-01 |
| 3 | 33.10 | 3.58E-01 | 3.47E-01 | 2.38E-02 | 1.51E-01 |

The updated values of the updating parameters used in the finite model updating of the overall wing structure are shown in Table 5.13. The initial value of the flat plate thickness has decreased by about 5.5 percent and two iterations are required to converge. Meanwhile the Young's Modulus has increased by about 2.59 percent with three iterations taken to converge.

Table 5.13: The updated values of the updating of the overall wing structure

| Parameter | Initial Value | Updated Value | Unit |
|---|---|---|---|
| Flat Plate Thickness | 1 | 0.945 | mm |
| Young's Modulus | 210 | 215.43 | GPa |

The updating procedure for the overall wing structure is performed by minimising the objective function as given by Equation (5.1) and tabulated in Table 5.14. The first three natural frequencies have improved significantly and reduced from 1.15% average percentage of error initially to 0.30% average percentage of error after the updating process. Each mode of the natural frequencies contributes less than 0.59% of error.

Table 5.14: Summarised results of the updating of overall wing structure.

| Mode | Natural Frequencies (Hz) | | Initial Percentage of Error (%) | Natural Frequencies (Hz) Updated Numerical | Updated Percentage of Error (%) | Initial Error – Updated Error |
|---|---|---|---|---|---|---|
| | Initial Numerical | Experimental | | | | |
| 1 | 15.25 | 15.09 | 1.06 | 15.11 | 0.13 | 0.93 |
| 2 | 18.40 | 18.40 | 0 | 18.40 | 0 | 0 |
| 3 | 33.10 | 32.33 | 2.38 | 32.48 | 0.46 | 1.92 |
| Average Percentage of Error | | | 1.15 | | 0.30 | 0.95 |

## 5.5 Summary

Finite element modelling and model updating analysis of the engine pylon and overall wing structure have been discussed in this chapter. The discrepancies between the experimental and numerical results of both structures are calculated in terms of average percentage of error have been successfully reduced below 5%. The large discrepancies between measured and predicted frequencies of the engine pylon have been successfully reduced from 6.56 to 1.13%. The challenge in modelling is to defined gap between two blocks before running finite element normal mode analysis. Initially, big discrepancies occur at the beginning due to assumptions made in the finite element model based on nominal values which are insufficient to represent the real test model.

In this work, the sensitivity analysis has become a successful tool for localising the sources of errors that are believed to arise as a result of excluding the effects of boundary conditions and initial displacement or stress.

# Chapter 6

# Nonlinear Identification of the Engine Pylon and Overall Wing Structure

## 6.1 Introduction

This chapter will discuss nonlinear identification of the engine pylon and overall wing structure. The combination force appropriation and restoring forces is applied to the both structures. This combination method is similar to the nonlinear resonant decay method (NLRDM). Platten et al. (2009a) applied NLRDM to multi degree of freedom structures using an extended modal space model. The NLRDM was applied to the structure using two shakers with an appropriated excitation pattern for each mode of interest. The theoretical basis of force appropriation and the restoring method can be referred in Chapter 3.

## 6.2 Force Appropriation Method for Engine Pylon Structure

Force appropriation method for engine pylon structure with fixed-free boundary condition as shown in Figure 6.1. There are 102 nodes at this model and fixed at all degree of freedom at node 1,2,3 and 4. This simplified FE model of a single engine pylon is initially modelled by using MD NASTRAN and compute SOL 103 to run normal mode analysis. Output pch file from NASTRAN output is needed in order to extract **M** and **K** matrices. Matlab coding is developed to process pch output file to extract **M** and **K** matrices as shown in Appendix 1.

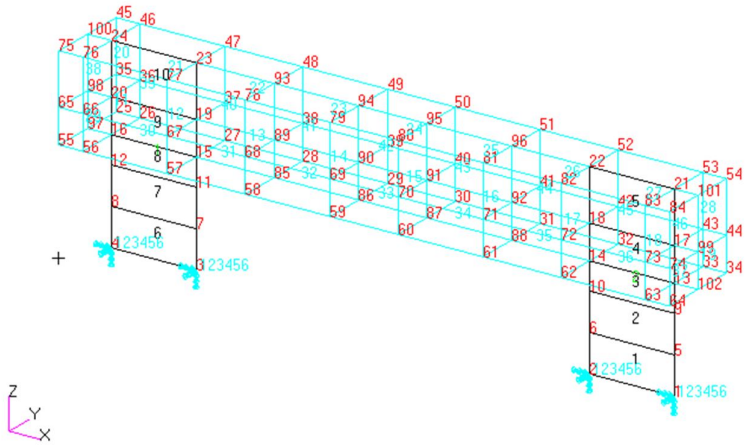

Figure 6.1: FE Engine Pylon Simplified Model for
Fixed Free Boundary Condition

**M** and **K** matrices are needed to run eigenvalue problems in the force appropriation method. However, **C** matrices can be developed using proportional damping (Rayleigh Method) is commonly used in nonlinear dynamics analysis and be defined as below

$$\mathbf{C} = \alpha_1 \mathbf{M} + \alpha_2 \mathbf{K} \tag{6.1}$$

where $\alpha_1$ is mass proportional damping coefficient and $\alpha_2$ is stiffness proportional damping coefficient. Proportional damping is the most common approach to model dissipative forces in complex engineering structures and it has been used in various dynamic problems. Relationships between the modal equations and orthogonality conditions allow this equation to be rewritten as:

$$\zeta_n = \frac{1}{2\omega_n}\alpha_1 + \frac{\omega_n}{2}\alpha_2 \tag{6.2}$$

where $\zeta_n$ is the critical damping ratio and $\omega_n$ is the natural frequency. It can be seen that the critical damping ratio varies with natural frequency. The values of $\alpha_1$ and

$\alpha_2$ are usually selected, according to engineering judgments, such that the critical damping ratio is given at two known frequencies.

Matlab coding for force appropriation was developed to run eigenvalues problem of engine pylon structure as shown in Appendix 2. Table 6.1 shows the force appropriation and MMIF result for the engine pylon structure with setting 12$r$ (response) x 4$e$ (excitation). A forward analysis for the normal mode test of this structure gave the natural frequency for mode 1 as 178.54 rad/s (28.42 Hz), mode 2 as 775.88 rad/s (123.49 Hz) and mode 3 as 1630.94 rad/s (259.57 Hz). Higher frequency step (1 rad/s) provides a satisfactory result for natural frequencies and mode shapes, but not for force vector and minimum eigenvalue. Smaller frequency step (0.01 rad/s) gives more accurate results for natural frequencies, mode shapes and force vector, but has a longer computational time.

The target of this method is to determine the monophase force vector, $f_1$, $f_2$, $f_3$ and $f_4$ when applied at undamped natural frequencies and to excite the corresponding undamped pure mode. Modal assurance criteria (MAC) and modal purity indicator (MPI) shows good correlation between each other. The function of the modal assurance criterion (MAC) is to provide a measure of consistency (degree of linearity) between estimates of a modal vector, which provides an additional confidence factor in the evaluation of a modal vector from different excitation (reference) locations or different modal parameter estimation algorithms. Perfect purity (MPI=1) of the mode shape is obtained from engine pylon structure when multiple of freedoms are applied at effective natural frequencies.

Table 6.1: Force Appropriation and MMIF Result for a system of Engine Pylon Structure (12 responses and 4 excitations)

| | Frequency Step ( 1 rad/s) | | |
|---|---|---|---|
| | Mode 1 | Mode 2 | Mode 3 |
| Frequencies, ω (Hz) | 28.4887 | 123.5042 | 259.7409 |
| Minimum Eigenvalue | 0.1303 | 0 | 0.0023 |
| Appropriated Force Vector | 1:1: -0.065: -0.065 | -0.1681:0.1681 :-1:1 | -7.064: -7.064 :1:1 |
| Computational Time (s) | 17.31 | | |
| MAC | 1 | 1 | 1 |
| MPI | 1 | 1 | 1 |
| | Frequency Step (0.1 rad/s) | | |
| | Mode 1 | Mode 2 | Mode 3 |
| Frequencies, ω (Hz) | 28.4251 | 123.4883 | 259.6613 |
| Minimum Eigenvalue | 0.0001 | 0 | 0.0023 |
| Appropriated Force Vector | -4.92:-4.92: 1: 1 | -0.006:0.006 :-1:1 | -6.76: -6.76 :1:1 |
| Computational Time (s) | 190.40 | | |
| MAC | 1 | 1 | 1 |
| MPI | 1 | 1 | 1 |
| | Frequency Step (0.01rad/s) | | |
| | Mode 1 | Mode 2 | Mode 3 |
| Frequencies, ω (Hz) | 28.4235 | 123.4883 | 259.6677 |
| Minimum Eigenvalue | 0 | 0 | 0.0023 |
| Appropriated Force Vector | 0.4146:0.4146: 1: 1 | -0.0061:0.0061 :-1:1 | -6.784: -6.784 :1:1 |
| Computational Time (s) | 2295.50 | | |
| MAC | 1 | 1 | 1 |
| MPI | 1 | 1 | 1 |

Figure 6.2 to 6.4 shows the MMIF graphs of eigenvalues, λ versus frequency, ω for different frequency steps.

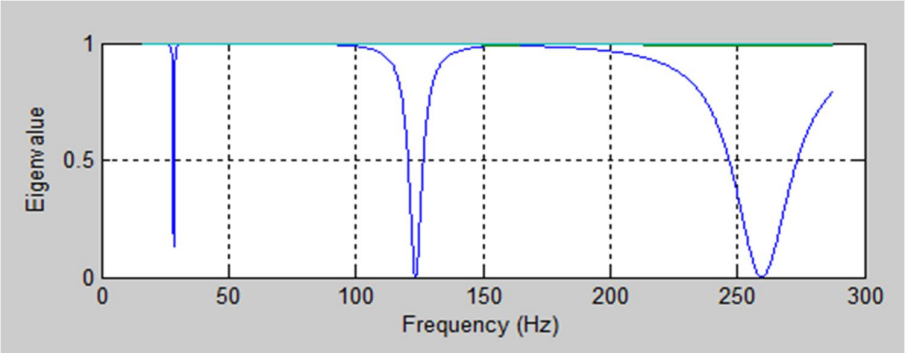


Figure 6.2: MMIF of Engine Pylon: Eigenvalue, λ versus Frequency, ω (1 rad/s frequency step)

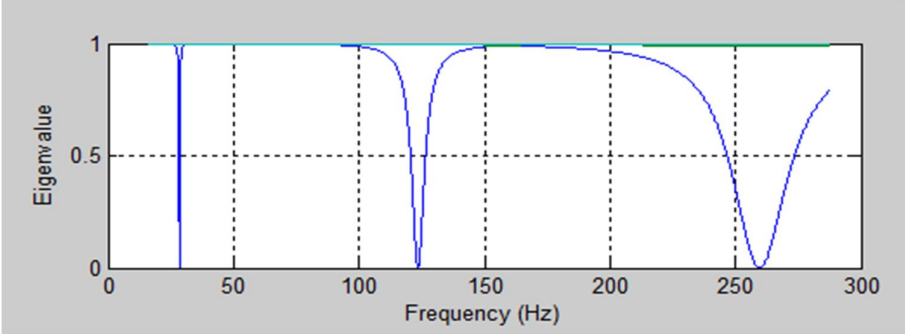


Figure 6.3: MMIF of Engine Pylon: Eigenvalue, λ versus Frequency, ω (0.1 rad/s frequency step)

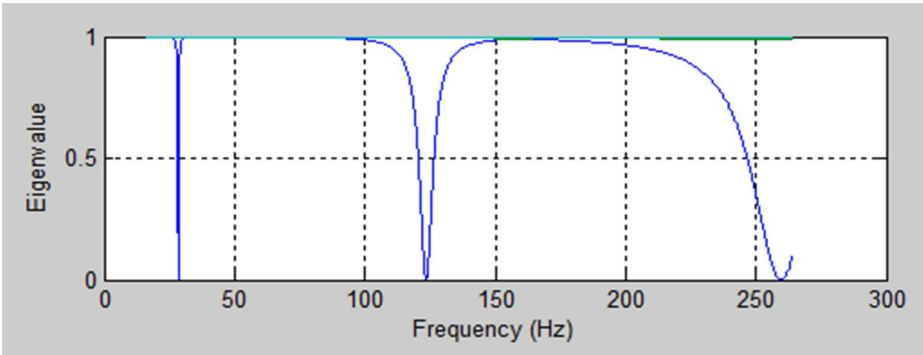


Figure 6.4: MMIF of Engine Pylon: Eigenvalue, λ versus Frequency, ω (0.01 rad/s frequency step)

## 6.3 Force Appropriation Method for Overall Wing Structure

The force appropriation method for overall wing structure with free-free boundary condition as shown in Figure 6.5. There are 1824 nodes at this model and this FE model of overall wing structure is modelled by using MD NASTRAN and compute SOL 103 to run normal mode analysis. The output pch file from NASTRAN output is needed in order to extract **M** and **K** matrices. Matlab coding is developed to process the pch output file to extract **M** and **K** matrices as shown in Appendix 1.

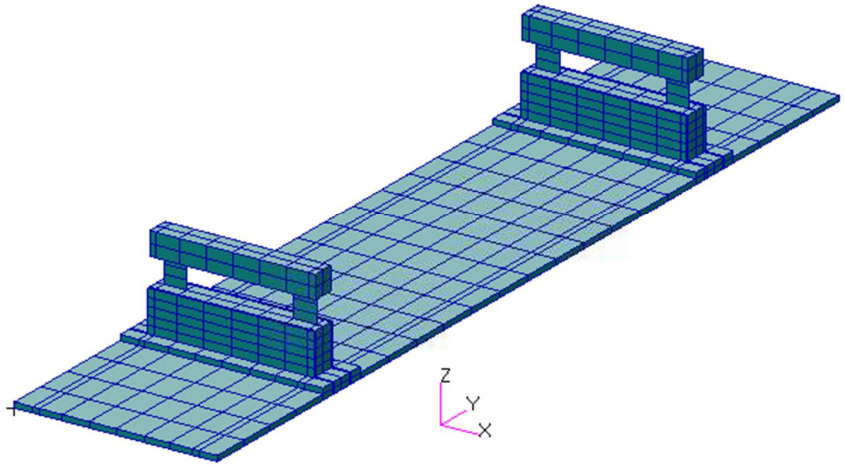


Figure 6.5: FE Modelling of Overall Wing Structure

Matlab coding for force appropriation was developed to run eigenvalues problem of overall wing structure as shown in Appendix 2. Table 6.2 shows the force appropriation and MMIF result for overall wing structure with setting 12*r* (response) x 2*e* (excitation). A forward analysis for the normal mode test of this structure gave the natural frequency for mode 1 as 95.818 rad/s (15.25 Hz), mode 2 as 115.61 rad/s

(18.40 Hz) and mode 3 as 207.97 rad/s (33.10 Hz). Higher frequency step (1 rad/s) provides a satisfactory result for natural frequencies and mode shapes, but not for force vector and minimum eigenvalue. A smaller frequency step (0.01 rad/s) gives more accurate results for natural frequencies, mode shapes and force vector, but has longer computational time.

Table 6.2: Force Appropriation and MMIF Result for a system of Overall Wing Structure (12 responses and 2 excitations)

| | Frequency Step ( 1 rad/s) | | |
|---|---|---|---|
| | Mode 1 | Mode 2 | Mode 3 |
| Frequencies, ω (Hz) | 15.7551 | 18.5102 | 33.2309 |
| Minimum Eigenvalue | 0.2703 | 0 | 0.0007 |
| Appropriated Force Vector | 1:0.87 | 1:-0.83 | 1:05 |
| Computational Time (s) | 55.72 | | |
| MAC | 1 | 1 | 1 |
| MPI | 1 | 1 | 1 |
| | Frequency Step (0.1 rad/s) | | |
| | Mode 1 | Mode 2 | Mode 3 |
| Frequencies, ω (Hz) | 15.4251 | 18.4283 | 33.2013 |
| Minimum Eigenvalue | 0.0001 | 0 | 0.0005 |
| Appropriated Force Vector | 1:0.90 | 1:-0.85 | 1:1.07 |
| Computational Time (s) | 712.92 | | |
| MAC | 1 | 1 | 1 |
| MPI | 1 | 1 | 1 |
| | Frequency Step (0.01rad/s) | | |
| | Mode 1 | Mode 2 | Mode 3 |
| Frequencies, ω (Hz) | 15.2460 | 18.4132 | 33.1187 |
| Minimum Eigenvalue | 0 | 0 | 0.0005 |
| Appropriated Force Vector | 1:0.93 | 1:-0.88 | 1:1.10 |
| Computational Time (s) | 9522.50 | | |
| MAC | 1 | 1 | 1 |
| MPI | 1 | 1 | 1 |

## 6.4 Nonlinear Identification of Overall Wing Structure

The identification of the overall wing structure using two shakers (two excitations) and 12 accelerometer (response) with an appropriated pattern for first 5 modes. The physical forces and accelerations were measured during MIMO normal mode test. The modal forces and responses were calculated by transforming the physical coordinate forces and responses to modal space using the modal matrix composed of the five mode shapes from the earlier linear identification at suitable excitation levels. The modal accelerations were integrated in time to determine modal velocities and displacements for each mode of interest. These integrations were performed after a transformation to the frequency domain.

Polynomial basis functions of order 3 were used for the nonlinear models to keep the order of the model as low as possible and yet have sufficient accuracy. Static load test on two pylons and wing were performed. Equations (6.3) and (6.4) below show the nonlinearity in the pylons and wing structure contains cubic and quadratic terms (nonlinear modal model in section 3.6). The curve for each pylon was fitted using a cubic polynomial and the formulas were:

$$L_1 = (2.65 \times 10^8)x_1^3 + (2.76 \times 10^5)x_1^2 + (6.65 \times 10^3)x_1 - 0.05 \qquad (6.3)$$

$$L_2 = (2.93 \times 10^8)x_2^3 + (3.87 \times 10^5)x_2^2 + (6.35 \times 10^3)x_2 + 0.45 \qquad (6.4)$$

where $L_1$ is the load on the first pylon, $L_2$ is the load on the second pylon, $x_1$ is the deflection of first load and $x_2$ is the deflection of second load. From equation (6.3) and (6.4) it is seen that both pylons exhibit a moderate level of asymmetry, as the polynomials obtained contain constant and second order terms.

Further investigation is a dynamic test on overall wing structure using MIMO Normal mode test. This test was carried out on the unit to generate a freely decaying response. The existence of stiffness nonlinearity would be observed by a variation in natural frequency with amplitude and of a damping nonlinearity by changing damping ratio with amplitude. Damping effect on this study is very small and does not affect the identification so much. No nonlinear damping was considered as the random excitation test showed little evidence of nonlinearity in the system.

The modal mass values used in the nonlinear curve fits were determined from Table 4.8, chapter 4 at page 107. This modal mass is from modal estimation with low amplitude random excitation data set. The linear damping and stiffness term were calculated as part of the nonlinear curve fitting process. Comparison with the linear result in Table 4.8 showed a very good agreement for these term. The finalized nonlinear curve fit was therefore of the form:

$$g_{nl,r} = f_r - m_r\ddot{p}_r - c_r\dot{p}_r - k_r p_r - A_{1,r}p_1^3 - B_{1,r}p_1^2p_2 - C_{1,r}p_1^2p_3 - D_{1,r}p_1p_2^2 - E_{1,r}p_1p_2p_3 - F_{1,r}p_1\dot{p}_3^2 - G_{1,r}p_2^3 - H_{1,r}p_2^2p_3 - I_{1,r}p_2p_3^2 - J_{1,r}p_3^3 \quad (6.5)$$

for $r$=1,2,3, where the unknowns to be evaluated were $c_r$, $k_r$, $A_{1,r}$, $B_{1,r}$, $C_{1,r}$, $D_{1,r}$, $E_{1,r}$, $F_{1,r}$, $G_{1,r}$, $H_{1,r}$, $I_{1,r}$ and $J_{1,r}$. As the number of coefficient in this model is relatively small, the best model structure was chosen by implementing exhaustive search. Model structure selection is an important part of nonlinear system identification, because not every coefficient term need be included in the final model. In addition, some of the $A_{1,r}$ to $J_{1,r}$ coefficients may have values of 0. The resulting model is the complete optimum best curve fit given particular optimal structure of candidate terms and data. A procedure would be too computationally intensive for a large number of candidate terms but could be easily applied in the current project due to the low numbers of candidate terms. Therefore, one of the main advantages of the combination force appropriation and restoring forces is

highlighted. Because of the limited number of terms participating in the responses, the nonlinear models can be simpler and evaluated accurately.

Final selected models and parameter estimates for the first three modes are depicted in Table 6.3 and 6.4. Table 6.3 shows the estimates of the interest linear parameters, $c_r$ and $k_r$ determined from the nonlinear curve fits, compared with those obtained from the PolyMAX modal estimation model. It can be seen that the parameters show small differences between two set of estimation. Furthermore, Table 6.4 shows nonlinear term coefficients identified for first three modes of overall wing structure. A zero value denotes that the corresponding term was not included in the final model.

Table 6.3: Comparison linear direct term coefficients identified by combination force appropriation and restoring method with PolyMAX.

| Mode | Force Appropriation and Restoring Forces Method | | PolyMAX (MIMO Normal Mode Test) | |
|---|---|---|---|---|
| | $c_r$, modal damping | $k_r$, modal stiffness | $c_r$, modal damping | $k_r$, modal stiffness |
| 1 | 2.47 | 1.79E4 | 2.35 | 1.71E4 |
| 2 | 3.24 | 3.13E4 | 3.17 | 3.34E4 |
| 3 | 4.14 | 6.35E4 | 4.06 | 6.46E4 |

Table 6.4: Nonlinear term coefficients identified for first three modes

| Coefficient | Mode 1 | Mode 2 | Mode 3 |
|---|---|---|---|
| $A_{1,r}$ | $3.76 \times 10^8$ | 0 | $-2.56 \times 10^8$ |
| $B_{1,r}$ | $-1.66 \times 10^9$ | $6.06 \times 10^9$ | 0 |
| $C_{1,r}$ | $-7.87 \times 10^8$ | 0 | $1.58 \times 10^9$ |
| $D_{1,r}$ | $3.45 \times 10^9$ | 0 | 0 |

| | | | |
|---|---|---|---|
| $E_{1,r}$ | 0 | $-1.53 \times 10^{10}$ | $6.37 \times 10^{10}$ |
| $F_{1,r}$ | 0 | 0 | $-2.42 \times 10^{9}$ |
| $G_{1,r}$ | 0 | $1.33 \times 10^{9}$ | 0 |
| $H_{1,r}$ | 0 | $1.87 \times 10^{9}$ | 0 |
| $I_{1,r}$ | 0 | $2.32 \times 10^{10}$ | $1.42 \times 10^{9}$ |
| $J_{1,r}$ | $-9.72 \times 10^{7}$ | 0 | 0 |

Form Table 4.8, Table 6.3, Table 6.4 and the final model structure in Equation (6.5), identified equation of motion for the overall wing structure can be written as:

$$2.15\ddot{p}_1 + 2.47\dot{p}_1 + 1.79 \times 10^4 p_1 + 3.76 \times 10^8 p_1^3 - 1.66 \times 10^9 p_1^2 p_2 - 7.87 \times 10^8 p_1^2 p_3 + 3.45 \times 10^9 p_1 p_2^2 - 9.72 \times 10^7 p_3^3 = f_1(t) \quad (6.6)$$

$$2.44\ddot{p}_2 + 3.24\dot{p}_2 + 3.13 \times 10^4 p_2 + 6.06 \times 10^9 p_1^2 p_2 - 1.53 \times 10^{10} p_1 p_2 p_3 + 1.33 \times 10^9 p_2^3 + 1.87 \times 10^9 p_2^2 p_3 + 2.32 \times 10^{10} p_2 p_3^2 = f_2(t) \quad (6.7)$$

$$1.66\ddot{p}_3 + 4.14\dot{p}_3 + 6.35 \times 10^4 p_3 - 2.56 \times 10^8 p_1^3 + 1.58 \times 10^9 p_1^2 p_3 + 6.37 \times 10^{10} p_1 p_2 p_3 - 2.42 \times 10^9 p_1 p_3^2 + 1.42 \times 10^9 p_2 p_3^2 = f_3(t) \quad (6.8)$$

$$0.99\ddot{p}_4 + 2.95\dot{p}_4 + 2.21 \times 10^5 p_4 = f_4(t) \quad (6.9)$$

$$1.17\ddot{p}_5 + 5.35\dot{p}_5 + 7.19 \times 10^5 p_5 = f_5(t) \quad (6.10)$$

It should be noted that under appropriated excitation, the amplitudes of the cross coupled modal responses were about an order of magnitude lower than direct modal responses. Thus, all the cross coupled nonlinear terms in Equation (6.6) to (6.10) are at least an order of magnitude smaller than the direct nonlinear terms.

## 6.5 Summary

In this chapter, a nonlinear experimental structure a wing with pylons was identified using the force appropriation and restoring forces method. At the pylon's bending and rotational degrees-of-freedom, discrete hardening stiffness nonlinearity was identified. The results presented evidence of nonlinear stiffness at higher amplitudes for the first three modes. The combination of nonlinear identification methods succeeded in estimating good quality nonlinear modal models for the modes of interest. It can be concluded that modes 1 and 2 showed hardening stiffness nonlinearities, mode 3 just showed very weak nonlinearity because of the small degree of rotation at the anchor locations. However, modes 4 and 5 behaved linearly and so a linear modal model sufficed for the overall wing structure as far as these 2 modes are concerned.

# Chapter 7

# Conclusion and Future Work

## 7.1 Introduction

The aim of this work is to develop nonlinear identification methods of wing structure with attached two engine pylon. The force appropriation method is developed to excite single mode of the structure by applying multiple forces. If the response of the system can be reduced to that of the mode of interest, then a single degree of freedom restoring force identification could be performed to identify any nonlinearity present. Beside of that several methods of modal testing are used such as impact hammer, single shaker (spectral test), double shaker (spectral test), MIMO sine testing and MIMO normal mode tests were carried out to obtain dynamics properties and other parameters. Finite element modelling and model updating were applied to minimise the discrepancies between numerical and experimental dynamic results. As conclusion, this thesis covered numerical work (finite element normal mode analysis and model updating), experimental (impact hammer, single shaker and double shaker) and programming work (Matlab coding) to perform nonlinear identification of the wing structure.

## 7.2 Thesis Contribution

The main original contributions of this thesis are as follows:

a) Finite element and model updating – FE model of engine pylon and overall wing structure were successfully modelled and run the Nastran SOL 103 normal mode

analysis to obtain dynamic properties. The success of performed model updating using MSC Nastran SOL 200 for both structures allowed the discrepancies in natural frequency to be reduced below 5%. In this work, Matlab coding was developed to extract **M** and **K** matrices from NASTRAN output result (pch file). These **M** and **K** matrices were used when performing MMIF eigenvalue and also needed when identification process in nonlinear modal model.

b) Force Appropriation Method – The appropriated force vectors were applied to the simulated nonlinear system with single degree of freedom and two degree of freedom for simple validation. Validation and comparison of results were made to make sure that Matlab coding was developed correctly and in a simple way. Modal assurance criteria (MAC) and modal purity index (MPI) was successfully implemented in mode multivariate indicator function (MMIF). MMIF eigenvalues were found to provide a useful indication of the presence and type of nonlinearity obtained in the wing structure. Therefore, this method has been demonstrated on simulated and experimental data for the engine pylon and overall wing structure. This method successfully generated the appropriate force vectors for both structures. These force vectors are useful for exciting a single mode of the structure. A method has been devised for the identification of the nonlinear characteristics of a multi degree of freedom system on a mode by mode basis. The successful tuning of undamped normal modes of the overall wing structure have shown that MIMO Normal Mode Test provides a feasible testing approach, particularly when correcting the finite element models where undamped normal mode parameters are desirable.

c) Restoring Forces Method – Model in modal space and the restoring forces method have been presented. The sinusoidal generalised force and modal acceleration responses are used to determine the nonlinear restoring forces. Polynomial and curve fitting were applied for the construction of nonlinear models. This method was simulated with single degree of freedom and two degree of freedom at the beginning to validate that Matlab coding. The thesis

showed a successful application of combination force appropriation and restoring forces method to the overall wing structure in order to identify nonlinearity. Several adaptations to the restoring force method are proposed, which include the elimination of kinematic constraints and the regularization of ill-conditioned inverse problems. The validity of the resulting identified model is explored and the advantages of combination force appropriation and restoring method are discussed. The potential of this method is that the nonlinear identification of engineering structure with a large number of modes can be performed.

## 7.3 Suggestion of Future Work

Some general recommendation for future work in the area finite element modelling and updating, nonlinear identification methods are outlined below:

a) In this work, a simple model updating method was applied to the nonlinear structures. The stochastic model updating by using the perturbation method for estimation should be carried out. It would be interesting to investigate this method, so that a comparison can be made with direct model updating.

b) The development of expert computer aided interpretation of the eigenvalues, rank determination, effective number of degrees of freedom and appropriated force vectors for close mode should be investigated. The sensitivity of force vectors to very close modes needs to be explored further. The modal mass estimation technique implemented in experiments was found to be sensitive to measurement noise. The method used should be studied further and use of an algorithm which could be smooth the measured data should be investigated.

c) An alternative way to speed up the identification would be to reduce the number of iterations performed by the optimization. This could be done in a number of ways:
    - Further investigation of the parameters used in the optimization routine such as step size used in the calculation of gradient.
    - Investigate if it is possible to allow values to be chosen to cause optimization to function more efficiently.
    - More sophisticated optimization routines may allow less iteration.

# Appendix 1:
# Matlab coding for extract M and K matrices

```
close all;clear all;clc;format compact;
%%%%%%%%%%%%%%%%%%%%%%%%%%%%%%%%%%%%%%%%%%%%%%%%%%%%%%%%%%%%%%%%%%%%%%%%%%%%%%%
%%%%date : 5 Oct 2011
%%%%created by : yazdi, shahrir, Hamed
%%%%%%%%%%%%%%%%%%%%%%%%%%%%%%%%%%%%%%%%%%%%%%%%%%%%%%%%%%%%%%%%%%%%%%%%%%%%%%%
%%% to read the mass and stiffness matrices tht including the boundary
condition

fid = fopen('EN_Clamped_300112.pch');
% fid2 = fopen('EN_Clamped.DAT', 'wt');

while 1
    tline = fgetl(fid); % read line by line
    if strcmp(tline(1:11),'DMIG    VAX')
        break
    elseif strcmp(tline(1:12),'DMIG    KAAX')
        Kcol = str2num(tline(end-7:end));
        CASENAME = 'STIFFNESS'; %to trigger STIFFNESS case (switch)
        counter = 0;
    elseif strcmp(tline(1:12),'DMIG    MAAX')
        Mcol = str2num(tline(end-7:end));
        CASENAME = 'MASS'; %to trigger MASS case (switch)
        counter = 0;
    end

    switch CASENAME
        case 'STIFFNESS'
            if strcmp(tline(1:5),'DMIG*')
                A1 = str2num (tline(20:end));
            elseif length(tline)==56 && strcmp(tline(1),'*')
                counter = counter + 1;
                A2 = str2num(tline(2:40));
                A3 = str2num(tline(end-15:end));
                Kmat (counter,:) = [A1 A2 A3] ;
            else
            end

        case 'MASS'
            if strcmp(tline(1:5),'DMIG*')
                A1 = str2num (tline(20:end));
            elseif length(tline)==56 && strcmp(tline(1),'*')
                counter = counter + 1;
                A2 = str2num(tline(2:40));
                A3 = str2num(tline(end-15:end));
                Mmat (counter,:) = [A1 A2 A3] ;
            else
            end
    end

end

fclose('all');

KK = Kmat;
MM = Mmat;
```

```
%%%%-----------------------------------------------------------------
%%%% STIFFNESS MATRIK
%%%%-----------------------------------------------------------------
KK(:,1) = (KK(:,1)-1)*6;
KK(:,3) = (KK(:,3)-1)*6;
colpost = sum(KK(:,3:4),2);
rowpost = sum(KK(:,1:2),2);

stiff_data = [rowpost,colpost,KK(:,5)];
STIFFMAT = zeros(Kcol,Kcol);

for ii = 1:size(stiff_data,1)
    dummy = stiff_data(ii,:);
    STIFFMAT(dummy(1),dummy(2)) = dummy(3);
    STIFFMAT(dummy(2),dummy(1)) = dummy(3);
end

% indexcolumn = find(sum(abs(STIFFMAT),2)==0)';
% indexrow = find(sum(abs(STIFFMAT),1)==0);
% disp('STIFFMAT FULL');
% disp(STIFFMAT)
% counter1 = 0;
% removed = [];
% for ii = 1:length(indexcolumn)
%     counter1 = counter1+1;
%     Adummy = indexcolumn(counter1);
%     counter2 = 0;
%     for jj = 1:length(indexrow)
%         counter2 = counter2+1;
%         Bdummy = indexrow(counter2);
%         if Adummy == Bdummy
%             removed = [removed;Adummy Bdummy];
%         else
%         end
%     end
% end
%
% STIFFMAT(:,removed(:,1))=[];
% STIFFMAT(removed(:,2),:)=[];
% disp('STIFFMAT FILTERED');
% disp(STIFFMAT)


%%%%-----------------------------------------------------------------
%%%% MASS MATRIK
%%%%-----------------------------------------------------------------
MM(:,1) = (MM(:,1)-1)*6;
MM(:,3) = (MM(:,3)-1)*6;
colpost2 = sum(MM(:,3:4),2);
rowpost2 = sum(MM(:,1:2),2);

mass_data = [rowpost2,colpost2,MM(:,5)];
MASSMAT = zeros(Mcol,Mcol);

for ii = 1:size(mass_data,1)
```

```
    dummy = mass_data(ii,:);
    MASSMAT(dummy(1),dummy(2)) = dummy(3);
    MASSMAT(dummy(2),dummy(1)) = dummy(3);
end
indexcolumnM = find(sum(abs(MASSMAT),2)==0)';
indexrowM = find(sum(abs(MASSMAT),1)==0);
indexcolumnK = find(sum(abs(STIFFMAT),2)==0)';
indexrowK = find(sum(abs(STIFFMAT),1)==0);
disp('MASSMAT FULL');
disp(MASSMAT)
removedM = intersect(indexcolumnM,indexrowM);
removedK = intersect(indexcolumnK,indexrowK);
removed=intersect(removedM,removedK);
% if length(removedM)>length(removedK)
% else
%     zerorowsstiff=setdiff(removedM,removedK);
% end
STIFFMAT(:,removed)=[];
STIFFMAT(removed,:)=[];
MASSMAT(:,removed)=[];
MASSMAT(removed,:)=[];

indexcolumnM1 = find(sum(abs(MASSMAT),2)==0)';
indexrowM1 = find(sum(abs(MASSMAT),1)==0);
zerorowsmass=intersect(indexcolumnM1,indexrowM1);

STIFFMAT_A=STIFFMAT(1:120,1:120); %%%%%%FOR CQUAD4%%%%%
STIFFMAT_AA=STIFFMAT(1:120,121:354)
STIFFMAT_B=STIFFMAT(121:354,121:354);%%%%%%FOR CHEXA%%%%%

MASSMAT_A=MASSMAT(1:120,1:120);%%%%%%FOR CQUAD4%%%%%
MASSMAT_AA=MASSMAT(1:120,121:354)
MASSMAT_B=MASSMAT(121:354,121:354);%%%%%%FOR CHEXA%%%%%


%%%%%%%%%%%%%%%%%%%%%%%%%%%%%%%%%%%%
%%%%%%K and M for CQUAD4%%%%%%%%%%%%
%%%%%%NEEDS USE TRANS %%%%%%%%%%%%%%
%%%%%%%%%%%%%%%%%%%%%%%%%%%%%%%%%%%%

n_idx=length(STIFFMAT_A)/6;
KA=zeros(6*n_idx);
KB=KA;
jo=0;

 for i=1:n_idx;
     io=6*(i-1);
      for j=1:3;
          jo=jo+1;
        KA(jo,:)= STIFFMAT_A(io+j,:);
     end
 end

 for i=1:n_idx;
     io=6*(i-1);
```

```
     for j=4:6;
         jo=jo+1;
       KA(jo,:)= STIFFMAT_A(io+j,:);
    end
end

jo=0;
 for i=1:n_idx;
    io=6*(i-1);
     for j=1:3;
         jo=jo+1;
       KB(:,jo)= KA(:,io+j);
    end
end

for i=1:n_idx;
    io=6*(i-1);
     for j=4:6;
         jo=jo+1;
       KB(:,jo)= KA(:,io+j);
    end
end

K21= KB(1+3*n_idx:6*n_idx,1:3*n_idx);
K22= KB(1+3*n_idx:6*n_idx,1+3*n_idx:6*n_idx);
%%%%%%%%%%%%%%%%%%%%%%%%%%%%%%%%%%%%%%%%%%%%%%%%%%%%%%%%%%%%%%%%%%%%%%%%%%%%%%%
phiA= - K22\K21;

TRANS = zeros(6*n_idx,3*n_idx);
TRANS(1:3*n_idx, 1:3*n_idx)= eye (3*n_idx,3*n_idx);
TRANS(1+3*n_idx:6*n_idx,1:3*n_idx) = phiA;

%%%%%%%%%%%%%%%%%%%%%%%%%%%%%%%%%%%%
%%%%%%%%%%%%%%%%%%%%%%%%%%%%%%%%%%%%

n_idxA=length(STIFFMAT_AA(:,1))/6;
n_idxB=length(STIFFMAT_AA(1,:))/3;

KAA=zeros(6*n_idxA,3*n_idxB);
jo=0;

  for i=1:n_idxA;
    io=6*(i-1);
     for j=1:3;
         jo=jo+1;
         KAA(jo,:)= STIFFMAT_AA(io+j,:);
    end
end

for i=1:n_idxA;
    io=6*(i-1);
     for j=4:6;
         jo=jo+1;
         KAA(jo,:)= STIFFMAT_AA(io+j,:);
    end
```

```
 end

%  KAB=KAA(1:60,1:234);
  KAB=TRANS'*KAA;

 MAA=zeros(6*n_idxA,3*n_idxB);
jo=0;

  for i=1:n_idxA;
     io=6*(i-1);
      for j=1:3;
          jo=jo+1;
          MAA(jo,:)= MASSMAT_AA(io+j,:);
     end
 end

 for i=1:n_idxA;
     io=6*(i-1);
      for j=4:6;
          jo=jo+1;
          MAA(jo,:)= MASSMAT_AA(io+j,:);
     end
 end

%  MAB=MAA(1:60,1:234);
   MAB=TRANS'*MAA;



%%%%%%%%%%%%%%%%%%%%%%%%%%%%%%%%%%%%%%%%%%%%%%%%%%%%%%%%%%%%%%%%%%%%%%%%%%%%%%%
%%%%%%%%%%%%%%%%%%%%%%%%%%%%%%%%%%%%%%%%%%%%%%%%%%%%%%%%%%%%%%%%%%%%%%%%%%%%%%%
%%%%%%%%%%%%%%%%%%%%%%%%%%%%%%%%%%%%%%%%%%%%%%%%%%%%%%%%%%%%%%%%%%%%%%%%%%%%%%%
n_idx=length(MASSMAT_A)/6;
MA=zeros(6*n_idx);
MB=MA;
jo=0;

 for i=1:n_idx;
     io=6*(i-1);
      for j=1:3;
          jo=jo+1;
        MA(jo,:)= MASSMAT_A(io+j,:);
     end
 end

 for i=1:n_idx;
     io=6*(i-1);
      for j=4:6;
          jo=jo+1;
        MA(jo,:)= MASSMAT_A(io+j,:);
     end
 end

 jo=0;
  for i=1:n_idx;
```

```
    io=6*(i-1);
     for j=1:3;
         jo=jo+1;
       MB(:,jo)= MA(:,io+j);
    end
end

for i=1:n_idx;
    io=6*(i-1);
     for j=4:6;
         jo=jo+1;
       MB(:,jo)= MA(:,io+j);
    end
end

%%%%%%%%%%%%%%%%%%%%%%%%%%%%%%%%%%%%%%%%%%%%%%%%%%%%%%%%%%%%
%%%%%%%K AND M FOR CQUAD4 U-V-W FORMAT%%%%%%%%%%%%%

Knew= TRANS'*KB*TRANS;
Mnew= TRANS'*MB*TRANS;
%%%%%%%%%%%%%%%%%%%%%%%%%%%%%%%%%%%%%%%%%%%%%%%%%%%%%%%%%%%%

nn1=length(Knew)/6;
nn_idx=length(STIFFMAT)/6;
nn2=nn_idx-n_idx;

nn=nn1+nn2;

KT = zeros(nn*6,nn*6);
KT(1:3*n_idx, 1:3*n_idx)= Knew;
KT(1:3*n_idx, 1+3*n_idx:6*nn)= KAB;
KT(1+3*n_idx:6*nn,1:3*n_idx)= KAB';
KT(1+3*n_idx:6*nn,1+3*n_idx:6*nn) = STIFFMAT_B;

MT = zeros(nn*6,nn*6);
MT(1:3*n_idx, 1:3*n_idx)= Mnew;
MT(1:3*n_idx, 1+3*n_idx:6*nn)= MAB;
MT(1+3*n_idx:6*nn,1:3*n_idx)= MAB';
MT(1+3*n_idx:6*nn,1+3*n_idx:6*nn) = MASSMAT_B;

[phi omegarad2]=(eig(KT,MT));
omegarad2=diag(omegarad2);
omegarad2=real(omegarad2);
omegarad2=sort(omegarad2);

omegarad= sqrt(omegarad2);
w=(omegarad)/2/pi;
```

# Appendix 2:
# Matlab coding for
# force appropriation of engine pylon

```
clear all;clc;close all;format compact
tic
% load ('STIFFMAT.mat')
% load ('MASSMAT.mat')
load ('TRANS.mat')
load ('KMT.mat')
load ('KK')

EXP_DATA = xlsread('Mode1_Pylon.xlsx');
nop  = size(EXP_DATA,1);
MS_P=EXP_DATA(:,1);
MS_P2=EXP_DATA(:,2);
MS_P3=EXP_DATA(:,3);

% a = 0; b = 0.00165;  % Rayleigh Damping Coefs
zetaa = 0.01;
zetab = 0.01;

wa = 1*2*pi;    % 1 Hz in rads
wb = 50*2*pi;    %% 50 Hz in rads
a = 2*wa*wb*(zetab * wa - zetaa * wb)/(wa^2 - wb^2);
b = 2*(zetaa * wa - zetab * wb) / (wa^2 - wb^2);
[a b zetaa zetab];
C= b*KT + a*MT;
[phi omegarad2]=(eig(KT,MT));
omegarad2=diag(omegarad2);
omegarad2=real(omegarad2);
omegarad2=sort(omegarad2);

omegarad=sqrt(omegarad2);
wf=sqrt(omegarad2)/2/pi; %%%in Hz
% wf=sort(wf);


M = MT;  K = KT;

%%%%%%%%%%%%%%%%%%%%%%%%%%%%%%%%%%%%%%%%%%%%%%%%%%%%

wmax = 1800 ;%max(w);

irow = [2 5 8 11 26 29 32 35 50 53 56 59];
icol = [5 8 53 56];

nr = size(irow);
nc = size(icol);

Mevals = [];
Mevects1 = [];
Mevects2 = [];
icount = 0;


for w = 100:0.01: wmax+10
```

```
    icount = icount + 1;
    ww(icount) = w/2/pi; %%% plot in Hz
    HH  = inv(-M*w^2 + 1i*w*C + K);  %%%%%%%% FRF

     for ii = 1:length(irow);
        for jj= 1:length(icol);
        A(ii,jj) = HH (irow(ii),icol(jj));
    end
    end

    AA=real (A);
    BB=imag (A);

    MM = AA'*AA;
    NN = (AA'*AA + BB'*BB);
    [MMIFevect,MMIFevals] = eig(MM,NN);

    Mevals = [Mevals, diag(MMIFevals)];
    Mevects1 = [Mevects1, MMIFevect(:,1)];
    Mevects2 = [Mevects2, MMIFevect(:,2)];


end

%%%%%%%%%%%%%%%%%%%%%%%%%%%%%%%%%%%%%%%%%%%%%%%%
for w1 = 2*pi* 28.4235;  %%%

    HH1  = inv(-M*w1^2 + 1i*w1*C + K);  %%%%%%%% FRF

     for ii = 1:length(irow);
        for jj= 1:length(icol);
        A1(ii,jj) = HH1 (irow(ii),icol(jj));
    end
    end

    AA1=real (A1);
    BB1=imag (A1);

    MM1 = AA1'*AA1;
    NN1 = (AA1'*AA1 + BB1'*BB1);

    [MMIFevect1,MMIFevals1] = eig(MM1,NN1);

%     Mevals1 = [Mevals1, diag(MMIFevals1)];
%     Mevects11 = [Mevects11, MMIFevect11(:,1)];
%     Mevects22 = [Mevects22, MMIFevect11(:,2)];


end

xvect = MMIFevect1(:,1)/abs(max(MMIFevect1(:,1)));
MMIFevect1(:,1);
```

```
% orgphi=TRANS*phi;
% orgphi(:,1)=orgphi(:,1)./sqrt(orgphi(:,1)'*MASSMAT*orgphi(:,1));
%
for iii=1:length(irow);
%         for jjj= 1:length(icol);
        jjj=1;
        phiA(iii,jjj) = MS_P(irow(iii),1);
        phi1 = phiA;
%         end
end

x_1= 1i*BB1*MMIFevect1(:,1);

% phi1=phi(:,(KK(1,2)));

MPI=(1-((real(x_1')*x_1))/(x_1'*x_1));

x1= BB1*MMIFevect1(:,1);
RRR = (x1'*x1)*(phi1'*phi1);

MAC= (abs(x1'*phi1))/sqrt(RRR);

%%%%%%%%%%%%%%%%%%%%%%%%%%%%%%%%%%%%%%%%%%%%%%%%%%%%%%%%%%%%%%%%%%%%%%%
for w2 = 2*pi*123.4883;  %%%

    HH2  = inv(-M*w2^2 + 1i*w2*C + K);  %%%%%%%% FRF

     for ii = 1:length(irow);
        for jj= 1:length(icol);
        A2(ii,jj) = HH2 (irow(ii),icol(jj));
    end
    end

    AA2=real (A2);
    BB2=imag (A2);

    MM2 = AA2'*AA2;
    NN2 = (AA2'*AA2 + BB2'*BB2);

    [MMIFevect2,MMIFevals2] = eig(MM2,NN2);

end
for iii=1:length(irow);
%         for jjj= 1:length(icol);
        jjj=1;
        phiB(iii,jjj) = MS_P2(irow(iii),1);
        phi2 = phiB;
%         end
end

xvect2 = MMIFevect2(:,1)/abs(max(MMIFevect2(:,1)));
MMIFevect2(:,1);
```

```
x_2= 1i*BB2*MMIFevect2(:,1);

MPI2=(1-((real(x_2')*x_2))/(x_2'*x_2));

x2= BB2*MMIFevect2(:,1);
RRR2 = (x2'*x2)*(phi2'*phi2);

MAC2= (abs(x2'*phi2))/sqrt(RRR2);

%%%%%%%%%%%%%%%%%%%%%%%%%%%%%%%%%%%%%%%%%%%%%%%%%%%%%%%%%%%%%%%%%%%%%%%%%%%%%%%

for w3 = 2*pi*259.6677;  %%%

    HH3  = inv(-M*w3^2 + 1i*w3*C + K);  %%%%%%%% FRF

     for ii = 1:length(irow);
        for jj= 1:length(icol);
        A3(ii,jj) = HH3 (irow(ii),icol(jj));
    end
    end

    AA3=real (A3);
    BB3=imag (A3);

    MM3 = AA3'*AA3;
    NN3 = (AA3'*AA3 + BB3'*BB3);

    [MMIFevect3,MMIFevals3] = eig(MM3,NN3);

end
for iii=1:length(irow);
%         for jjj= 1:length(icol);
        jjj=1;
        phiC(iii,jjj) = MS_P3(irow(iii),1);
        phi3 = phiC;
%         end
end

xvect3 = MMIFevect3(:,1)/abs(max(MMIFevect3(:,1)));
MMIFevect3(:,1);

x_3= 1i*BB3*MMIFevect3(:,1);

MPI3=(1-((real(x_3')*x_3))/(x_3'*x_3));

x3= BB3*MMIFevect3(:,1);
RRR3 = (x3'*x3)*(phi3'*phi3);

MAC3= (abs(x3'*phi3))/sqrt(RRR3);


%%%%%%%%%%%%%%%%%%%%%%%%%%%%%%%%%%%%%%%%
figure(1)
```

```
subplot(211)

plot(ww,Mevals(1:4,:)); grid on
xlabel('Frequency (Hz)');
ylabel('Eigenvalue');


y = Mevals(1,:);
yend = length(Mevals(1,:));
y1 = y(1:yend-2);
y2 = y(2:yend-1);
y3 = y(3:yend);

imin = find((y2 < y1) & (y2 < y3))
ymin = y(imin + 1)
wwmin = ww(imin + 1)
toc
```

**BIBLIOGRAPHY**

ABDUL RANI, M. N. (2012). *Structural dynamic analysis and model updating for a welded structure made from thin steel sheets.* PhD Thesis, Department of Dynamics and Control, School of Engineering, University of Liverpool, UK.

ABU HUSSAIN, KHODAPARAST, H. H. and OUYANG, H. (2012). Parameter selection and stochastic model updating using perturbation methods with parameter weighting matrix assignment. *Mechanical System and Signal Processing,* vol. 32, pp. 135-152.

ABU HUSSAIN, N., KHODAPARAST, H. H., SNAYLAM, A., JAMES, S., DEARDEN, G. and OUYANG, H. (2010). Finite-element modelling and updating of laser spot weld joints in a top-hat structure for dynamic analysis *Proceedings of the Institution of Mechanical Engineers, Part C: Journal of Mechanical Engineering Science,* vol. 224, no. 4, pp. 851- 861.

ABU HUSSAIN, N., KHODAPARAST, H. H., SNAYLAM, A., JAMES, S., SHARP, M., DEARDEN, G. and OUYANG, H. (2009b). Modal testing and finite element model updating of laser spot welds. *Journal of Physics: Conference Series ,*vol. 181.

ABU HUSSAIN, N., SNAYLAM, A., KHODAPARAST, H. H., JAMES, S., DEARDEN, G. and OUYANG, H. (2009a). Finite model updating for damage detection – Application to a welded structure. *Key Engineering Materials Trans Tech Publication*, vol. 413-414, pp 393-400.

AGARWAL, G. S. and GUPTA, S. D. (1987). Effect of nonlinear boundary conditions on nonlinear phenomena in optical resonators. *Optics Letters,* vol. 12, no. 10, pp. 829-831.

AHMADIAN, H., MOTTERSHEAD, J. E., JAMES, S., FRISWELL, M.I. and REECE, C. A. (2006). Modelling and updating of large surface to surface joint in the awe mace structure. *Mechanical System and Signal Processing,* vol. 20, pp. 868-880.

ALEXIOU, K. (1990). *Comparison of multi-point vibration test methods.* PhD Thesis, Department of Aeronautical Engineering, Queen Mary and Westfield College, University of London, UK.

ALEXIOU, K. and WRIGHT, J. R. (1993) Comparison of some multipoint force appropriation methods. *Modal Analysis: The International Journal of Analytical and Experimental Modal Analysis* 8(2), pp. 119-136.

ALEXIOU, K. and WRIGHT, J. R. (1993). Comparison of some direct multi-point force appropriation methods. *International Journal of Analytical and Experimental Modal Analysis,* vol. 8, no. 2, pp. 119-136.

AL-HADID, M. A. and WRIGHT, J. R. (1989). Developments in the force-state mapping technique for non-linear systems and the extension to the location of nonlinear elements in a lumped-parameter system. *Mechanical Systems and Signal Processing*, vol. 3, no. 3, pp. 269-290.

ALLEMANG, R. J. and BROWN, D. L. (1986). Multi input experimental modal analysis – A survey. *International Journal of Analytical and Experimental Modal Analysis,* vol. 1, no. 1, pp. 37-44.

AMABILI, M. and PAÏDOUSSIS, M. P. (2003) Review of studies on geometrically nonlinear vibrations and dynamics of circular cylindrical shells and panels, with and without fluid-structure interaction. *Applied Mechanics Reviews*, vol. 56, no. 4, pp. 349- 381.

ANDERSON, T. J., NAYFEH, A. H. and BALACHANDRAN, B. (1996). Experimental verification of the importance of the nonlinear curvature in the response of a cantilever beam. *Journal of Vibration and Acoustics*, vol. 118, pp. 21-27.

ARRUDA, J. R. F. and SANTOS, J. M. C. (1993). Mechanical joint parameter estimation using frequency response functions and component mode synthesis. *Mechanical System and Signal Processing,* vol. 7, no. 6, pp. 493-508.

ARSLAN, O. (2008). *Modal identification of nonlinear substructures and implementation in structural coupling analysis*, M.Sc. Thesis, Department of Mechanical Engineering, Middle East Technical University, Ankara, Turkey.

ASHER, G. W. (1958). A method of normal mode excitation utilizing admittance matrices. *Proceeding of the National Specialist Meeting on Dynamics and Aeroelasticity, Journal of Aeronautical Science,* vol. 6, pp. 56-96.

ATKINS, P. and WORDEN, K. (1997). Identification of a multi-degree-of-freedom nonlinear system. *Proceedings of the 15$^{th}$ International Modal Analysis Conference,* Orlando, Florida, pp. 1023-1028.

ATLURI, S. (1973). Nonlinear vibrations of a hinged beam including nonlinear inertia effects. *Journal of Applied Mechanics*, vol. 40, pp. 121-126.

BARUCH, M. (1978). Optimization procedures to correct stiffness and flexibility matrices using vibration test. *AIAA Journal*, vol. 16, no. 11, pp 1208-1210.

BATHE, K. J. (1982). *Finite Element Procedure in Engineering Analysis,* Prentice-Hall, ISBN 0-13-317305-4.

BENDAT, J. S. (1990). *Nonlinear system analysis and identification from random data.* John Wiley & Sons. New York, U.S.A.

BERAN, P. S., STRGANAC, T.W., KIM, K. and NICHKAWDE, C. (2004). Studies of store induced limit cycle oscillation using a model with full system nonlinearities. *Nonlinear Dynamics,* vol. 37, no. 4, pp. 323-339.

BERMAN, A. and FLANNELLY, G. (1971). Theory of incomplete models of dynamic structures. *AIAA Journal*, vol. 9, no. 8, pp 1481-1487.

BERMAN, A. and NAGY, E. J. (1983). Improvement of a large analytical model using test data. *AIAA Journal*, vol. 21, no. 8, pp 1118-1173.

BILLINGS, S., CHEN, S., and KORENBERG, M. (1989). Identification of MIMO nonlinear systems using a forward regression orthogonal estimator. *International Journal of Control*, vol. 49, no. 6, pp. 2157-2189.

BILOSOVA, A. (2001). *Modal testing*. Technical Report: European Social Fund in Czech Republic.

BOIVIN, N., PIERRE, C. and SHAW, S. W. (1995). Nonlinear modal analysis of structural systems featuring internal resonances. *Journal of Sound and Vibration*, vol. 182 no. 2, pp. 225-230.

BRATOSIN, D. and SIRETEANU, T. (2002). Hysteretic damping modelling by nonlinear. *Proceedings of The Romanian Academy Series A: Mathematics, Physics, Technical Sciences, Information Science,* vol. 3, pp. 99-104.

BREITBACH, E. (1973). A semi-automatic modal survey test technique for complex aircraft and space structures. *Proceeding of the 3rd Esro Testing Smposium*. Frascati, Italy, pp. 519-528.

BRILLHART, R. D. and HUNT, D. L. (1992). Multiple input excitation methods for the C-17 transport aircraft Ground Vibration Testing. *Proceedings of the 10th International Modal Analysis Conference.*

CEASAR, B. (1986). Update and identification dynamic mathematical models. *Proceedings of the 5th International Modal Analysis Conference,* Los Angeles, pp. 394-401.

CEASAR, B. (1987). Updating system matrices using model test data. *Proceedings of the 4th International Modal Analysis Conference,* Los Angeles, pp. 453-459.

CHEN, Q., WORDEN, K., PENG, P. and LEUNG, A. (2007). Genetic algorithm with an improved fitness function for NARMAX modelling. *Mechanical Systems and Signal Processing*, vol. 21, no. 2, pp. 994-1007.

CLAEYS, M., SINOU, J., LAMBELIN, J.P. and TODESCHINI, R. (2016). Experiments and numerical simulations of nonlinear vibration responses of an assembly with friction joints – Application on a test structure named "Harmony". *Mechanical Systems and Signal Processing*, vol. 70-71, pp. 1097-1116.

COOPER, J. E. , HAMILTON, M.J. and WRIGHT, J. R. (1993) Experimental evaluation of various normal mode force appropriation methods on a rectangular perspex plate using four exciters. *Modal Analysis: The International Journal of Analytical and Experimental Modal Analysis* 10(2), pp. 118-130.

COOPER, J. E. and WRIGHT, J. R. (1997). To fit or to tune – That is the question. *Proceedings of the 15th International Modal Analysis Conference,* pp. 1353-1359.

CRAWLEY, E.F. and AUBERT, A.C. (1986). Identification of nonlinear structural elements by force-state mapping. *AIAA Journal,* vol. 24, pp. 155-162

DEARSON, R. K. (1994). *Discrete time dynamic model*. Oxford University Press.

DEBLAUWE, F., BROWN, D. L. and ALLEMANG, R. J. (1987). The polyreference time technique. *Proceedings of the 5th International Modal Analysis Conference,* pp. 832-845.

DEGENER, M. (1995). Ground vibration testing for validation of large aircraft structural dynamics. *Proceedings of the International Forum on Aeroelasticity and Structural Dynamics*, pp. 70.1-70.12.

DESFORGES, M.J., COOPER, J.E. and WRIGHT, J. R. (2004). Force appropriation for flight flutter testing. *Proceedings of The Institution of Mechanical Engineers Part G-Journal of Aerospace Engineering,* vol. 218 (3), pp. 189-198.

DIMITRIADIS, G. and COOPER, J.E. (1998). A method for the identification of non-linear multi-degree-of-freedom systems. *Proceedings of the Institute of Mechanical Engineers*, Part G 212, pp. 287-298.

EWINS, D. J. (1995). *Modal testing: Theory and practice*. Hertfordshire: Research Studies Press Ltd. 1st Edition.

EWINS, D. J. (2000). *Modal testing: Theory, practice and application*. Hertfordshire :Research Studies Press Ltd. 2nd Edition.

FELDMAN, M. (2007). Considering high harmonics for identification of non-linear systems by Hilbert transform. *Mechanical System and Signal Processing,* vol. 21, no. 2, pp 943-958.

FELDMAN, M. (2012). Nonparametric identification of asymmetric nonlinear vibration systems with the Hilbert transform. *Journal of Sound and Vibration*, vol. 331, pp. 3386-3396.

FRISWELL, M.I. and MOTTERSHEAD, J. E. (1995). *Finite element model updating in structural dynamics*, Kluwer Academic Publisher.

FRITZEN, C. P., JENNEEWEIN, D. and KIEFER, T. (1998). Damage detection based on model updating methods. *Mechanical System and Signal Processing,* vol. 12, pp 163-186.

GANT, F., ROUCH, PH. and CHAMPENEY, L. (2013). Updating of uncertain joint models using the lack of knowledge theory. *Computers and Structure,* vol. 128, pp. 128-135.

GATTO, M., PEETERS, B. and COPPOTELLI, G. (2010). Flexible shaker excitation signals for improved FRF estimation and and non-linearity assessment. *Proceedings of International Conference on Noise and Vibration Engineering,* Leuven, Belgium, pp. 2475-2488.

GAVASSONI, E., GONÇALVES, P. B., and ROEHL, D. E. M. (2015). Nonlinear vibration modes of an offshore articulated tower. *Ocean Engineering,* vol. 109, pp. 226-242.

GLOTH, G. and SINAPIUS, M. (2004). Influence and characterisation of weak nonlinearities in swept-sine modal testing. *Aerospace Science and Technology*, vol. 8, no. 2, pp. 111-120.

GÖGE, D., SINAPIUS, M., FÜLLEKRUG, U. and LINK, M. (2005). Detection and description of non-linear phenomena in experimental modal analysis via linearity plots. *International Journal of Non-Linear Mechanics*, vol. 40, no. 1, pp. 27-48.

GUILLAUME, P., SCHOUKENS, J., PINTELON , R. and KOLLAR, I. (1991). Crest-factor minimization using nonlinear chebyshev approximation methods. *IEEE Trans. Instrumentation and Measurement*. vol. 40, pp. 982-989.

GUILLAUME, P., VERBOVEN, P., VANLANDUIT, S. and PARLOO, E. (2001). Multisine excitations - new developments and applications in modal analysis. *Proc. IMAC 19 Int. Modal Analysis Conf.*, Kissimmee (FL), USA., pp. 1543-1549.

GUO, X. Y. and ZHANG, W. (2016). Nonlinear vibrations of a reinforced composite plate with carbon nanotubes. *Composite Structures,* vol. 135, pp. 96-108.

HAMILTON, M. J. (1993). *Multipoint vibration testing methods for undamped normal mode identification.* PhD Thesis, Department of Mechanical Engineering, University of Manchester, UK.

HEYLEN, W., LAMMENS, S. and SAS, P. (1998). *Modal Analysis: Theory and Testing,* KULeuven Publisher, 2nd Edition.

HOLMES, P. S., COOPER, J. E. and WRIGHT, J. R. (1996). Normal mode estimation from non-proportionally damped systems. *Proceedings of the 21st International Seminar on Modal Analysis,* pp. 1237-1249.

IBANEZ, P. (1973). Identification of dynamic parameters of linear and nonlinear structural models from experimental data. *Nuclear Engineering and Design*, vol. 25, pp. 30-41.

IBANEZ, P. (1976). Force appropriation by Extended Asher's method. *SAE Aerospace Engineering and Manufacturing Meeting,* SAE Paper, no.760873.

IMEGRUN, M. and VISSER, W.J. (1991). A review of model updating techniques, *The Shock and Vibration Digest,* vol. 23, no. 1, pp 9-20

JUANG, J.N. and WRIGHT, J. R. (1991). A multipoint force appropriation method based upon a singular value decomposition approach. *Journal of Vibration and Acoustics,* vol. 113, pp. 176-181.

KENIGBUCH, R. and HALEVI, Y. (1998). Model updating in structural dynamics: A generalised reference basis approach, , *Mechanical Systems and Signal Processing,* vol. 12, no. 1, pp 575-90.

KERSCHEN, G. (2002). *On the model validation in non-linear structural dynamics.* PhD Thesis, Department of Aeronautical, University of Liege, Belgium.

KERSCHEN, G., GOLINVAL, J.C. and WORDEN, K. (2001). Theoretical and experimental identification of a non-linear beam. *Journal of Sound and Vibration,* vol. 244, pp. 597-613.

KERSCHEN, G., WORDEN, K., VAKAKIS, A.F. and GOLINVAL, J. C. (2006). Past, present and future of nonlinear system identification in structural dynamics, *Mechanical Systems and Signal Processing,* vol. 20, no. 3, pp 505-592.

KIM, G.H. and PARK, Y. S. (2001). Finite element modal updating using multi-objective optimization techniques. *Proceedings of the 19th International Modal Analysis Conference,* Orlando, Florida, pp. 348-354.

KIM, T. R., WU, S.M. and EMAN, K.F. (1989). Identification of joint parameters for a taper joint. *Journal of engineering for industry,* vol. 111, no. 3, pp 282-287.

KRAGH, K. A., THOMSEN, J. J. and TCHERNIAK, D. (2010). Experimental detection and quantification of structural nonlinearity using homogeneity and Hilbert transform methods. *Proceedings of 24th International Conference on Noise and Vibration engineering (ISMA2010)*, Leuven, pp. 3159-3171.

KÜMMEL, M., GLODSCHMIDT, S. and WALLASCHEK, J. (1998). Theoretical and experimental studies of a piezoelectric ultrasonic linear motor with respect to damping and nonlinear material behaviour. *Ultrasonics*, vol. 35, no. 1-5, pp. 103-109.

LAU, J., PEETERS, B., DEBILLE, J., GUZEK, Q., FLYNN, W., LANGE, D. S. and KAHLMANN, T. (2011). Ground vibration testing master class: modern testing and analysis concepts applied to an f-16 aircraft. *Proceedings of the 29th International Modal Analysis Conference,* Jacksonville, Florida, USA.

LEMBREGTS, F., LEURIDAN, J. and VAN BRUSSEL, H. (1989). Frequency domain direct parameter identification: state space formulation. *Proceedings of the 7th International Modal Analysis Conference,* pp. 1271-1277.

LEONTARITIS , I. J. and BILLINGS, S. A. (1985). Input-output parametric models for nonlinear systems, part I: deterministic nonlinear systems, vol. 41, pp. 303–328.

LEY, W., WITTMANN, K. and HALLMANN, W. (2009). *Handbook of Space Technology*. John Wiley & Sons, ISBN: 978-0-470-74241-9.

LIN, R. M., EWINS, D. J. and LIM, M. K. (1993). Identification of nonlinearity from analysis of complex modes. *International Journal of Analytical and Experimental Modal Analysis*, vol. 8, no. 3, pp. 290-306.

MAIA, N. M. M. and SILVA, J. M. M. (1997). *Theoretical and experimental modal analysis.* Baldock Research Studies Press.

MALATKAR, P. (2003). *Nonlinear vibrations of cantilever beams and plate.* PhD Thesis, Virgina Polytechnic Institute and State University,US.

MARCHESIELLO, S. (2003). Application of the conditioned reverse path method, *Mechanical Systems and Signal Processing*, vol. 17, pp. 183-188.

MAREISHI, S., RAFIEE, M., HE, X. Q. and LIEW, K. M. (2014). Nonlinear free vibration, postbuckling and nonlinear static deflection of piezoelectric fiber-reinforced laminated composite beams. *Composite Part B: Engineering*, vol. 59, pp. 123-132.

MARWALA, T. (2010). *Finite Element Model Updating Using Computational Intelligence Techniques: Applications to Structural Dynamics. Heidelberg:* Springer, ISBN 978-1-84996-322-0.

MASRI, S.F. and CAUGHEY, T.K. (1979). A nonparametric identification technique for nonlinear dynamic problems. *Journal of Applied Mechanics*, vol. 46, pp. 433-447

MASRI, S.F., SASSI, H. and CAUGHEY, T.K. (1982). Nonparametric identification of nearly arbitrary nonlinear systems. *Journal of Applied Mechanics*, vol. 49, pp. 619-628

McEWAN, M. I., WRIGHT, J. R., COOPER, J. E. and LEUNG, A. Y. T. (2001). A combined modal/finite element analysis technique for the dynamic response of a nonlinear beam to harmonic excitation. *Journal of Sound and Vibration*, vol. 243, pp. 601-624.

MOROSOW, G. and AYRE, R. S. (1978). Force appropriation for modal vibration testing using excitation. *Shock and Vibration Bulletin*, vol. 48, part 1, pp. 39-48.

MOTTERSHEAD, J. E. and FRISWELL, M.I. (1993). Model updating in Structural Dynamics – A survey. *Journal Sound and Vibration*, vol. 167, no. 2, pp 347-375.

MOTTERSHEAD, J. E., FRISWELL, M.I., NG, G. H. T. and BRANDON, A. (1996). Geometric parameters for finite element model updating of joints and constraints. *Mechanical Systems and Signal Processing*, vol. 10, no. 2, pp 171-182.

MOTTERSHEAD, J. E., LINK, M. and FRISWELL. (2011). The sensitivity method in finite element model updating: A tutorial. *Mechanical Systems and Signal Processing*, vol. 25, pp 2275-2296

MOTTERSHEAD, J. E., MARES, C. and FRISWELL, M.I. (2010). The sensitivity method in finite element model updating: A tutorial. *Mechanical Systems and Signal Processing*, vol. 25, no. 7, pp. 2275-2296.

MOTTERSHEAD, J. E., MARES, C. JAMES, S. and FRISWELL, M.I. (2006). Stochastic model updating: Part 2 – Application to a set physical structures. *Mechanical Systems and Signal Processing*, vol. 20, no. 8, pp 2171-2185.

MOTTERSHEAD, J. E., MARES, C., FRISWELL, M.I. and JAMES, S. (2000). Selection and updating of parameters for an aluminium space frame model. *Mechanical Systems and Signal Processing*, vol. 14, no. 6, pp 923-944.

MSC.2 (2010). *MD/MSC NASTRAN 2010 Quick Reference Guide,* MSC Software.

NASH, M. (1991). A modification of the multivariate mode indicator function employing principal force vectors. *Proceedings of the 9th International Modal Analysis Conference*, pp. 688-693.

NATKE, H. G. (1998). Updating computational models in the frequency domain based on measured data: a survey. *Probabilistic Engineering Mechanics,* vol. 3, no. 1, pp 28-35.

NAYFEH, A. H. and PAI, P. F. (2004). *Linear and nonlinear structural mechanics*. John Wiley & Sons, Inc., New York.

NIEDBAL, N. (1985). Advanced in ground vibration testing using a combination of phase resonance and phase resonance method. *Proceedings of the 2nd International Symposium on Aero-elasticity and Structural Dynamics,* pp. 523-528.

NOËL, J.P., RENSON, L., GRAPPASONNI, C. and KERSCHEN, G. (2016). Identification of nonlinear normal modes of engineering structures under broadband forcing. *Mechanical Systems and Signal Processing*, vol. 74, pp. 95-110.

ORLANDO, S., PEETERS, B. and COPPOTELLI, G. (2008). Improved FRF estimators for MIMO Sine Sweep data. *Proceedings of International Conference on Noise and Vibration Engineering*, Leuven.

OTTE, D., VAN DER AUWERAER, H., DEBILLE, J. and LEURIDAN, J. (1993). Enhanced force vector appropriation methods for normal mode testing. *Proceedings of the 11th International Seminar on Modal Analysis Conference,* Kissimmee, Florida, USA pp. 1310-1316.

OUYANG, H., OLDFIELD, M. J. and MOTTERSHEAD, J. E.(2006). Experimental and theoretical studies of a bolted joint excited by a torsional dynamic load. *International Journal of Mechanical Sciences*, vol. 48, no. 12, pp. 1447-1455.

PALMONELLA, M. , FRISWELL, M. I., MARES, C. and MOTTERSHEAD, J. E. (2003). Improving spot weld models in structural dynamics. *ASME Design Engineering Technical Conference and Computer Information in Engineering Conference,* vol. 1A, pp 379-388.

PESHECK, E., BOIVIN, N. and PIERRE, C. (2001). Nonlinear modal analysis of structural systems using multi-mode invariant manifolds. *Nonlinear Dynamics,* vol. 25, pp. 183-205.

PLATTEN, M. F., WRIGHT, J. R. and COOPER, J.E. (2002). The use of a noncontact acoustic excitation array for the estimation of damping in aircraft panels. *Proceedings of the 25th International Seminar on Modal Analysis (ISMA2002)*. Leuven, Belgium, pp. 451–460.

PLATTEN, M. F., WRIGHT, J. R., COOPER, J.E. and DIMITRIADIS, G. (2009b). Identification of a nonlinear wing structure using an extended modal model. *Journal of Aircraft*, vol. 46, no. 5, pp. 1614-1626.

PLATTEN, M. F., WRIGHT, J. R., DIMITRIADIS, G. and COOPER, J.E. (2009a). Identification of multi degree of freedom nonlinear systems using an extended modal space model. *Mechanical Systems and Signal Processing*, vol. 23, no. 1, pp. 8-29.

RADES, M. (1992). A comparison of some mode indicator functions. *Proceedings of the17th International Seminar on Modal Analysis*, pp. 563-581.

RICE, H. J. (1995). Identification of weakly nonlinear systems using equivalent linearization. *Journal of Sound and Vibration,* vol. 185, no. 3, pp. 473-481.

RICE, H. J. and FITZPATRICK, J.A (1991). A procedure for the identification of linear and non-linear multi-degree-of freedom systems. *Journal of Sound and Vibration*, vol. 149, pp. 397-411.

RICHARDS, C. M. and SINGH, R. (1998). Identification of multi-degree-of-freedom non-linear systems under random excitations by the reverse-path spectral method. *Journal of Sound and Vibration*, vol. 213, pp. 673-708.

RICHARDS, C. M. and SINGH, R. (2001). Characterization of rubber isolator nonlinearities in the context of single- and multi-degree-of-freedom experimental systems. *Journal of Sound and Vibration*, vol. 247, pp. 807-834.

ROACHE, P.J. (1998). *Verification and Validation in Computational Science and Engineering*, Hermosa Publications, Albuquerque.

RODDEN, W.P. (1967). A method for deriving influence coefficients from ground vibration test. *AIAA Journal*, vol. 5, no. 5, pp 991-1000.

ROSA, L. F., MAGLUTA, C. and ROITMAN, N. (1999). Estimation of modal parameters through a nonlinear optimisation technique. *Mechanical Systems and Signal Processing*, vol. 13, no. 4, pp. 593-607.

RUI, Q., OUYANG, H. and WANG, H. Y. (2013). An efficient statistically equivalent reduced method on stochastic model updating. *Applied Mathematical Modelling*, vol. 37, no. 8, pp. 6079-6096.

SAADA, M. M., ARAFA, M. H. and NASEEF, A. O. (2013). Finite element model updating approach to damage identification in beams using particle swarm optimization. *Engineering Optimization,* vol. 45, no. 6, pp. 677-696.

SANI, M.S.M., OUYANG, H., COOPER, J.E. and HUSIN, C.K.E.N.C.K. (2013) Smart Methodology of Stiffness Nonlinearity Identification Vibration System, *2nd International Conference on Mechanical Engineering Research 2013 (ICMER 2013),* 1-3 July 2013, Bukit Gambang Resort, Gambang, Pahang Malaysia.

SARMAST, M. and WRIGHT, J. R. (2010). Residual modes on non-linear resonant decay method. *Proceedings of the World Congress on Engineering (WEC 2010)*, vol. II.

SCHOUKENS, J., ROLAIN ,Y., SWEVERS ,J. and CUYPER, J. D. (2000). Simple methods and insights to deal with non-linear distortions in FRF-measurements, *Mechanical Systems and Signal Processing*, vol. 14, no. 4, pp. 657-666.

SHAW, S. W. and PIERRE, C. (1991). Normal modes for nonlinear vibratory systems. *Journal of Sound and Vibration*, vol. 164, no. 1, pp. 85–124.

SHI, G. and ATLURI, S.N. (1991). Nonlinear dynamic response of frame-type structures with hysteretic damping at the joints. *AIAA Journal* vol. 30, no. 1, pp 234-240.

SILLER, H. R. E. (2004). *Nonlinear modal analysis methods for engineering structures.* PhD Thesis, Department of Mechanical Engineering, Imperial College London, UK.

SIMOEN, E., ROECK, G. D. and LOMBAERT, G. (2015). Dealing with uncertainty in model updating for damage assessment: A review. *Mechanical Systems and Signal Processing*, vol. 56-57, pp. 123-149.

SIMON, M. and TOMLINSON, G. R. (1984). Use of the Hilbert transform in modal analysis of linear and non-linear structures. *Journal of Sound and Vibration*, vol. 96, pp. 421-436.

SLAATS, P. M., A., JONGH, J. De and SAUREN, A. A. H. J. (1995). Model reduction tools for nonlinear structural dynamics. *Computers & structures*, vol. 54, no. 6, pp. 1155-1171.

SOIZE, C. and Le Fur, O. (1997). Modal identification of weakly nonlinear, multidimensional dynamical systems using a stochastic linearisation method with random coefficients. *Mechanical Systems and Signal Processing*, vol. 11, no. 1, pp. 37-49.

STAHLE, C. V. (1962). Phase separation technique for ground vibration testing. *Aerospace Engineering,* vol. 21, no. 7, pp. 56-96.

TAYLOR, G. A., GAUKROGER, D. R. and SKINGLE, C.W. (1967). A semi-automatic technique for exciting the principle modes of vibration of complex structures. *RAE Technical Report*, 677211.

THOUVEREZ, F. and JEZEQUEL, L. (1996). Identification of NARMAX models on a modal base. *Journal of Sound and Vibration*, vol. 89, pp. 193-213.

TOMLINSON, G. R. (1987). Developments in the use of the Hilbert transform for detecting and quantifying non-linearity associated with frequency response functions. *Mechanical Systems and Signal Processing*, vol. 1, no. 2, pp. 151-171.

TURNER, J. A. (2004). Non-linear vibrations of a beam with cantilever-Hertzian contact boundary conditions. *Journal of Sound and Vibration,* vol. 275, no. 1-2, pp. 177-191.

WEI, F. S. (1980). Stiffness matrix correction from incomplete test data. *AIAA Journal*, vol. 18, no. 10, pp 1274-1275.

WHITE, S. W., KIM, S. K., BAJAJ, A. K., DAVIES P., SHOWERS , D. K. and LIEDTKE, P. E. (2000). Experimental techniques and identification of nonlinear and viscoelastic properties of flexible polyurethane foam. *Nonlinear Dynamics,* vol. 22, pp. 281-313.

WILLIAMS, R. , CROWLEY, J. and VOLD, H. (1986). The multivariate mode indicator function in modal analysis. *Proceeding of the 4th International Modal Analysis Conference (IMAC)*. Los Angeles pp. 66-70.

WILLIAMS, R. , CROWLEY, J. and VOLD H. (1986) The multivariate mode indicator function in modal analysis. *Proceedings of the 3rd International Modal Analysis Conference,* Orlando, Florida pp. 66-70.

WORDEN, K. (1990). Data processing and experiment design for the restoring force surface method, Part II :choice of excitation signal. *Mechanical System Signal Process,* vol. 4, pp. 321-44.

WORDEN, K. and TOMLINSON, G. R. (2001). *Nonlinearity in structural dynamics: detection, identification and modelling*. Institute of Physics Publishing.

WRIGHT, J. R., COOPER, J.E. and DESFORGES, M.J. (1999). Normal mode force appropriation – theory and application. *Mechanical Systems and Signal Processing* 13(2), pp. 217-240.

WRIGHT, J. R., PLATTEN, M. F., COOPER, J. E. and SARMAST, M. (2001) Identification of multi degree of freedom weakly nonlinear systems using a model based in modal space. *Proceedings of the International Conference on Structural System Identification*, Kassel, Germany, pp. 49-68.

YUNUS, M. A. (2012). *Finite element modelling and updating of structure of sheet metal with bolted and welded joints.* PhD Thesis, Department of Dynamics and Control, School of Engineering, University of Liverpool, UK.

ZHANG, L. (2004). An overview of major developments and issues in modal identification. *Proceedings of the 22nd International Modal Analysis Conference (IMAC)*. Detroit, Michigan.

ZIENKIEWIEZ, O. C. and TAYLOR, R. L. (1994). *The finite element method.* Mc-Graw-Hill, ISBN 0-07-084072-5.